Computational methods for microbial cell factory engineering aided by evolution

PhD Thesis by Kristian Jensen

December 2018

The Novo Nordisk Foundation Center for Biosustainability

Technical University of Denmark

Computational methods for microbial cell factory engineering aided by evolution

PhD thesis by Kristian Jensen

Principal supervisor: Markus Herrgård

Co-supervisor: Nikolaus Sonnenschein

Preface

This thesis is written as partial fulfillment of the requirements for obtaining a PhD degree at the Technical University of Denmark. The work included in the thesis has been carried out at the Novo Nordisk Foundation Center for Biosustainability in the period from January 2016 to December 2018. Part of the work was done in Uwe Sauer's lab at the Eidgenössiche Technische Hochschule Zürich in Switzerland in the fall of 2017. The work has been supervised by Professor Markus Herrgård and Senior Researcher Nikolaus Sonnenschein and was funded by the Technical University of Denmark and the Novo Nordisk Foundation.

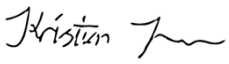

Kristian Jensen

Kgs. Lyngby, December 2018

Abstract

Increasing global temperatures and limited fossil resources make it increasingly urgent to find alternative ways of producing fuels and chemicals. Metabolic engineering offers a promising solution to this problem by using microbes as cell factories for manufacturing a diverse set of products from renewable resources. However, cell factory development requires extensive knowledge of microbial biology as well as expensive and time-consuming strain engineering. Non-rational methods allow the strain development process to be accelerated by taking advantage of evolutionary processes.

This thesis addresses the integration of adaptive laboratory evolution into cell factory development workflows through computational methods. By studying a large set of *Escherichia coli* strains evolved to tolerate 11 different chemicals of industrial relevance, it was shown that there is significant cross-tolerance between compounds of the same chemical class, and that pre-evolving strains to tolerate a product can improve production rates when the evolved strain is engineered with a production pathway. Metabolic profiling of the evolved strains using direct-injection mass spectrometry showed that strains evolved in the same conditions had converged to similar metabolic phenotypes, suggesting that metabolism is involved in chemical tolerance. It was shown that the effects of individual mutations could be predicted, both by directly comparing the metabolic profiles of evolved strains to previously measured metabolic profiles of knockout strains, as well as using deep neural networks to predict metabolite level changes directly from genetic perturbations.

Adaptive laboratory evolution can be used to optimize growth rates under various growth conditions, but through clever strain engineering it is possible to couple production to growth, thereby allowing optimization of production rate. This thesis also presents an algorithm based on genome-scale metabolic modelling that can predict genetic modifications that enable growth-coupling in combination with addition of specific supplements to the growth medium. The algorithm could predict known growth-coupled strain designs that are shown to work *in vivo* as well as novel promising strain designs, for production of itaconic acid, propionic acid and for product methylation.

Resumé

På grund af stigende globale temperaturer og begrænsede fossile ressourcer er det kritisk at finde alternative måder at producere kemikalier og brændstoffer. Dette problem kan løses ved at konstruere mikrobielle cellefabrikker der kan producere en bred vifte af produkter fra vedvarende ressourcer. Anvendelse af cellefabrikker kræver dog en vidtrækkende viden om mikrobiel biologi såvel som dyr og tidskrævende udvikling af mikrobielle stammer. Gennem brug af non-rationelle metoder kan stammeudviklingsprocessen accelereres ved at udnytte evolutionære processer.

Denne afhandling omhandler integrering af adaptiv laboratorieevolution i udvikling af cellefabrikker gennem beregningsmetoder. Ved at studere et stort antal Escherichia coli stammer der er evolutionært udviklet til at tolerere 11 forskellige industrielt relevante kemikalier, blev det vist at der er betydelig kryds-tolerans mellem stoffer der har kemiske ligheder. Derudover blev det vist at brugen af laboratorieevolution til at forbedre en stammes produkttolerans også kan øge stammens evne til at producere stoffet, når der er blevet indsat en produktionspathway. Metabolisk profilering af de evolutionært udviklede stammer ved hjælp af direct-injection massespektrometri viste at stammer udviklet under de samme betingelser havde konvergeret til lignende metaboliske profiler, hvilket tyder på at metabolisme er involveret i kemisk tolerans. Det blev yderligere vist at individuelle mutationers effekter kunne forudsiges både ved at sammenligne de målte metaboliske profiler med tidligere målte metaboliske profiler for knockout-stammer, samt ved at anvende dybe neurale netværk til at forudsige ændringer i metabolitniveauer direkte fra genetiske ændringer.

Adaptiv laboratorieevolution kan bruges til at optimere vækstrate under forskellige betingelser, men gennem snedige stammedesigns er det muligt at koble produktion til vækst, hvorved produktionsraten kan optimeres. Denne afhandling præsenterer også en algoritme baseret på metaboliske modeller i genoskala, som kan forudsige genetiske ændringer der kan forårsage vækstkobling i kombination med at specifikke supplementer tilføjes til vækstmediet. Algoritmen kunne forudsige kendte vækstkoblede stammedesigns som tidligere er valideret in vivo, og kunne også forudsige nye lovende designs til produktion at itakonsyre, propionsyre samt til produkt-methylering.

Acknowledgements

Even though the last three year have been hard, they have also been extremely rewarding. There are a number of people without whom I could not have completed this thesis, and who have made the process more enjoyable. I owe those people a lot of gratitude.

First, I would like to thank Markus Herrgård for giving me the opportunity to do a PhD at the Center for Biosustainability, and who has helped me with lots of guidance, advice and feedback along the way. I would also like to thank Nikolaus Sonnenschein who has co-supervised my work and helped with good ideas and critical questions. Furthermore, I would like to thank Joaõ Cardoso, who as my master thesis supervisor introduced me to the world of metabolic modelling and computational strain design. I also want to thank Anne Sofie Lærke Hansen for directing my attention towards the Center for Biosustainability in the first place, and for many fun and inspiring conversations ever since.

During my PhD I have been lucky to supervise several talented master students: I am grateful to Anders Ellegaard, Christina Bligaard Pedersen and Valentijn Broeken for their excellent work and for many interesting discussions along the way.

Several of the projects described in this thesis have been done in collaboration with other researchers whom I thank for their respective contributions. During my stay at ETH Zürich I received lots of valuable help and support from Mattia Zampieri, for which I am also very grateful.

Additionally, I am thankful to a large group of people who have made the past three years a lot more fun: Kristian for the many evenings we spent on crazy engineering projects; Christian, Christian, Niko, Christoffer and Carsten for all the fun hours playing music in the bunker; Phillpp and Karin for being great office mates at ETHZ; Biotek-10 for making every Wednesday something to look forward to; a long list of colleagues including (in no particular order) Ida, Ruben, Kira, Pasquale, Svetlana, Alexandra, Maja, Alicia and Michael for lots of fun at various parties, balls, and bar crawls; and all past and present members of the SIMS group for the fantastic work environment.

Finally, I want to thank my parents and Mikkel, Sif and Agnes for many enjoyable times during holidays and weekends, as well as Eya for your company and all your support, which means the world to me.

List of publications

Publications included in this thesis

Lennen, R., Jensen, K., Mohammed, E., Malla, S., Börner, R., Özdemir, E., Bonde, I., Koza, A., Pedersen, L., Schöning, L., Sonnenschein, N., Palsson, B., Sommer, M., Feist, A., Nielsen, A., Herrgård, M. (in preparation). Parallel laboratory evolutions reveal general chemical tolerance mechanisms and enhance chemical production. **(Chapter 1)**

Jensen, K., Gudmundsson, S., & Herrgård, M. (2018). Enhancing Metabolic Models with Genome-Scale Experimental Data. Systems Biology, 337–350. **(Chapter 4)**

Jensen, K., Broeken, V.F., Hansen, A.S.L., Sonnenschein, N., Herrgård, M. (submitted). OptCouple: Joint simulation of gene knockouts, insertions and medium modifications for prediction of growth-coupled strain designs. **(Chapter 5)**

Contributions to the following publications were made during the work of this thesis, but are not included in the thesis

Jensen, K., Cardoso, J., & Sonnenschein, N. (2016). Optlang: An algebraic modeling language for mathematical optimization. Journal of Open Source Software.

Cardoso, J.G.R., Jensen, K., Lieven, C., Hansen, A.S.L., Galkina, S., Beber, M., Özdemir, E., Herrgård, M.J., Redestig, H., Sonnenschein, N. (2018). Cameo: A Python Library for Computer Aided Metabolic Engineering and Optimization of Cell Factories. ACS Synthetic Biology, 7(4), 1163-1166.

Cardoso, J. G. R., Zeidan, A. A., Jensen, K., Sonnenschein, N., Neves, A. R., & Herrgård, M. J. (2018). MARSI: metabolite analogues for rational strain improvement. Bioinformatics, 34(13), 2319-2321.

Rugbjerg, P., Genee, H. J., Jensen, K., Sarup-Lytzen, K., & Sommer, M. O. A. (2016). Molecular Buffers Permit Sensitivity Tuning and Inversion of Riboswitch Signals. A C S Synthetic Biology, 5(7), 632-638.

List of abbreviations

12PD: 1,2-propanediol

23BD: 2,3-butanediol

ADIP: Adipate

AKG: Alpha-ketoglutarate

ALE: Adaptive laboratory evolution

BUT: Butanol

COUM: p-Coumarate

FC: Fold-change

FBA: Flux balance analysis

GIMME: Gene Inactivity Moderated by Metabolism and Expression

GLUT: Glutarate

HEXA: Hexanoate

HPLC: High-performance liquid chromatography

HMDA: Hexamethylenediamine

IBUA: Isobutyrate

MCMC: Markov-chain monte carlo

MCS: Minimal cut sets

MFA: Metabolic flux analysis

MILP: Mixed integer linear programming

MLP: Multilayer perceptron

OCTA: Octanoate

PEP: Phosphoenolpyruvate

PUTR: Putrescine

RBA: Resource balance analysis

RI: Refractive index

SAH: S-adenosylhomocysteine

SAM: S-adenosylmethionine

t-SNE: t-distributed Stochastic Neighbour Embedding

Table of contents

Thesis outline

A major challenge of modern society is the need to find sustainable methods for upholding our current way of living. This necessitates the development of renewable alternatives to oil-derived fuels and chemicals. Using microbial cell factories to produce useful and valuable chemicals from sustainable resources is a promising solution to this problem. However, developing successful cell factories by employing metabolic engineering is a slow and difficult process that is impeded by our limited understanding of microbial metabolism.

This thesis addresses the use of so-called non-rational engineering – specifically adaptive laboratory evolution (ALE) – which leverages evolutionary processes to quickly optimize cell factories without requiring comprehensive knowledge about the functioning of the cell. The thesis, which will focus on computational methods that can be used in combination with ALE, is divided into two parts: Part I (Chapter 1-3) focuses on methods that can help understand the evolved strains resulting from ALE, while Part II (Chapters 4-5) focuses on the use of mathematical models to design selection conditions that can be used to optimize production characteristics.

Chapter 1 contains a manuscript for a research article describing study where *Escherichia coli* was evolved to tolerate high concentrations of various potential products. Through genome sequencing and growth characterization we found that overall chemical tolerance obtained in the different evolution conditions varied widely, and that only very few mutations were universally observed across strains from a given condition. Furthermore, we find that evolving strains to tolerate a compound can also have beneficial effects on the strains' ability to produce the compound. This work was done in collaboration with other researchers at the Center for Biosustainability, and mainly the data analysis parts, i.e. analysis of genome sequences and growth profiles, were done as part of this thesis.

Chapter 2 describes a follow-up study to Chapter 1, where all the evolved tolerant strains were subjected to metabolomics analysis in order to study how the evolution of tolerance affects metabolism. It is found that strains evolved under the same condition tend to be very similar metabolically, such that all the tested conditions have a specific characteristic metabolic phenotype. This suggests that strains evolved on the same condition reach the same phenotype despite

considerable differences in genotype. Furthermore, the metabolic profiles of the evolved strains were combined with previously published metabolomics data and used to predict how each observed mutation impacts the function of the gene(s) it affects. Finally, a time-series perturbation analysis was used to investigate how different toxic environments affect metabolism.

Chapter 3 describes a machine learning method for predicting how genetic perturbations affect metabolite levels. The method is based on a deep neural network and the main novelty is using biological networks through which signals in the input data are propagated. The motivation for developing such a method was to take advantage of prior knowledge encoded in networks for various prediction tasks using graph-structured input and output data. While the obtained predictive performance limits the practical use of the method, it represents a proof-of-concept of the technical feasibility of propagating input signals through a graph in a way that is inferred from the data.

Chapter 4 contains a published book chapter about metabolic modeling and methods for integration of genome-scale experimental data. The chapter is a review of existing literature and serves as an introduction to the field of metabolic modeling.

Chapter 5 contains a manuscript for a research article presenting OptCouple, a new modeling algorithm for identifying strain designs where production is coupled to growth, such that ALE can be used to optimize production. The main novelty of the algorithm is the possibility of simultaneously finding knockouts, gene insertions and additions to the growth medium, which in combination cause production to be growth-coupled. The algorithm is validated by showing that it can predict existing growth-coupled strain designs, that are shown to work *in vivo*, as well as new strain designs that are predicted to be growth-coupled *in silico*.

Both Part I and Part II begin with a short overview that introduces key concepts and frames the chapters in a larger context. While Chapters 2 and 3 are not manuscripts in preparation, they are both structured as research articles and will be adapted and submitted for publication in scientific journals in the future.

Part I: Metabolic engineering and evolutionary methods

The use of microbes in the production of various commodities is an old practice that has been around for many centuries across most known cultures. The two major examples of this – bread and beverages – are both based on the growth of yeast in a sugary substrate taking advantage of microbe's natural production of carbon dioxide and ethanol. In more recent times the use of microorganisms to produce chemicals has become increasingly deliberate and directed. Early examples of microbial chemical production include using filamentous fungi to produce organic acids, e.g. citric acid (Max et al., 2010), and using the bacterium *Clostridium acetobutylicum* to produce acetone and butanol (Weizmann and Rosenfeld, 1937). Culturing microbes solely for the purpose of production, in contrast to as part of food production, allows employing various process optimizations to maximize production outcomes specifically. Through such process optimization techniques, the efficiency of industrial applications of microbial production has steadily increased. While manufacturers up until the late 20th century have had to rely on optimizations regarding the physicochemical parameters of the processes, the possibility of modifying the production strain allowed further improvements to be made. This was first done through a process of random mutagenesis and subsequent screening (Rowlands, 1884), while the later availability of genetic engineering techniques opened new venues to the targeted creation of mutant strains with modified characteristics, including production capabilities (Nielsen, 2001). An example of targeted engineering of a production strain is the insertion of genes from other organisms, introducing a new metabolic pathway in the production strain. This can be beneficial as many natural producers of a target compound may be hard to culture in a production process. Transferring the pathway to another organism can thus improve production. An example of this was the production of cephalosporin antibiotics, which are naturally produced by fungal *Acremonium* species, in the common laboratory organism *Penicillium chrysogenum* (Cantwell et al., 1992). Another type of modifications frequently made during strain engineering is the deletion of native genes to improve production, e.g. by reducing formation of byproducts. An example of this was a reduction in oxalic acid formation during expression of heterologous proteins in the fungus *Aspergillus niger*, by deleting a gene encoding an oxaloacetate hydrolase (Pedersen et al., 2000).

The practice of genetically modifying microbial organisms to obtain good production strains is known as metabolic engineering and has become increasingly widespread since the 1990's (Bailey, 1991; Nielsen, 2017). Even though examples of successful metabolic engineering abound, it is by no means an easy process, owing to the overwhelming complexity of microbial biology. Most efforts to engineer useful production strains follow an iterative process, commonly called the Design-Build-Test-Learn cycle (Nielsen and Keasling, 2016), shown in Figure 1. In the design step, the metabolic engineer plans a set of genetic modifications, which are expected to improve production characteristics. These modifications are introduced into the organism in the build step, whereby a new strain is made. The resulting strain is subjected to testing to evaluate how production characteristics have been affected by the modifications. In the learn step, the results from the tests are evaluated in order to gain insight into the functioning of the production process, which leads to new hypotheses about the production organisms that can be used to generate new designs. This process is known as rational engineering, as each strain is designed based on the best current understanding of the process.

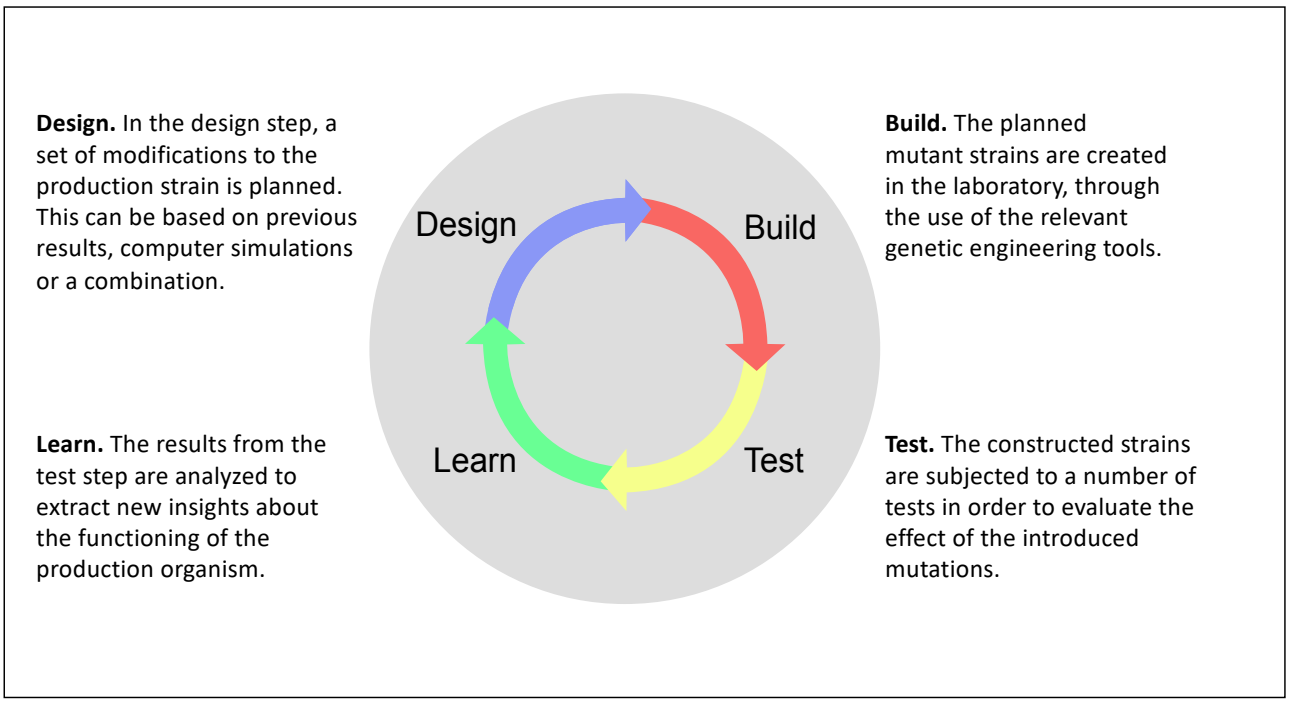

Figure 1: The Design-Build-Test-Learn cycle.

Each of the steps in the cycle requires a significant amount of work, but in the last decade a disparity between the steps has emerged. New advances in genetic engineering technology has allowed

genetic modifications to be performed faster than ever (Schmidt and Platt, 2017), and even the synthesis of completely novel DNA sequences can now be done routinely (Chao et al., 2015). Additionally, many assays in the testing step can be done with a very high throughput, due to the increasing availability of laboratory automation systems (Nielsen and Keasling, 2016). This leaves a significant bottleneck in the design and learn steps. In other words, the main challenges in metabolic engineering are currently more concerned with deciding what do to than with actually doing it.

Several approaches to evening out this disparity have been developed. One approach is to simply take advantage of the increased testing throughput to collect more extensive systems data on the production strains. This allows more comprehensive characterization of the developed strains, such that subsequent strain design can focus on addressing the specific problems that are identified (Lee and Kim, 2015). An example is to use transcriptomics analyses to identify problematic regulatory effects of overproducing the target compound, e.g. causing inhibition in the production pathway or precursor supply (Shimizu, 2011). Overproducing a target compound can also lead to broad physiological problems in the cell such as cofactor imbalances or energy deficits, which can also be identified through detailed strain analysis and subsequently addressed by targeted modifications (Liu et al., 2018).

Another approach for overcoming the bottleneck in the learn and design steps is to also take advantage of the high throughput in the build step, to create and screen a large number of strains thereby increasing the chance that one of them has improved production properties. The effectiveness of this depends on the throughput of the screening assay being used. This approach represents a deviation from the Design-Build-Test-Learn cycle towards what could be called non-rational engineering, where decisions are not made based on a theoretical understanding, but on the achieved screening results alone (Shepelin et al., 2018). Non-rational engineering is an alternative to the Design-Build-Test-Learn cycle and the process is illustrated in Figure 2A, where the design and build steps are replaced by generation of variation while the test and learn steps are replaced by selection. The higher the screening throughput, the more of a compromise can be accepted with regard to the rational design and learn steps, as even random generation of modifications can lead to better strains if enough candidates are screened. Very high throughputs can be achieved if the desired phenotype can be selected for under certain growth conditions. This

allows rapid identification of the best performing mutants among millions of variants. The non-rational engineering process can either utilize artificially created genetic variation in specific regions, e.g. through error-prone PCR, resulting in a method known as directed evolution (Vick and Schmidt-Dannert, 2011), or, if the desired phenotype can be selected for, it can rely on the naturally occurring mutations in a continuously grown culture, giving rise to an iterative selection process known as adaptive laboratory evolution (ALE) (Portnoy et al., 2011). Directed evolution is useful if the metabolic engineer has a good idea of which genes or DNA regions should be mutated to improve the desired strain characteristic, as a large and diverse library of variants can be generated quickly. It has for example been used to modify heterologous pathway enzymes taken from thermophilic organisms to function better in *Escherichia coli* (Atsumi and Liao, 2008; Wang et al., 2000). ALE takes advantage of natural selection by continuously passaging a culture to fresh media, whereby mutants with increased growth rates will outcompete the other cells and become enriched in the culture (Winkler et al., 2013). The ALE process can be used to optimize microbial strains on a systems level, without any prior hypotheses about which genes should be targeted to increase growth and is very similar to natural evolution. After application of ALE, the final culture, or isolates from it, is subjected to sequencing to learn which mutations have arisen and might be responsible for the improved growth rate (Figure 2B).

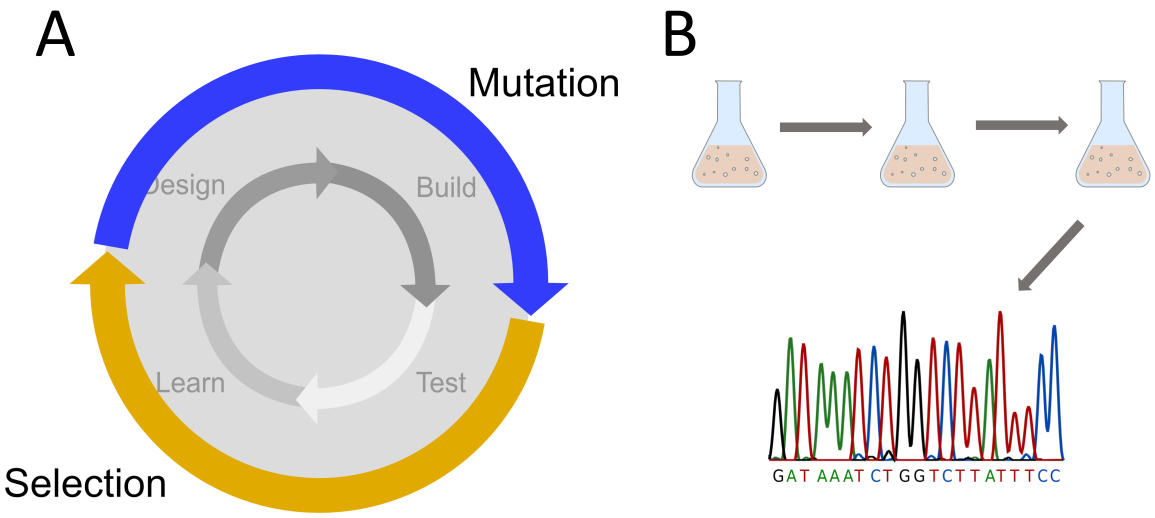

Figure 2: A) Illustration of how ALE can replace manual iterations through the Design-Build-Test-Learn cycle. B) The process of ALE through serial passaging of cultures. After a desired increase in fitness has been observed, isolates from the ALE experiment may be sequenced to investigate which mutations are responsible for the improvements.

Some traits of production strain performance are inherently related to growth and can thus be easily optimized with ALE. An example of this is substrate utilization. Growing cells on a sub-optimal substrate allows them to gradually adapt to the new condition, as there is a constant selection pressure for the cells that grow fastest on the new substrate (Apel et al., 2016). Evolution for substrate utilization can be a very useful part of strain engineering, as economic considerations can constrain the use of usual laboratory substrates in the production process (Hansen et al., 2017). Another growth-related trait that is easy to evolve is tolerance to toxic environments (Mohamed et al., 2017). This can also be easily achieved by growing cells in the toxic environment, whereby the most tolerant mutant strains will continuously be selected. In strain engineering this can be useful for overcoming product toxicity, which is the phenomenon where the production strain is inhibited by the compound it is producing. Product toxicity limits the attainable titers in the production process and thus the economic feasibility (Hansen et al., 2017). Additionally, during production processes the production strains are often grown under stressful conditions, e.g. due to suboptimal aeration and mixing and the use of complex feedstocks that may contain inhibitors or toxic residue from pretreatment. Chapter 1 describes these issues in more detail as well as an application of ALE to study the evolution of tolerance and the effect this has on the production characteristics of the strains.

Arguably the most important characteristic of a production strain, at least for high-value products, is the production rate of the compound of interest. The production rate is not inherently related to growth, rather there is in general a tradeoff between biomass production and product formation. This tradeoff is a consequence of mass balance as both are sinks for limited cellular resources, the most important of which being carbon. Some compounds, however, are obligate by-products of growth, which means that the cell cannot grow without producing them. Such compounds are said to be growth-coupled and include for example ethanol and lactate under anaerobic growth of *Saccharomyces cerevisiae* and *E. coli* respectively (Clark, 1989; Deken, 1966). In addition to compounds that are naturally growth-coupled it is possible, through clever strain engineering, to construct mutant strains where the compound of interest is coupled to growth (von Kamp and Klamt, 2017). If a compound is growth-coupled it is possible to use ALE to indirectly optimize the production rate through selection of faster growing strains. Making production of a target compound growth-coupled often requires introduction of genetic modifications that are not

intuitively obvious. It can therefore be beneficial to use model-based computational methods in the strain design process in order to engineer specific desired phenotypes, such as growth-coupling (Feist et al., 2010). Computational strain design and methods for constructing growth-coupled strains will be addressed in Part II of this thesis.

After performing ALE and obtaining one or more mutant strains with improved characteristics, it is most often of interest to sequence the genome of the strains. The mutants might have accumulated random mutations that can have a detrimental effect on overall strain performance and must be reverted before the strain is used for production. Alternatively, a core set of mutations responsible for improved growth, can be identified and reintroduced into the background strain (Shepelin et al., 2018). Additionally, sequencing the mutants can allow investigation of the mechanisms through which growth was improved (Sandberg et al., 2014). This can be useful for gaining an understanding of the strain's characteristics and might allow for more direct rational strain engineering in the future. Unfortunately, it is rarely obvious why the mutations that arise in the evolved strains confer improvements in the phenotype. This challenge raises the need for a variety of experimental and computational methods for interpreting the sequencing results of strains evolved using ALE (Shepelin et al., 2018). Furthermore, the evolved strains can be probed in other ways to explore how their physiology has been altered through the ALE process. This can include growth characterization in various conditions or systems analyses such as transcriptomics or metabolomics. In combination with the genomic information gained from sequencing this can give a deeper understanding of the process through which the evolved strain improved. An example of how metabolomics can be used to elucidate details about evolved strains and the evolution process is described in Chapter 2, using the strains constructed in the study described in Chapter 1. Chapter 3 describes a novel machine learning method for relating genetic mutations to changes in metabolism in a systematic way. Such a method can potentially help understand the effects of mutations observed in ALE experiments, as well as integrate other systems-level data obtained from evolved strains.

References

Apel, A.R., Ouellet, M., Szmidt-middleton, H., Keasling, J.D., 2016. Evolved hexose transporter enhances xylose uptake and glucose / xylose co-utilization in Saccharomyces cerevisiae. Nat.

Publ. Gr. 1–10. https://doi.org/10.1038/srep19512

Atsumi, S., Liao, J.C., 2008. Directed evolution of Methanococcus jannaschii citramalate synthase for biosynthesis of 1-propanol and 1-butanol by Escherichia coli. Appl. Environ. Microbiol. 74, 7802–7808. https://doi.org/10.1128/AEM.02046-08

Bailey, J.E., 1991. Toward a science of metabolic engineering. Science (80-.). 252, 1668–1675.

Cantwell, C., Beckmann, R., Whiteman, P., Queener, S.W., Abraham, E.P., 1992. Isolation of deacetoxycephalosporin C from fermentation broths of Penicillium chrysogenum transformants: Construction of a new fungal biosynthetic pathway. Proc. R. Soc. B Biol. Sci. 248, 283–289. https://doi.org/10.1098/rspb.1992.0073

Chao, R., Yuan, Y., Zhao, H., 2015. Building biological foundries for next-generation synthetic biology. Sci. China Life Sci. 58, 658–665. https://doi.org/10.1007/s11427-015-4866-8

Clark, D.P., 1989. The fermentation pathways of Escherichia coli. FEMS Microbiol. Rev. 63, 223–234.

Deken, R.H., 1966. The Crabtree Effect: A Regulatory System in Yeast. J. Gen. Microbiol. 149–156.

Feist, A.M., Zielinski, D.C., Orth, J.D., Schellenberger, J., Herrgard, M.J., Palsson, B.O., 2010. Model-driven evaluation of the production potential for growth-coupled products of Escherichia coli. Metab. Eng. 12, 173–186. https://doi.org/10.1016/j.ymben.2009.10.003

Hansen, A.S.L., Lennen, R.M., Sonnenschein, N., Herrgård, M.J., 2017. Systems biology solutions for biochemical production challenges. Curr. Opin. Biotechnol. 45, 85–91. https://doi.org/10.1016/j.copbio.2016.11.018

Lee, S.Y., Kim, H.U., 2015. Systems strategies for developing industrial microbial strains. Nat. Biotechnol. 33, 1061–1072. https://doi.org/10.1038/nbt.3365

Liu, J., Li, H., Zhao, G., Caiyin, Q., Qiao, J., 2018. Redox cofactor engineering in industrial microorganisms: strategies, recent applications and future directions. J. Ind. Microbiol. Biotechnol. 45, 313–327. https://doi.org/10.1007/s10295-018-2031-7

Max, B., Salgado, J.M., Rodríguez, N., Cortés, S., Converti, A., Domínguez, J.M., 2010. Biotechnological production of citric acid. Brazilian J. Microbiol. 41, 862–875. https://doi.org/10.1590/S1517-83822010000400005

Mohamed, E.T., Wang, S., Lennen, R.M., Herrgård, M.J., Simmons, B.A., Singer, S.W., Feist, A.M., 2017. Generation of a platform strain for ionic liquid tolerance using adaptive laboratory evolution. Microb. Cell Fact. 16, 1–15. https://doi.org/10.1186/s12934-017-0819-1

Nielsen, J., 2017. Systems Biology of Metabolism. Annu. Rev. Biochem. 86, 245–275. https://doi.org/10.1146/annurev-biochem-061516-044757

Nielsen, J., 2001. Metabolic engineering. Appl. Microbiol. Biotechnol. 55, 263–283. https://doi.org/10.1007/s002530000511

Nielsen, J., Keasling, J.D., 2016. Engineering Cellular Metabolism. Cell 164, 1185–1197. https://doi.org/10.1016/j.cell.2016.02.004

Pedersen, H., Christensen, B., Hjort, C., Nielsen, J., 2000. Construction and characterization of an oxalic acid nonproducing strain of Aspergillus niger. Metab. Eng. 2, 34–41. https://doi.org/10.1006/mben.1999.0136

Portnoy, V.A., Bezdan, D., Zengler, K., 2011. Adaptive laboratory evolution-harnessing the power of biology for metabolic engineering. Curr. Opin. Biotechnol. 22, 590–594. https://doi.org/10.1016/j.copbio.2011.03.007

Rowlands, R.T., 1884. Industrial strain improvement: mutagenesis and random screening procedures. Enzym. Microb. Technol. 6, 3–10.

Sandberg, T.E., Pedersen, M., Lacroix, R.A., Ebrahim, A., Bonde, M., Herrgard, M.J., Palsson, B.O., Sommer, M., Feist, A.M., 2014. Evolution of Escherichia coli to 42 C and Subsequent Genetic Engineering Reveals Adaptive Mechanisms and Novel Mutations. Mol. Biol. Evol. 31, 2647–2662. https://doi.org/10.1093/molbev/msu209

Schmidt, F., Platt, R.J., 2017. Applications of CRISPR-Cas for synthetic biology and genetic recording. Curr. Opin. Syst. Biol. 5, 9–15. https://doi.org/10.1016/j.coisb.2017.05.008

Shepelin, D., Hansen, A.S.L., Lennen, R., Luo, H., Herrgård, M.J., 2018. Selecting the best: Evolutionary engineering of chemical production in microbes. Genes (Basel). 9. https://doi.org/10.3390/genes9050249

Shimizu, K., 2011. Metabolic Regulation Analysis and Metabolic Engineering, Second Edition. ed, Comprehensive Biotechnology, Second Edition. Elsevier B.V. https://doi.org/10.1016/B978-0-08-088504-9.00117-3

Vick, J., Schmidt-Dannert, C., 2011. Directed Enzyme and Pathway Evolution, in: Enzyme Technologies: Metagenomics, Evolution, Biocatalysis, and Biosynthesis. John Wiley and Sons, pp. 41–75.

von Kamp, A., Klamt, S., 2017. Growth-coupled overproduction is feasible for almost all metabolites

in five major production organisms. Nat. Commun. 8, 1–10. https://doi.org/10.1038/ncomms15956

Wang, C., Oh, M., Liao, J.C., 2000. Directed Evolution of Metabolically Engineered Escherichia coli for Carotenoid Production. Biotechnol. Prog. 16, 922–926.

Weizmann, C., Rosenfeld, B., 1937. The activation of the butanol-acetone fermentation of carbohydrates by Clostridium acetobutylicum (Weizmann). Biochem. J. 31, 619–639.

Winkler, J., Reyes, L.H., Kao, K.C., 2013. Adaptive Laboratory Evolution for Strain Engineering, in: Alper, H.S. (Ed.), Systems Metabolic Engineering: Methods and Protocols. Humana Press, Totowa, NJ, pp. 211–222. https://doi.org/10.1007/978-1-62703-299-5_11

Chapter 1: Parallel laboratory evolutions reveal general chemical tolerance mechanisms and enhance chemical production

Rebecca Lennen[1]*, Kristian Jensen[1]*, Elsayed T. Mohammed[1], Sailesh Malla[1], Rosa A. Börner[1], Emre Özdemir[1], Ida Bonde[1], Anna Koza[1], Lasse E. Pedersen[1], Lars Y. Schöning[1], Nikolaus Sonnenschein[1], Bernhard Ø. Palsson[1,2], Morten A. Sommer[1], Adam Feist[1,2], Alex T. Nielsen[1]**, Markus J. Herrgård[1]**

* These authors contributed equally to the work

** Co-corresponding authors

1) The Novo Nordisk Foundation Center for Biosustainability, Technical University of Denmark, Building 220, Kemitorvet, 2800 Kgs. Lyngby, Denmark

2) Department of Bioengineering, University of California, San Diego

Abstract

Tolerance toward high concentrations of product is a major barrier to achieving economically viable processes for biobased chemical production. Product tolerance cannot currently be rationally engineered due to lack of knowledge of the cellular mechanisms of chemical toxicity and tolerance. We used an automated platform to evolve parallel populations of *Escherichia coli* to tolerate previously toxic concentrations of 11 chemicals that have applications as polymer precursors, chemical intermediates, or biofuels. Re-sequencing of isolates from 88 independently evolved populations, reconstruction of mutations, transcriptomic and proteomic analyses, and cross-compound tolerance profiling was employed to uncover general and specific tolerance mechanisms. We found that the broad tolerance of strains to chemicals varied significantly depending on the condition under which the strain was evolved in and that strains that acquired high levels of osmotolerance were also tolerant to most chemicals. Specific genetic tolerance mechanisms included alterations in regulatory, cell wall, and broad transcriptional and translational functions, as well as more chemical-specific mechanisms related to transport and metabolism. Finally, we show that pre-tolerizing the host strain can significantly enhance endogenous production of chemicals and is especially valuable when a large number of independently evolved isolates are screened.

1.1 Introduction

Despite significant advances in synthetic and systems biology tools to engineer and study metabolism, developing microbial strains for commercial-level production of chemicals still remains a challenge (Van Dien, 2013). One of the major problems relates to the stressful conditions that production strains encounter in large-scale industrial production processes where numerous stresses that are not encountered in laboratory conditions are present (Deparis et al., 2017). Some of these stresses relate to the presence of high concentrations of a carbon source or toxic compounds related to feedstock processing such as ionic liquids (Mohamed et al., 2017). Irrespective of the production system or substrate, cells will encounter high intracellular and extracellular levels of the primary product that they have been engineered to produce. Frequently, high levels of such products can have inhibitory effects on the host organism, which effectively limits the titers that can be achieved and thereby the economic feasibility of the process. This issue can be overcome by engineering a production strain that is tolerant to higher titers of the product, however rational engineering of tolerance to either native or non-native chemical products is rarely possible due to a lack of knowledge about the molecular mechanisms of tolerance. This often necessitates choosing an otherwise difficult to engineer production host that already has desirable tolerance characteristics. Alternatively, one can use non-rational approaches to obtain strains with high chemical tolerance by mutagenesis, screening of transporter and other libraries, or adaptive laboratory evolution (ALE) (Hansen et al., 2017). ALE in particular has been successfully used to obtain strains that tolerate product chemicals (Winkler and Kao, 2014). In some cases the mechanisms of chemical tolerance have been at least partially deciphered through resequencing and other omics approaches applied to evolved strains (Haft et al., 2014; Kildegaard et al., 2014; Reyes et al., 2013), but in most cases the full toxicity and tolerance mechanisms remain to be determined. While ALE applied to product tolerance has resulted in strains that increase actual production of the target chemical (Mundhada et al., 2017), in many cases these strains have not shown improved production (Atsumi et al., 2010; Kildegaard et al., 2014).

Here we take a broad approach to elucidating mechanisms of chemical tolerance across a wide spectrum of chemicals enabled by automated ALE as well as systematic genomic and phenotypic analyses of the resulting large collection of evolved strains. This approach allows us to determine

general features of chemical tolerance and build a large dataset as a reference for future tolerance studies. For two products we also investigate whether pre-evolving for tolerance can significantly improve production. A similar approach has been previously take to study adaptation to diverse stresses including some non-native chemical stresses in *E. coli* (Horinouchi et al., 2017), but in the present study we use significantly higher concentrations of chemicals to mimic industrially relevant conditions and evolve and characterize a significantly larger number of strains per condition.

1.2 Materials and Methods

1.2.1 Strains and media

E. coli K-12 MG1655 (ATCC 47076) strain was used as a starting point strain for the adaptive laboratory evolution experiments and as reference strain for all subsequent characterization. Chemicals were purchased from either Sigma-Aldrich (Merck KGaA, Darmstadt, Germany) or Fisher Scientific (Part of Thermo-Fisher Scientific). Plasmids for isobutyric acid and 2,3-butanediol production were obtained from the authors (Xu et al., 2014; Zhang et al., 2011).

M9 glucose medium supplemented with 10 g/L glucose was formulated with 1x M9 salts, 2 mM $MgSO_4$, 100 µM $CaCl_2$ and 1x trace elements. A stock solution of 10x M9 salts consisted of 68 g/L Na_2HPO_4 anhydrous, 30 g/L KH_2PO_4, 5 g/L NaCl, and 10 g/L NH_4Cl dissolved in Milli-Q filtered water and autoclaved. M9 trace elements stock concentration was a 2000x solution containing of 3.0 g/L $FeSO_4 \cdot 7H_2O$, 4.5 g/L $ZnSO_4 \cdot 7H_2O$, 0.3 g/L $CoCl_2 \cdot 6H_2O$, 0.4 g/L $Na_2MoO_4 \cdot 2H_2O$, 4.5 g/L $CaCl_2 \cdot H_2O$, 0.2 g/L $CuSO_4 \cdot 2H_2O$, 1.0 g/L H_3BO_3, 15 g/L disodium ethylene-diamine-tetra-acetate, 0.1 g/L KI, 0.7 g/L $MnCl2 \cdot 4H_2O$ in Milli-Q filtered water and sterile filtered.

1.2.2 Selection of initial chemical concentrations

The toxicity of each of the chemicals was tested by screening growth of MG1655 in different concentrations. Biological triplicates of *E. coli* MG1655 were cultivated at 37 °C with 300 RPM shaking. After 14 to 18 h, the cultures were inoculated into M9 + 0.2 % glucose and one of the chosen chemicals at different concentrations. The cultures were then incubated in a BioLector microbioreactor system (m2p-labs GmbH, Baesweiler, Germany) at 37 °C with 1,000-rpm shaking. The growth rates at different concentrations were calculated for each chemical (Supplementary

Figure 1). Initial concentrations for adaptive laboratory evolution were chosen so that MG1655 could obtain a growth rate of approximately 0.4 /h.

The initial and final evolution concentrations, as well as the screening concentrations for all the chosen chemicals are shown in Table 1.

Table 1: *Concentrations of each chemical used during ALE and for growth screening. All concentrations are g/L.*

	Initial ALE concentration	Final ALE concentration	Isolate screening concentration	Cross-tolerance screening concentration
1,2-propanediol	52	83	83	62
2,3-butanediol	49	79	69	59
Hexamethylenediamine	20	38	38	32
Putrescine	20	38	38	32
Glutarate	20	47.5	47.5	40
Adipate	25	50	50	45
Hexanoate	2	7.5	5	3
Octanoate	3.5	10	8	8
Isobutyrate	3	12.5	12.5	7.5
Coumarate	4	20	10	7.5
Butanol	5.7	16.2	11.34	11.34

1.2.3 Adaptive laboratory evolution

The starting strain K-12 MG1655 was adaptively evolved for higher concentrations of each chemical through independent parallel replicates. Bacterial cells were cultivated in M9 + glucose supplemented with the initial chemical concentration listed in Table 1, with gradual increase in each chemical concentration over the time span of the adaptation. Cells were serially passaged during exponential growth for approximately 40 days using an automated liquid-handler platform as described by LaCroix et al. (2017). Cells were cultured at 37 °C with full aeration at 1200 RPM stirring speed. Once OD_{600} reached approximately 1.0, 150 µL was passed into a new tube with 15 mL fresh media containing the respective chemical concentration. Over the course of the experiment, cells were kept in exponential growth phase in order to keep a constant selection pressure for growth rate. The OD_{600} was measured by a Sunrise Plate Reader (Tecan Inc., Switzerland). Growth rates were determined by computing the slope of log(OD) using linear regression with the Polyfit function in MATLAB (The Mathworks Inc., Natick, Massachusetts). When an increase in the apparent growth

rate was achieved (average growth rate for all of the parallel replicates) at a particular concentration, the chemical concentration was increased by 10-15%. This process was repeated in cycles until a significant increase in tolerated concentration was achieved. In incidents where the increase in the chemical concentration caused cells to crash, i.e. cell death, chemical concentration was reduced to a level that allowed cell growth. Periodically, samples were frozen in 25% v/v glycerol and stored at -80 °C for further use.

1.2.4 Growth screening of ALE isolates

1.2.4.1 Primary tolerance screening

Populations from evolution endpoints were plated on LB agar plates and 10 individual colonies from each population were screen for growth at the maximum concentration for which robust growth rates were achieved during the evolution. Cultures of wild-type strain, *E. coli* K-12 MG1655, were used as controls. The isolates were inoculated in 500 µL M9 + glucose in deep-well plates and incubated in plate shaker at 37 °C and 300 RPM. The next day, cells were diluted 10X in M9 + glucose and 30 µL was transferred to clear-bottom 96 half-deep plates containing M9 + glucose supplemented with the corresponding toxic chemical at concentrations as in Table 1 (isolate screening concentration). The plates were incubated at 37 °C with 225 RPM shaking in a Growth Profiler screening platform (EnzyScreen BV, Heemstede, Netherlands). The resulting growth curves for all isolates were inspected qualitatively for isolates exhibiting robust growth as assessed by lag time, final OD and growth rate. Each of the 10 isolates from the primary screening was grouped according to close similarities based on the above criteria. For each population, isolates representative of each group were picked (2-3 isolates per population).

1.2.4.1 Cross-tolerance screening

The *E. coli* strains were inoculated into 300 µl of M9 + glucose medium in 96 deep well plates (in biological triplicates) and the cultures were incubated at 37°C and 300 RPM for overnight. Next day, 30 µl of a 10-fold was added to 270 µl of M9 + glucose supplemented with chemicals in 96 well plate and the plates incubated in growth profiler (EnzyScreen BV, Heemstede, The Netherlands) at 37 °C and 225 RPM. The chemical concentrations are shown in Table 1 (Cross-tolerance screening concentration).

1.2.5 Genome editing of *E.coli*

Strains containing the relevant single gene deletions were obtained from the Keio Collection and were transduced into the MG1655 background strain using the protocol described in (Lennen et al., 2011). Multiple gene deletions were constructed using the protocol described in (Lennen et al., 2011). Site directed changes in the *E. coli* genome of evolved strains were done using the protocol described in (Lennen et al., 2015).

1.2.6 Quantification of 2,3-butanediol production

The *hsdR* gene was deleted from each of the strains evolved on 2,3-butanediol. The strains were then transformed with pET-RABC plasmid (Xu et al., 2014) and precultured in 300 µl of M9 + glucose supplemented with 5 g/L yeast extract and kanamycin (50 µg/mL) in 96 deep well plate and incubated at 37 °C with 300 RPM overnight (incubated for 20 h) in quadruplicates. *E. coli* MG1655 Δ*hsdR*/pET-RABC was used as a control. The following day, 20 µL of pre-inoculum was transferred into 2 mL of ALE-M9-YE-Km media in 24 deep well plates and incubated at 30 °C and 300 RPM. At 24 h and 48 h, optical densities of the culture broths were determined at 600 nm (OD_{600nm}). Then, 400 µL of the cultures were harvested, centrifuged at 4000 RPM for 10 min and 30 µL of the collected supernatants were injected into high performance liquid chromatography (HPLC). Subsequently, the samples were subjected to electrospray ionization mass analysis.

The amounts of 2,3-butanediol in the supernatants were quantified by HPLC (Ultimate 3000, Thermo Scientific, USA) equipped with an organic acid analysis column, Aminex® HPX-87H ion exclusion column (300 mm x 7.8 mm, Bio-Rad Laboratories, Denmark) connected to a refractive Index (RI) detector and a UV detector (205 nm, 210 nm, 254 nm and 280 nm). An isocratic elution with flow rate of 0.5 mL/min of 5 mM sulphuric acid was used for 30 min. Under these conditions, stereoisomers of 2,3-butanediol were detected under the RI detector channel at the retention times of 17.4 min and 18.3 min. Using the peak areas of the stereoisomers, total amount of 2,3-butanediol was calculated. For absolute quantification a calibration curve was drawn using 1, 5, 10, 12.5, 15 and 25 g/L concentrations ($y = 6.5119x + 0.5464$, $R^2 = 0.9999$).

The exact mass of the compounds was analyzed by using Oribtrap Fusion (Thermo Scientific, USA) with a Dionex 3000 RX HPLC system (Thermo Scientific, USA) in the positive and negative ion mode.

1.2.7 Quantification of isobutyrate production

The *yqhD* gene was deleted from each of the strains evolved on isobutyrate. The strains were then transformed with pIBA1 and pIBA7 plasmids (Zhang et al., 2011) and precultured into 300 µl of LB media supplemented with kanamycin (50 µg/mL) and ampicillin (100 µg/mL) in 96 deep well plate and incubated at 37 ºC with 300 RPM overnight (incubated for 18 h) (in quadruplicates). *E. coli* MG1655 Δ*yqhD*/pIBA1/pIBA7 was used as a control. The following day, 24 µL of pre-inoculum was transferred into 2.4 mL of half-FIT media (1:1 FIT media: MOPS of 200 mM) media supplemented with antibiotics. Then the culture plates were incubated at 30 °C and 300 RPM. After 6 hours of incubation, OD_{600} was measured and the cultures were induced with 100 µM of IPTG and continued the incubation at 30 °C and 300 RPM. At 24 h, 48 and 72 h, OD_{600} was measured again. Then, 300 µl of the cultures were harvested, centrifuged at 4000 RPM for 10 min and 30 µL of the collected supernatants were injected into HPLC. Subsequently, the samples were subjected to electrospray ionization mass analysis.

The amounts of isobutyrate in the supernatants were quantified by HPLC (Ultimate 3000, Thermo Scientific, USA) equipped with an organic acid analysis column, Aminex® HPX-87H ion exclusion column (300 mm x 7.8 mm, Bio-Rad Laboratories, Denmark) connected to a refractive Index (RI) detector and a UV detector (205 nm, 210 nm, 254 nm and 280 nm). An isocratic elution with flow rate of 0.5 mL min^{-1} of 5 mM sulphuric acid was used for 30 min. Under these conditions, isobutyrate was detected under the 210 nm UV channel at a retention time of 20.3 min. Using the peak area, total amount of isobutyrate was calculated. For absolute quantification a calibration curve was drawn using 0.5, 1, 2.5, 4, 5, 7.5 10, and 12.5 g/L concentrations ($y = 35.487x - 2.3142$, $R^2 = 0.9993$).

1.2.8 Resequencing

Genomic libraries were generated using the TruSeq® Nano DNA LT Library Prep Kit (Illumina Inc., San Diego CA). Briefly, 100 ng of genomic DNA diluted in 52.5 µL TE buffer was fragmented in Covaris Crimp Cap microtubes on a Covaris E220 ultrasonicator (Woburn, MA) with 5% duty factor, 175 W peak incident power, 200 cycles/burst, and 50-s duration under frequency sweeping mode at 5.5 to 6°C (Illumina recommendations for a 350-bp average fragment size). The ends of fragmented DNA were repaired by T4 DNA polymerase, Klenow DNA polymerase, and T4 polynucleotide kinase. The Klenow exo minus enzyme was then used to add an 'A' base to the 3' end of the DNA fragments.

The adapters were ligated to the ends of the DNA fragments, and the DNA fragments ranging from 300 - 400 bp were recovered by beads purification. Finally, the adapter-modified DNA fragments were enriched by 3 cycle PCR. Final concentration of each library was measured by Qubit® 2.0 Fluorimeter and Qubit DNA Broad range assay (Life Technologies). Average dsDNA library size was determined using the Agilent DNA 7500 kit on an Agilent 2100 Bioanalyzer. Libraries were normalized and pooled in 10 mM Tris-Cl, pH 8.0, plus 0.05% Tween 20 to the final concentration of 10 nM. Denaturated in 0.2N NaOH, 10 pm pool of 20 libraries in 600 µL ice-cold HT1 buffer was loaded onto the flow cell provided in the MiSeq Reagent kit v2 (300 cycles) (Illumina Inc., San Diego CA) 300 cycles and sequenced on a MiSeq (Illumina Inc., San Diego CA) platform with a paired-end protocol and read lengths of 151 nt.

1.2.9 Resequencing data analysis

The Illumina sequencing reads were analyzed with the Breseq pipeline (Deatherage and Barrick, 2014) through the ALEdb platform (Phaneuf et al., 2018) to generate lists of mutations for each evolved strain. The reference strain for this analysis was *E. coli* K-12 MG1655 with the Genbank accession number NC_000913.3.

1.2.9.1 Mapping mutations to genes

Each mutation was mapped to one or more genes. Intragenic mutations were mapped to any gene(s) whose coding sequence overlapped with the mutation. Intergenic mutations were mapped to the closest gene downstream from the mutation.

1.2.10 Growth data analysis

The growth curves generated by the instruments were processed using the *croissance* python package (http://github.com/biosustain/croissance), which performs automated growth phase identification and growth parameter fitting. Biomass concentration was quantified by OD_{600} values. For each extracted growth rate, a normalized growth rate was calculated by subtracting the mean growth rate of the wild-type strain, MG1655, on the same plate and in the same medium. This was done to remove the effects of any between-plate and between-experiment growth variations.

The *croissance* algorithm consists of two separate steps:

Step 1: The growth curve is smoothed and analyzed to find regions of exponential growth. This is done by identifying time intervals where the first- and second-order time derivatives of the smoothed biomass function are strictly positive.

Step 2: Each growth phase identified in step 1 is fitted with an exponential function of the form

$$x(t) = a \cdot e^{\mu \cdot t} + b \quad (1)$$

where μ (growth rate) is of particular interest in this study. The offset parameter *b* is included to enable analysis of growth curves that are not background-subtracted.

Post-processing was done to filter the returned growth rates. This served both to exclude growth rates from growth phases that were not thought to be real, and to select between several growth phases in the same growth curve. Growth rates higher than 1.5 h^{-1} were excluded, as were growth phases where the absolute value of the fitted offset parameter *b* was larger than a certain threshold, *c* (0.5 for growth profiler curves, 4 for Biolector curves). Growth phases where the initial biomass concentration deviated more than *c* from the fitted offset *b* were also excluded, as these were likely to be secondary growth phases. Furthermore, growth curves starting after a certain time point were also excluded. This was done to prevent growth from contaminations from being used. The chosen time cutoff was dependent on the growth conditions (30-40 hours). Very short growth phases were also excluded as they were most likely artifacts. For standard M9 glucose cultures growth phases shorter than 2 hours were excluded, while the cutoff was 5 hours for cultures in the stress conditions.

1.3 Results

We selected 11 chemical compounds representing a diversity of chemical categories with variable initial levels of toxicity to *E. coli* (Figure 1a). We chose the chemicals to 1) include compounds that have potential as a bio-based product, 2) have examples of multiple chemical compound classes (diols, diamines, diacids, fatty acids, aromatic compounds), 3) include in four cases two examples of the same compound class, and 4) to have compounds that had the right solubility and volatility profile to allow ALE and downstream characterization. We included two compounds (octanoate and n-butanol) that have previously been used in ALE studies in *E. coli* (Reyes et al., 2013; Royce et al.,

2015). For the majority of the compounds there have been efforts to engineer improved production in *E. coli*. All but one of the compounds (putrescine) are compounds that do not occur naturally in *E. coli* metabolism. The initial concentrations of the compounds were chosen so that the wild type strain would grow at a growth rate of approximately 0.4 h^{-1}.

We used an automated serial passaging platform to independently evolve a total of 88 populations of *E. coli* MG1655 in M9 glucose base media to tolerate previously toxic levels of the 11 target chemicals. For each chemical, 8 independent populations were evolved. The growth medium was kept at neutral pH to ensure an evolutionary pressure for tolerating the specific chemical compounds rather than tolerance towards low or high pH. During the laboratory evolution process, we increased the chemical concentrations from the initial concentration in a stepwise manner over approximately 800 generations. The starting and end concentrations that allowed population growth are listed in Table 1 and shown in Figure 1b. From each endpoint population, we isolated 10 strains that were subjected to growth screening, to test their ability to tolerate the chemical they had been evolved in the presence of. Among these isolates, 2-3 isolates per population were selected for further characterization, representing as diverse growth characteristics as possible. This resulted in a total of 224 strains that showed robust tolerance to the chemical that they were evolved in the presence of. All 224 strains were subjected to whole genome resequencing and cross-compound tolerance screening. A subset of the mutations were reconstructed in clean background strains to confirm their causative role in tolerance. Finally, in the cases of isobutyrate and 2,3-butanediol we engineered production pathways into all genetically distinct isolates in order to determine if evolved product-tolerant strains actually show increased production when the product is made endogenously. The overall workflow of the study is shown in Figure 1c.

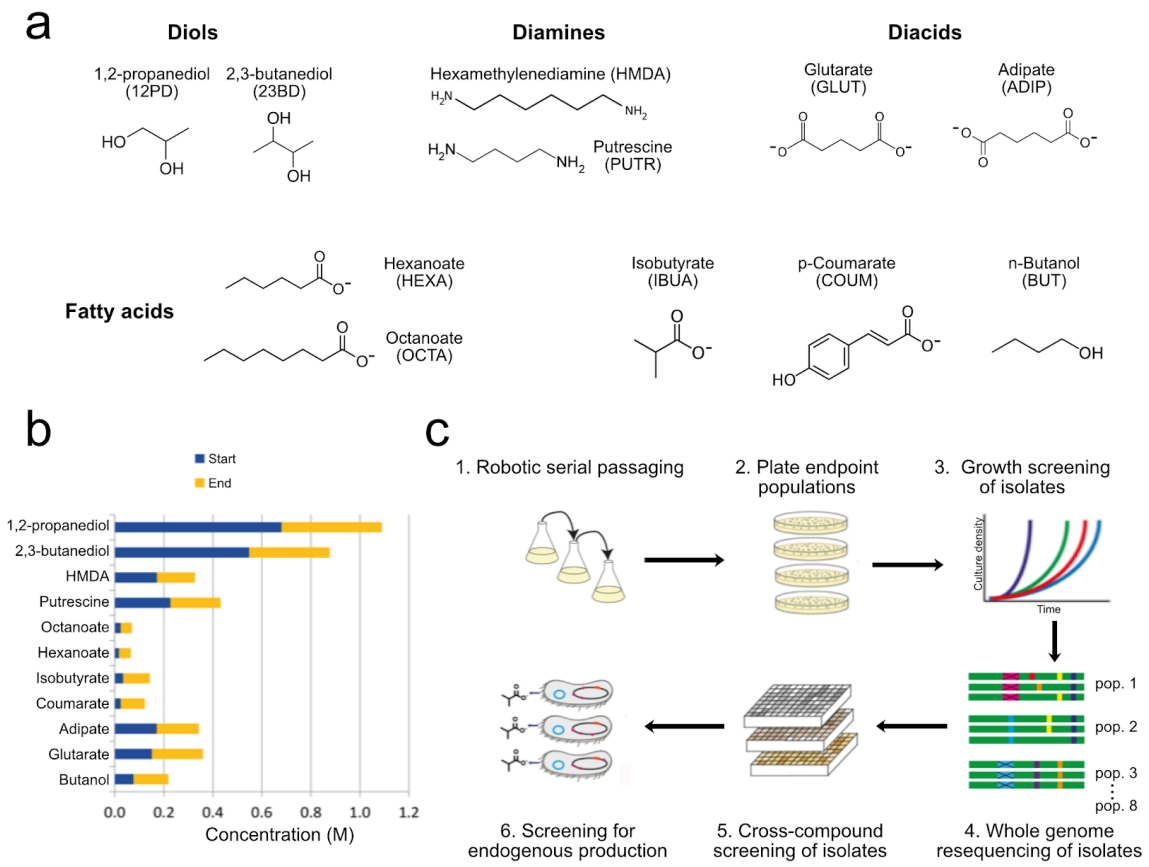

***Figure 1**: a) Chemicals selected for the study grouped by chemical category. b) Initial and final concentrations of the chemicals used during ALE. c) Overall workflow of the study.*

Resequencing of the evolved isolates showed that the median number of sequence variants per strain was 6, although a subset of the strains had more than 10 times this number. This drastic difference was determined to be caused by a hypermutator phenotype, as all the strains in question had *mut** mutations (e.g. *mutS*). Since these hypermutator strains were assumed to have accumulated mostly random neutral variants, they were not included in further analysis of sequence variants in the evolved strains. The 1,2-propanediol condition was also dropped from the sequence variant analyses as only three isolates from a single population were not hypermutators. The median number of variants per strain among the remaining 189 strains was 5 and the numbers of variants for strains evolved in different conditions were quite similar (Figure 2a). A subset of strains contained large duplications - these were especially common in strains evolved on isobutyrate and coumarate (Figure 2a). A full list of the mutations in each strain can be found in Supplementary Table 1.

To investigate which cellular functions were affected by the mutations, the functional domains of all the mutated genes were analyzed (Figure 2b). More than half of the variants affect genes with regulatory or transport functions, indicating that these gene classes play a significant role in the evolution of tolerance.

Even in the non-mutator strains, it is likely that a subset of the observed mutations have arisen by random chance and are thus not associated with tolerance. However, the availability of isolates from independent parallel ALE populations allows some degree of distinction between random and adaptive mutations. Specifically, if a mutation is observed in isolates from several independent populations, it is quite unlikely that it is a product of chance. In four conditions we identified genes that were mutated in all isolates from that condition: all glutarate and adipate strains had *kgtP* mutations while all isobutyrate strains had *pykF* mutations and all 2,3-butanediol strains had *relA* mutations. Aside from these, mutations in a number of other genes were observed in at least one strain from each population or in almost all populations as shown in Table 2. We observed limited overlap between the different evolution conditions in terms of the of the genes that were mutated - this set of genes included primarily global regulators (e.g. *rpoB*, rpoC and rpoA) and a handful of other genes that are commonly found to be mutated in *E. coli* ALE studies (Wang et al. 2018). In cases where the same gene was mutated in different evolution conditions, e.g. the RNA polymerase genes, the specific mutations were usually distinct indicating that the effects of the mutations may also be different (Supplementary Figure 2).

***Table 2**: The five most commonly mutated genes for each condition. The numbers in parentheses denote the number of ALE populations in which mutations in the given gene were observed in at least one strain.*

HMDA	PUTR	23BD	GLUT	ADIP	HEXA	OCTA	IBUA	COUM	BUT
pyrE (4/6)	mreB (5/7)	metJ (7/7)	kgtP (8/8)	kgtP (7/7)	rpoA (7/7)	rpoC (3/6)	pykF (8/8)	rho (7/8)	pyrE (7/8)
proV (3/6)	spoT (4/7)	relA (7/7)	spoT (7/8)	ybjL (5/7)	sapB (3/7)	rpoA (2/6)	rpoB (6/8)	nadR (4/8)	manY (7/8)
nagC (3/6)	rpoC (3/7)	rpoC (5/7)	rpoC (5/8)	proV (4/7)	mdtK (3/7)	dusB (2/6)	glyQ (2/8)	pyrE (4/8)	rob (7/8)
ptsP (2/6)	proV (3/7)	nanK (5/7)	nagC (4/8)	pyrE (3/7)	rpoC (3/7)	gtrS (2/6)	rpoC (2/8)	manY (4/8)	marC (6/8)
ybeX (2/6)	rpsA (3/7)	purT (5/7)	proV (3/8)	sspA (3/7)	ompC (2/7)	mreB (2/6)	rpoS (2/8)	mprA (3/8)	yobF (4/8)

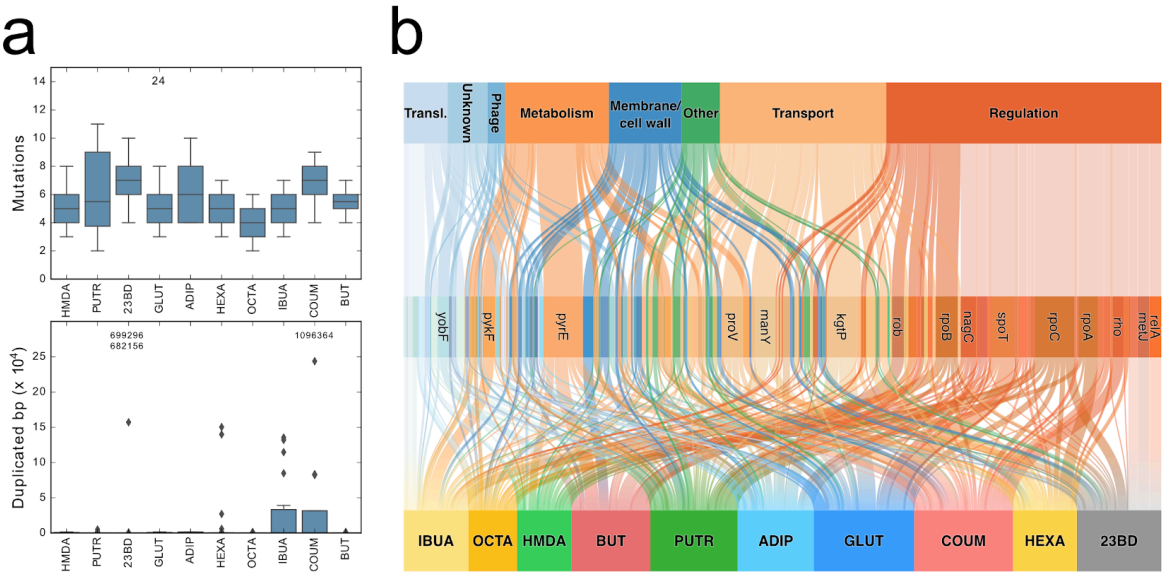

Figure 2: *a) Boxplots showing the distributions of mutations per strain and duplication size per strain for each condition. The numbers above the boxes show the values of outliers not shown in the plots. b) Genetic variant landscape. The chart shows an overview of the genes mutated in the different conditions and the functional classifications of these genes. The width of the lines is proportional to the number of strains in which a given gene was mutated.*

In order to determine whether the strains had tolerance to a broad range of chemicals, we measured growth rates of all 224 isolates in the presence of moderately toxic levels of each of the 11 chemicals. In addition, we measured growth rates of all the strains on M9 glucose to determine general growth improvements and on M9 glucose + 0.6 M NaCl to determine osmotic stress resistance of the strains. We found that strains evolved on diamines, diols and diacids were in general resistant to the other chemical of the same functional class (Figure 3a). In contrast, strains evolved on either of the medium chain-length fatty acids were not tolerant to the other medium chain-length fatty acid. We also tested whether strains that were tolerant to four specific compounds (HMDA, 2,3-butanediol, adipate and isobutyrate) were also tolerant to other similar compounds (diamines, diols, diacids or carboxylic acids, respectively; Figure 3b). We found that in most cases strains tolerant to one compound also have significantly higher growth rates on similar compounds compared to the ancestral strain.

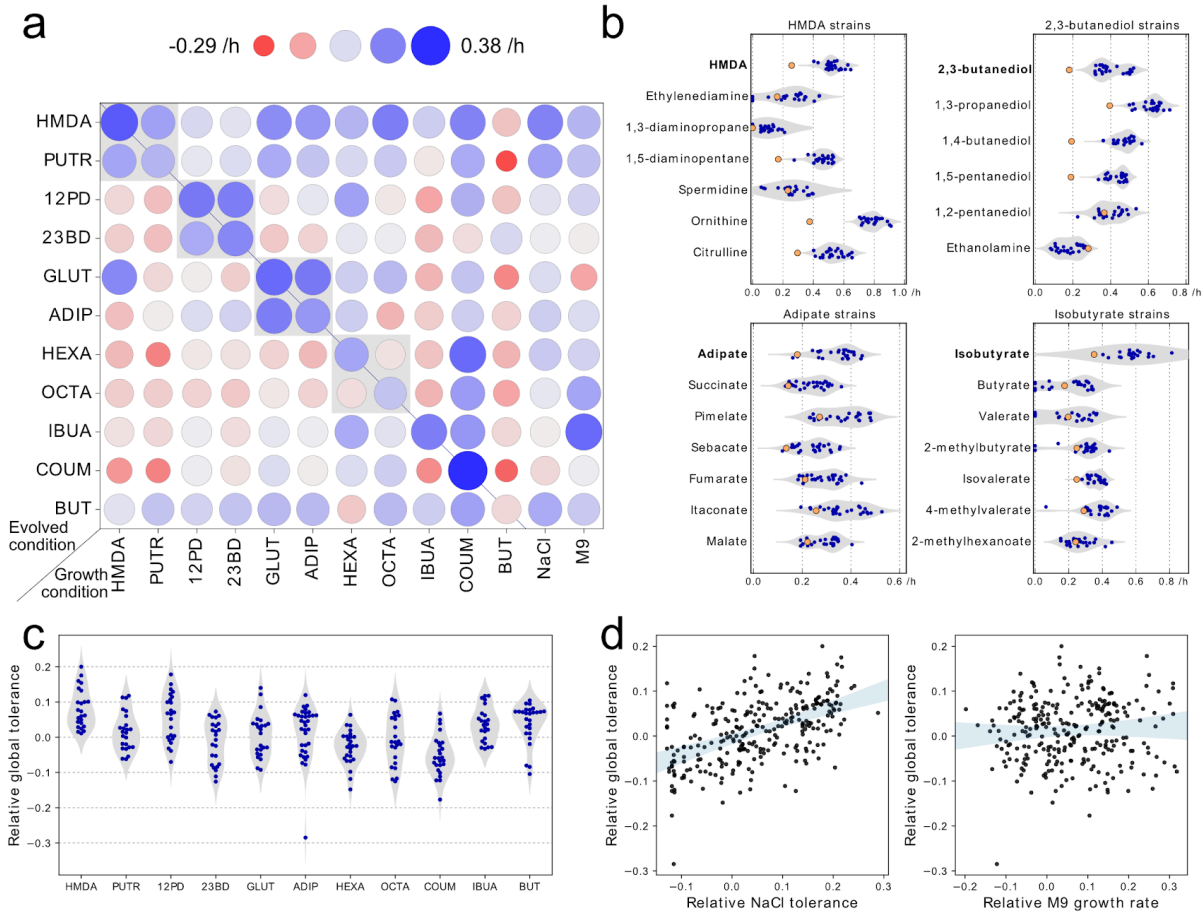

Figure 3: *Chemical cross-tolerance between similar and dissimilar compounds. a) Cross-tolerance between the compounds used for ALE. Circle color and size represent the mean growth rate of the group of strains relative to the unevolved reference strain. The grey boxes indicate pairs of compounds that are structurally similar. The growth rates on 0.6 M NaCl and M9 are also shown. b) Tolerance to compounds structurally related to four of the compounds used for ALE. Blue points represent growth rates of evolved strains, while the orange points show the growth rates of the reference strain. c) Distribution of global tolerance values for strains evolved on each of the 11 compounds d) Global tolerance as a function of osmotolerance (growth rate on NaCl) and improvement in baseline growth (growth on M9 glucose).*

We sought to understand some of the general mechanisms that make an *E. coli* strain tolerant to a broad range of chemicals. We used the average growth rate of an ALE strain relative to the wild type strain across all 11 chemicals as a metric of global chemical tolerance of a strain. The global chemical tolerance of strains depended significantly on what chemical the specific strain had been evolved to tolerate (F-test, $F = 10.06$, $p < 10^{-13}$; Figure 3c). Strains evolved on HMDA had typically high chemical tolerance whereas strains evolved on coumarate and hexanoate were significantly less tolerant to most other chemicals than the wild-type strain. We found that osmotic stress tolerance (as measured by the growth rate of the strain in 0.6 M NaCl) was predictive of global chemical

tolerance (Pearson's r = 0.52, $p < 10^{-20}$) (Figure 3d) whereas growth rate of the ALE strain in M9 glucose minimal media was not (Pearson's r = 0.06, p = 0.31) (Figure 3d). Interestingly, the osmolarity of the medium at the end of the ALE experiments did not seem to be associated with either osmotolerance or global tolerance of the strain (Supplementary Figure 3).

The mechanisms by which strains acquired tolerance to each chemical were usually quite complex and hard to decipher from the resequencing data alone. However, in the cases where transporter mutations were found in many strains it was possible to formulate a clear mechanistic hypothesis and test it experimentally. All strains evolved to tolerate adipate and glutarate contained mutations in the *kgtP* gene, which encodes an active alpha-ketoglutarate importer (Seol and Shatkin, 1991). Approximately half of these mutations were clearly deleterious for the transport function, i.e. deletions or insertions causing frameshifts or SNPs causing premature stop codons. We tested the ability of a *kgtP* deletion strain to grow in the presence of high levels of glutarate or adipate and found that especially on glutarate a *kgtP* deletion strain grew significantly faster than the wild type strain (Figure 4a and b). Some of the diacid-evolved strains also contained apparent loss-of-function mutations in two other transporters, *proV* (ATP-binding subunit of the glycine-betaine transporter ProVWX) and *ybjL* (putative uncharacterized transporter). Deleting these transporters in addition to *kgtP* deletion increased the growth rate further on glutarate and adipate (Figure 4a and 4b) with the triple deletion strain reaching approximately the same growth rate on glutarate as the best evolved strains. Furthermore, the strains where *kgtP* was either deleted or otherwise inactive were not able to grow with glutarate as a carbon source whereas the wild type and *proV* and *yjbL* single deletion strains were able to grow in this condition (data not shown).

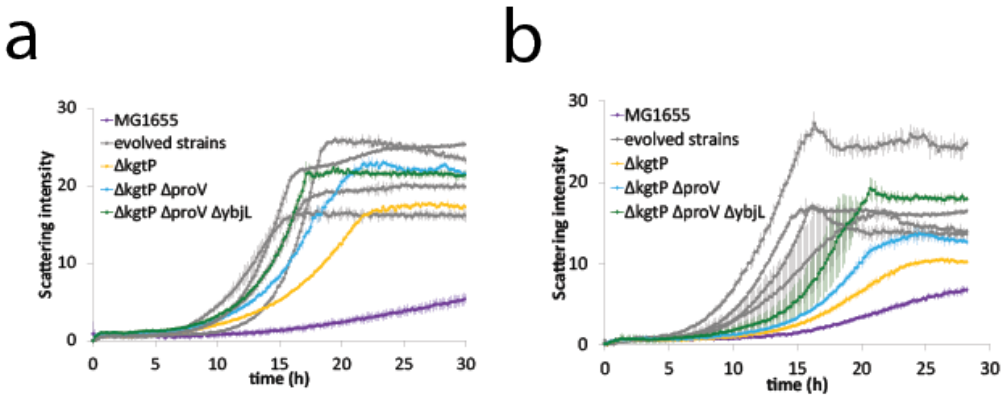

Figure 4: *Transport modulation as a tolerance mechanism for diacids. a) Growth curves of reference strain MG1655, four genetically distinct glutarate-evolved strains as well as single, double and triple transporter deletion strains on 47.5 g/L glutarate (in M9 Glucose media). b) Growth curves of reference strain MG1655, four genetically distinct adipate-evolved strains as well as single, double and triple transporter deletion strains on 50 g/L adipate (in M9 Glucose media).*

We wanted to determine whether pre-evolving strains to tolerate a non-native chemical product would result in enhanced production when the relevant pathways are engineered into a tolerant host strain. We chose the two relatively simple pyruvate-derived compounds isobutyrate and 2,3-butanediol as examples for this study because production of these compounds had previously been demonstrated in *E. coli* (Xu et al., 2014; Zhang et al., 2011) and engineering the production background into a large number of background strains was feasible. In the case of isobutyrate we also have some understanding of tolerance mechanisms from resequencing and mutation reconstructions. As previously mentioned, all isobutyrate-evolved strains had deletions of the *pykF* isozyme of pyruvate kinase, and this deletion alone was demonstrated to significantly improve isobutyrate tolerance (Figure 5a). In addition to *pykF* deletions some of the strains also had point-mutations in acetolactate synthase regulatory subunits *ilvH/N* that are involved in feedback inhibition by valine. These mutations alone or in combination with *pykF* deletions did not confer improved isobutyrate tolerance (Figure 5b), but significantly improved strain growth in the presence of exogenous valine (Figure 5c), suggesting that they disable or reduce valine feedback inhibition. We hypothesize that the mechanism of isobutyrate toxicity is inhibition of 2-isopropylmalate synthase (encoded by the gene *leuA*) due to the similarity between isobutyrate and the native substrate alpha-ketoisovalerate (KIV) (Figure 5d). This inhibition would lead to overproduction of valine and feedback inhibition of the biosynthesis of all branched-chain amino acids.

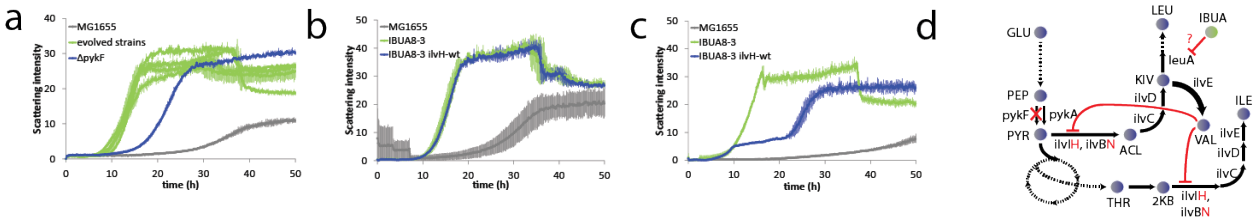

Figure 5: *Isobutyrate tolerance modulated by variants in metabolic genes. a) pykF deletion strain growth compared to growth of evolved and wild type strains in the presence of toxic concentrations of isobutyrate (12.5 g/L). b) Growth comparison of the reference strain, the IBUA8-3 isolate, and the same isolate where the ilvH point-mutation was reverted to wild type in the presence of toxic concentrations of isobutyrate. c) Comparison of growth curves of the same strains shown in panel b in the presence of 1 g/L valine. d) Schematic description of the proposed mechanism of toxicity and role of the major genetic changes identified in IBUA8-3 strain.*

We engineered the native production of isobutyrate into wild type MG1655 and 12 genetically distinct isobutyrate-tolerant strains by expressing three heterologous genes from plasmids and deleting a competing pathway in each strain (Figure 6a). The engineered ALE strains had highly variable levels of production of isobutyrate compared to the engineered reference strain (Figure 6b). In particular some strains produced almost no isobutyrate and also grew very poorly. On the other hand, there were ALE strains that produced more than three times more isobutyrate than the engineered wild-type with a particularly large difference in production during the first 24 hours. The strains that produced and grew best (IBUA8-3 and IBUA8-10) both had *ilvH/N* mutations whereas the other strains lacked these mutations, indicating that the removal of acetolactate synthase feedback inhibition was beneficial to production.

We also engineered production of 2,3-butanediol into MG1655 and 20 tolerant ALE strains by expressing three heterologous genes in the strains (Figure 6c). Deletion of the native gene *hsdR* encoding a restriction enzyme was necessary to perform the transformation. Again, there was significant variation in 2,3-butanediol among the engineered ALE strains, but in this case the majority of strains had production levels similar to the engineered wild type strain with only two specific ALE strains showing improved production of 2,3-butanediol compared to engineered wild type strain (Figure 6d). We could not identify a mechanistic basis for the improved production even if we could quite clearly pinpoint which mutations were responsible for the improved production due to differences between isolates obtained from the same ALE populations (Supplementary Table 1).

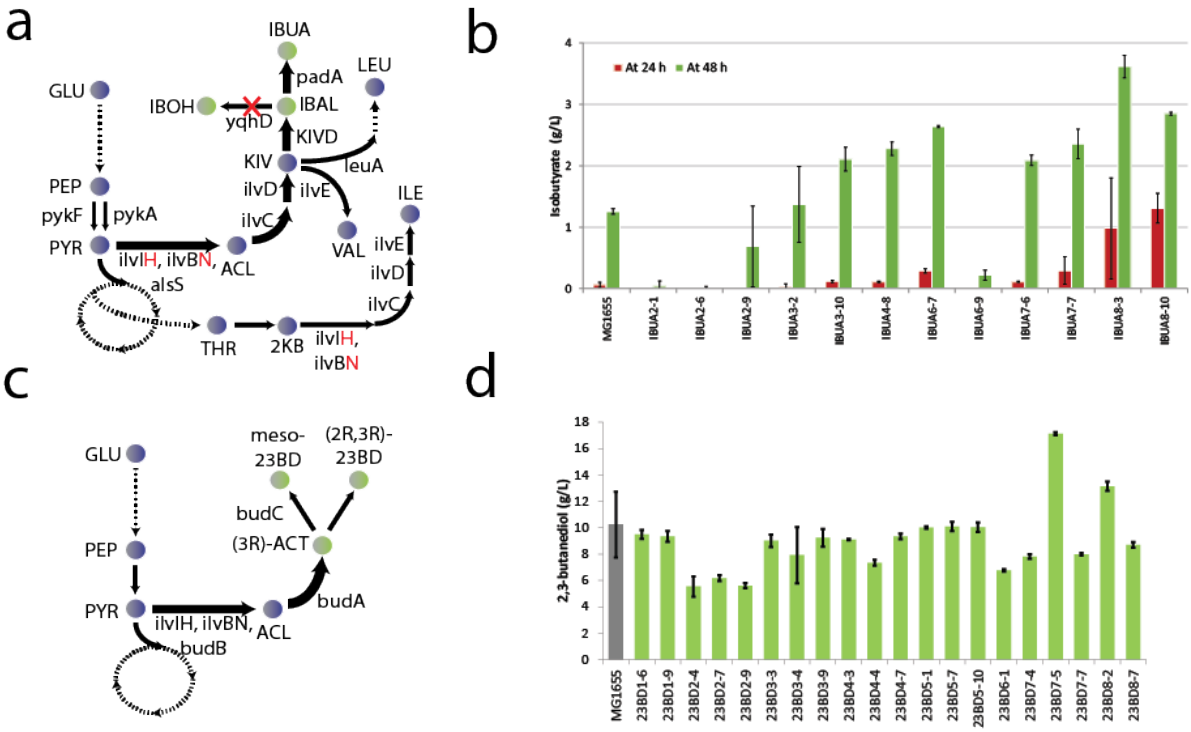

Figure 6: *Production of isobutyric acid and 2,3-butanediol using pre-tolerized strains. a) Production pathway schematic for isobutyrate, with heterologous expression of an acetolactate synthase AlsS, ketoisovalerate decarboxylase KIVD, and PadA to generate isobutyric acid from ketoisovalerate (KIV), with deletion of native yqhD to prevent reduction of isobutyraldehyde (IBAL) to isobutanol (IBOH). b) Production of isobutyrate in wild-type and evolved isolates harboring production plasmids for isobutyrate and deletion of yqhD after 24 and 48 hours growth in FIT (feed-in-time) medium. c) Production pathway schematic for 2,3-butanediol from pyruvate, with heterologous expression of BudA, BudB, and BudC. d) Production of 2,3-butanediol in wild-type and evolved isolates harboring a production plasmid for 2,3-butanediol and deletion of hsdR after 48 hours in M9 + 5% glucose + 0.5% yeast extract.*

1.4 Discussion

Consistent with previous findings described in the literature, our results show that ALE can be used to significantly increase the tolerance of microbial cells to an exogenously supplied chemical of interest. The relative increases in tolerance were largest for the chemicals that initially were most toxic to *E. coli* (primarily acids) whereas tolerance to compounds that were initially tolerated at high levels, such as diols, was increased more modestly. Since we neutralize the acids, the reasons for limited ability of *E. coli* to tolerate acids is not related to low pH. It is likely that further increases in tolerance would be achievable for most compounds by continuing the evolution experiments at ever increasing chemical concentrations, however, physico-chemical properties such as volatility and solubility become issues for many of the compounds at higher concentrations, thus limiting the ability to further evolve tolerant strains. In comparison to previous ALE studies, the systematic approach used here allows direct comparisons of the evolvability of *E. coli* to different conditions.

Resequencing of 224 tolerant strains obtained from 88 independently evolved populations revealed that most strains had a relatively modest number of mutations and that large genome rearrangements were also rare. In principle, this makes it possible to develop a good understanding of which genes are important for tolerance to a given compound. However, the overall genomic variant landscape across all strains is quite complex with most genes targeted by mutations only in specific evolution conditions. These results indicate that there is high diversity in mechanisms of toxicity and tolerance between the different chemicals. The interpretation of the resequencing data alone is also made difficult by the high frequency of mutations in regulatory genes that are known to have pleiotropic effects (RNA polymerase subunits, genes involved in stringent response, termination factors, etc.). The overall conclusions from the resequencing results is that there are no universal chemical tolerance mechanisms at the genetic level and that tolerance usually involves both specific (e.g. transporters) and general (e.g. adjustments in global regulation) adaptations.

The cross-tolerance screening showed that in the case of diacids, diols and diamines, strains evolved to tolerate one specific chemical usually had tolerance to the other chosen chemical of the same class (Figure 3a). However, for the medium chain fatty acids hexanoate and octanoate, this pattern of cross-tolerance was not observed. It is not clear why this is the case, in particular since the genetic adaptations were not necessarily more similar between e.g. diamines than medium chain fatty acids. Furthermore, strains evolved to tolerate a specific chemical (Figure 3b) tend to be tolerant to a wide range of highly similar chemicals, which is of great practical relevance. Because of this, it is only necessary to perform ALE once for a category of chemicals (e.g. diols) in order to obtain a series of potential platform strains that have high levels of tolerance within the category.

Cross tolerance profiling could also be used to define a measure of global chemical tolerance of each evolved strain. Global tolerance was found to be highly variable within the set of genetically distinct strains evolved under each condition and even more so between strains evolved under different conditions. Global tolerance was found to be unrelated to the growth rate of the strain on the base M9 glucose medium (Figure 3d) indicating that the fast growth and stress tolerance phenotypes are not related to each other biologically. On the other hand, the ability of a strain to grow in osmotic stress conditions (NaCl) was found to be significantly predictive of the global chemical tolerance of the strain (Figure 3d). This result is expected due to the high osmolarity of the final growth medium for many chemicals although the osmolarity of the evolution condition was not predictive of global

tolerance of a strain. Some of the strains that were highly osmotolerant (and hence globally chemical tolerant) contained mutations in genes such as *nagC* and *proV* that have previously been implicated in osmotolerance in ALE experiments (Winkler et al., 2014). Unfortunately, the exact mechanisms by which many of the observed mutations or their combinations confer osmotolerance remain somewhat elusive. The result that osmotolerance is predictive of general chemical tolerance indicates that choosing a well-characterized osmotolerant strain as a starting platform strain for metabolic engineering efforts may in general be a good strategy for any target chemical.

Determining the exact mechanisms of chemical tolerance was challenging, but in specific cases where convergent mutation targets in either transporters or metabolic genes were discovered in independently evolved strains, mechanistic hypotheses could be generated and validated experimentally. Since all strains evolved on adipate and glutarate contained apparent loss-of-function mutations in a gene encoding a known alpha-ketoglutarate transporter (*kgtP*), this transporter was likely the primary transporter importing the two diacids. Indeed, deletion of the transporter conferred a large increase in tolerance and prevented growth with glutarate as the sole carbon source. As alpha-ketoglutarate is structurally similar to glutarate and adipate, the transporter most likely has significant promiscuous activity towards the two diacids. Two further transporters were mutated in specific diacid-tolerant strains and a triple deletion of these transporters was sufficient to achieve levels of tolerance to glutarate and adipate almost on par with the evolved strains. One of these genes encoding transporters (*proV*, encoding the ATP-binding subunit of the ProVWX glycine betaine transporter complex) is a known to import the osmoprotectant glycine betaine whereas the other one (*yjbL*) is previously completely uncharacterized. As *proV* mutations were also observed in many other strains, it is likely that the ProVWX transporter can promiscuously import many of the chemicals and deleting *proV* is therefore beneficial for chemical tolerance in general.

Exogenous chemical tolerance alone is not a very useful phenotype for metabolic engineering applications where the strains are engineered to produce a chemical endogenously. In order to demonstrate that pre-evolving for exogenous tolerance could help in obtaining better endogenous production strains we engineered production pathways for isobutyrate and 2,3-butanediol into genetically distinct strains that had been evolved to tolerate the respective compounds. In both cases we found that engineered ALE strains did not generally show increased production compared

to the similarly engineered wild-type strain. However, for both isobutyrate and 2,3-butanediol we could identify specific strains that did have significantly higher production. This indicates that pre-evolving for exogenous tolerance would be a viable strategy for obtaining improved production strains as long as a sufficient number of independently evolved and genetically distinct strains are created and screened. With rapid improvements in genetic manipulation and automation technologies, engineering the same pathway into multiple strain backgrounds can be readily done, making this approach feasible.

All isobutyrate-evolved strains contained *pykF* mutations the majority of which were clear loss-of-function mutations. *pykF* mutations are commonly seen in many *E. coli* ALE experiments (Wang et al. 2018; Phaneuf et al. 2018) and *pykF* deletions have also been proven to allow increased production of many metabolites (Harder et al., 2016; Sengupta et al., 2015). It is not clear exactly how *pykF* deletion would specifically increase isobutyrate tolerance, but this deletion has been shown to have broad effects in redirecting fluxes in central carbon metabolism and in changing the regulation of pyruvate supply (Al Zaid Siddiquee et al., 2004). Deleting *pykF* conferred significantly improved tolerance to isobutyrate, but in terms of production the different ALE strains showed very different levels ranging from no production to three times higher production than the wild type strain, indicating that *pykF* mutations alone did not explain production differences. The highest producing strains from population IBUA8 had mutations in *ilvH/N* encoding regulatory subunits of acetolactate synthases. These mutations were shown to alleviate feedback inhibition by valine, which may explain their ability to produce higher levels of isobutyrate as the engineered strains contain a heterologously expressed acetolactate synthase AlsS, which increases not only isobutyrate production but also production of branched-chain amino acids including valine. In the case of 2,3-butanediol production, only one of the engineered evolved strains had considerably higher production than the wild-type strain. The genotype of the strain did not provide clear clues to the reasons for improved production although the high producing strain was the only one containing a mutation in the *acrB* gene encoding a subunit of the AcrB/AcrB/AcrZ/TolC multidrug efflux pump. However, the mutation present in the strain was a frameshift mutation close to the 5’ end of the gene indicating that the efflux pump was likely inactivated.

1.5 Conclusion

In this study we used ALE to evolve strains of *E. coli* to tolerate high concentrations of 11 different industrially relevant chemicals. The tolerated concentrations increased by factors of 60 % to 400 %. Genome sequencing of the evolved strains showed that the median number of mutations per strain was 6, and that only a small degree of mutation overlap was seen between conditions and even between independently evolved strains in the same condition. This made it difficult to infer mechanisms of tolerance in all but a couple of cases. Cross-compound tolerance screening revealed a general trend of cross-tolerance between compounds of the same class. This suggests that a single broadly tolerant platform strain could be used for production of several compounds of the same class. Furthermore, we observed that tolerance to high osmolarity was predictive of the overall tolerance to all 11 compounds, suggesting that high osmolarity is a significant factor of toxicity at the utilized concentrations. For two compounds, the evolved strains were transformed with plasmids carrying production pathways and screened for improved production compared to the wild-type. In both cases we could identify strains that produced considerably better than the wild-type, although the majority of evolved strains had similar or reduced production compared to the wild-type. This suggests that pre-evolving a strain to tolerate the target compound before engineering production can be a viable strategy as long as a large number of independently evolved strains can be isolated and screened.

1.6 References

Al Zaid Siddiquee, K., Arauzo-Bravo, M.J., Shimizu, K., 2004. Metabolic flux analysis of pykF gene knockout Escherichia coli based on 13C-labeling experiments together with measurements of enzyme activities and intracellular metabolite concentrations. Appl. Microbiol. Biotechnol. 63, 407–417. https://doi.org/10.1007/s00253-003-1357-9

Atsumi, S., Wu, T.Y., Machado, I.M.P., Huang, W.C., Chen, P.Y., Pellegrini, M., Liao, J.C., 2010. Evolution, genomic analysis, and reconstruction of isobutanol tolerance in Escherichia coli. Mol. Syst. Biol. 6, 1–11. https://doi.org/10.1038/msb.2010.98

Deatherage, D.E., Barrick, J.E., 2014. Identification of mutations in laboratory evolved microbes from next-generation sequencing data using breseq. Methods Mol. Biol. 1151, 165–188.

https://doi.org/10.1007/978-1-4939-0554-6

Deparis, Q., Claes, A., Foulquié-Moreno, M.R., Thevelein, J.M., 2017. Engineering tolerance to industrially relevant stress factors in yeast cell factories. FEMS Yeast Res. 17, 1–17. https://doi.org/10.1093/femsyr/fox036

Haft, R.J.F., Keating, D.H., Schwaegler, T., Schwalbach, M.S., Vinokur, J., Tremaine, M., Peters, J.M., Kotlajich, M. V., Pohlmann, E.L., Ong, I.M., Grass, J.A., Kiley, P.J., Landick, R., 2014. Correcting direct effects of ethanol on translation and transcription machinery confers ethanol tolerance in bacteria. Proc. Natl. Acad. Sci. 111, E2576–E2585. https://doi.org/10.1073/pnas.1401853111

Hansen, A.S.L., Lennen, R.M., Sonnenschein, N., Herrgård, M.J., 2017. Systems biology solutions for biochemical production challenges. Curr. Opin. Biotechnol. 45, 85–91. https://doi.org/10.1016/j.copbio.2016.11.018

Harder, B.J., Bettenbrock, K., Klamt, S., 2016. Model-based metabolic engineering enables high yield itaconic acid production by Escherichia coli. Metab. Eng. 38, 29–37. https://doi.org/10.1016/j.ymben.2016.05.008

Horinouchi, T., Suzuki, S., Kotani, H., Tanabe, K., Sakata, N., Shimizu, H., Furusawa, C., 2017. Prediction of Cross-resistance and Collateral Sensitivity by Gene Expression profiles and Genomic Mutations. Sci. Rep. 7, 1–11. https://doi.org/10.1038/s41598-017-14335-7

Kildegaard, K.R., Hallström, B.M., Blicher, T.H., Sonnenschein, N., Jensen, N.B., Sherstyk, S., Harrison, S.J., Maury, J., Herrgård, M.J., Juncker, A.S., Forster, J., Nielsen, J., Borodina, I., 2014. Evolution reveals a glutathione-dependent mechanism of 3-hydroxypropionic acid tolerance. Metab. Eng. 26, 57–66. https://doi.org/10.1016/j.ymben.2014.09.004

LaCroix, R.A., Palsson, B.O., Feist, A.M., 2017. A model for designing adaptive laboratory evolution experiments. Appl. Environ. Microbiol. 83. https://doi.org/10.1128/AEM.03115-16

Lennen, R.M., Kruziki, M.A., Kumar, K., Zinkel, R.A., Burnum, K.E., Lipton, M.S., Hoover, S.W., Ranatunga, D.R., Wittkopp, T.M., Marner, W.D., Pfleger, B.F., 2011. Membrane stresses

induced by overproduction of free fatty acids in Escherichia coli. Appl. Environ. Microbiol. 77, 8114–8128. https://doi.org/10.1128/AEM.05421-11

Lennen, R.M., Nilsson Wallin, A.I., Pedersen, M., Bonde, M., Luo, H., Herrgård, M.J., Sommer, M.O.A., 2015. Transient overexpression of DNA adenine methylase enables efficient and mobile genome engineering with reduced off-target effects. Nucleic Acids Res. 44, 1–14. https://doi.org/10.1093/nar/gkv1090

Mohamed, E.T., Wang, S., Lennen, R.M., Herrgård, M.J., Simmons, B.A., Singer, S.W., Feist, A.M., 2017. Generation of a platform strain for ionic liquid tolerance using adaptive laboratory evolution. Microb. Cell Fact. 16, 1–15. https://doi.org/10.1186/s12934-017-0819-1

Mundhada, H., Seoane, J.M., Schneider, K., Koza, A., Christensen, H.B., Klein, T., Phaneuf, P. V., Herrgard, M., Feist, A.M., Nielsen, A.T., 2017. Increased production of L-serine in Escherichia coli through Adaptive Laboratory Evolution. Metab. Eng. 39, 141–150. https://doi.org/10.1016/j.ymben.2016.11.008

Phaneuf, P. V, Gos, D., Palsson, B.O., Feist, A.M., 2018. ALEdb 1.0: A Database of Mutations from Adaptive Laboratory Evolution Experimentation.

Reyes, L.H., Abdelaal, A.S., Kao, K.C., 2013. Genetic determinants for n-butanol tolerance in evolved escherichia coli mutants: Cross adaptation and antagonistic pleiotropy between n-butanol and other stressors. Appl. Environ. Microbiol. 79, 5313–5320. https://doi.org/10.1128/AEM.01703-13

Royce, L.A., Yoon, J.M., Chen, Y., Rickenbach, E., Shanks, J. V., Jarboe, L.R., 2015. Evolution for exogenous octanoic acid tolerance improves carboxylic acid production and membrane integrity. Metab. Eng. 29, 180–188. https://doi.org/10.1016/j.ymben.2015.03.014

Sengupta, S., Jonnalagadda, S., Goonewardena, L., Juturu, V., 2015. Metabolic engineering of a novel muconic acid biosynthesis pathway via 4-hydroxybenzoic acid in Escherichia coli. Appl. Environ. Microbiol. 81, 8037–8043. https://doi.org/10.1128/AEM.01386-15

Seol, W., Shatkin, A.J., 1991. Escherichia coli kgtP encodes an alpha-ketoglutarate transporter.

Proc. Natl. Acad. Sci. 88, 3802–3806.

Van Dien, S., 2013. From the first drop to the first truckload: Commercialization of microbial processes for renewable chemicals. Curr. Opin. Biotechnol. 24, 1061–1068. https://doi.org/10.1016/j.copbio.2013.03.002

Winkler, J.D., Garcia, C., Olson, M., Callaway, E., Kao, K.C., 2014. Evolved osmotolerant escherichia coli mutants frequently exhibit defective N-acetylglucosamine catabolism and point mutations in cell shape-regulating protein MreB. Appl. Environ. Microbiol. 80, 3729–3740. https://doi.org/10.1128/AEM.00499-14

Winkler, J.D., Kao, K.C., 2014. Recent advances in the evolutionary engineering of industrial biocatalysts. Genomics 104, 406–411. https://doi.org/10.1016/j.ygeno.2014.09.006

Xu, Y., Chu, H., Gao, C., Tao, F., Zhou, Z., Li, K., Li, L., Ma, C., Xu, P., 2014. Systematic metabolic engineering of Escherichia coli for high-yield production of fuel bio-chemical 2,3-butanediol. Metab. Eng. 23, 22–33. https://doi.org/10.1016/j.ymben.2014.02.004

Zhang, K., Woodruff, A.P., Xiong, M., Zhou, J., Dhande, Y.K., 2011. A synthetic metabolic pathway for production of the platform chemical isobutyric acid. ChemSusChem 4, 1068–1070. https://doi.org/10.1002/cssc.201100045

1.7 Supplementary Materials

Supplementary Table 1: *Summary of the mutations and mutated genes in all the non-mutator strains. The mutation names denote the type, location and change of the mutations.*

	GENES	MUTATIONS
12PD4-6	relA, metJ, yeaR, sspA, rpsA	SNP-3377240-G, SNP-4128078-G, SNP-2912634-G, SNP-962923-T, MOB-1879829-Δ1-:
12PD6-3	lrhA, rpoA, fabR, dusA, yfgF	SNP-4161155-A, SNP-4261586-C, SNP-3440194-A, MOB-2628616-IS2-5, MOB-2406831-IS2-5
12PD6-9	rpoA, fabR, yfgF, ypjA	SNP-3440194-A, MOB-2628616-IS2-5, SNP-2780609-C, SNP-4161155-A
23BD1-6	gabP, nanK, rnb, metJ, elfA, rpoB, purT, relA	MOB-998193-IS5-4, SNP-4182583-T, SNP-2794550-G, SNP-1931977-G, SNP-3369969-A, DEL-2911491-7528, SNP-4128380-A, MOB-1347480-IS5-4
23BD1-9	gabP, nanK, rnb, metJ, elfA, rpoB, purT, relA	MOB-998193-IS5-4, SNP-4182583-T, SNP-2794550-G, SNP-1931977-G, SNP-3369969-A, DEL-2911491-7528, SNP-4128380-A, MOB-1347480-IS5-4
23BD2-4	nanK, uspC, metJ, rpoC, rpsA, gtrS, relA	SNP-1979639-C, MOB-4128293-IS5-4, SNP-4186152-G, SNP-3369969-A, SNP-962056-T, MOB-580116-IS5-4, SNP-2470411-G, DEL-2911491-7528
23BD2-7	metJ, rpoC, nanK, relA, rpsA	MOB-4128293-IS5-4, MOB-1096841-IS2-5, SNP-4186152-G, SNP-3369969-A, SNP-962056-T, MOB-580116-IS5-4, DEL-2911491-7528
23BD2-9	metJ, rpoC, nanK, relA, rpsA	MOB-4128293-IS5-4, SNP-4186152-G, SNP-3369969-A, SNP-962056-T, MOB-580116-IS5-4, DEL-2911491-7528
23BD4-3	yeaR, mprA, rnb, fadB, umuD, metJ, rpoC, purT, relA	SNP-1347775-A, SNP-4128361-C, SNP-2810756-T, SNP-2913536-T, DEL-4187816-15, SNP-1931977-G, MOB-1879829-Δ1-:, SNP-4031019-A, SNP-1230727-A
23BD4-4	yeaR, umuD, rpoC, metJ, purT, relA	SNP-4128361-C, SNP-1931977-G, MOB-1879829-Δ1-:, SNP-2913536-T, DEL-4187816-15, SNP-1230727-A
23BD4-7	rpoC, nanK, metJ, relA	SNP-4186274-T, SNP-3369969-A, SNP-4128169-G, DEL-2911491-7528
23BD5-1	yeaR, spoT, umuD, metJ, rpoC, purT, relA	SNP-4128361-C, MOB-1879829-Δ1-:, SNP-3823036-C, SNP-2913536-T, DEL-4187816-15, SNP-1931977-G, SNP-1230727-A
23BD5-7	ybeT, nanK, ybhP, ydhK, rpoC, metJ, zntR, relA	SNP-4186274-T, SNP-1722386-T, SNP-4128379-T, SNP-824028-G, SNP-3369969-A, SNP-3438773-G, DEL-2911491-7528, SNP-679090-G
23BD5-10	rpoC, nanK, metJ, relA	SNP-4186274-T, SNP-3369969-A, SNP-4128169-G, DEL-2911491-7528
23BD6-1	essD, rpoC, metJ, nusG, purT, relA	DEL-575786-3027, DEL-2912618-10, SNP-4185573-G, SNP-1930993-G, SNP-4128250-C, SNP-4178172-G
23BD7-4	treR, nanK, elfD, tolC, metJ, rpoC, yhjA, flu, purT, relA	SNP-4128386-C, MOB-3668878-IS2-5, SNP-4186152-G, MOB-4466841-IS5-4, SNP-1931668-G, SNP-3369969-A, DEL-2911491-7528, SNP-3178128-G, SNP-2073463-A, MOB-998719-IS2-5
23BD7-5	acrB, nanK, elfD, metJ, rpoC, flu, purT, relA	SNP-4128386-C, SNP-4186152-G, SNP-3369969-A, MOB-998719-IS2-5, DEL-2911491-7528, INS-484102-AT, SNP-2073463-A, MOB-1931499-IS5-4
23BD7-7	treR, nanK, elfD, tolC, metJ, rpoC, yhjA, flu, purT, relA	SNP-4128386-C, MOB-3668878-IS2-5, SNP-4186152-G, MOB-4466841-IS5-4, SNP-1931668-G, SNP-3369969-A, DEL-2911491-7528, SNP-3178128-G, SNP-2073463-A, MOB-998719-IS2-5
23BD8-2	ygaH, iscR, relA, rpoB, pyrE, lon	SNP-2661816-G, SNP-2913641-T, SNP-4184579-G, DEL-3815810-1, SNP-2810459-C, SNP-461034-G
23BD8-7	ygaH, iscR, metJ, lacZ, rpoB, pyrE, relA	DEL-3815810-1, DEL-365742-1, SNP-2661816-G, SNP-4128212-G, SNP-2810459-C, SNP-2913641-T, SNP-4184579-G
ADIP1-1	sspA, kgtP, gltP, ybjL, proV, yicC, uvrB, pyrE	SNP-814029-G, DEL-3377068-21, MOB-2725207-IS1-9, SNP-3815823-A, DEL-2804648-38, SNP-4294366-T, DEL-889569-1, SNP-3816848-T
ADIP1-9	allD, sspA, kgtP, ligA, gltP, ybjL, proV, yicC, pyrE	DEL-3377068-21, SNP-2530235-T, MOB-2725207-IS1-9, SNP-3815823-A, SNP-546309-T, DEL-2804648-38, SNP-4294366-T, DEL-889569-1, SNP-3816848-T
ADIP2-5	lacY, rph, nagC, kgtP	SNP-362830-A, MOB-700529-IS1-9, DEL-3815884-2, SNP-2725613-A
ADIP2-6	lacY, rph, nagC, kgtP	MOB-700529-IS1-9, SNP-362830-A, SNP-2725613-A, DEL-3815884-2
ADIP2-10	ydcD, pyrE, nagC, kgtP	SNP-1530007-A, MOB-700628-IS5-4, DEL-3815810-1, SNP-2725613-A
ADIP3-2	yfgO, sspA, kgtP, ybjL, proV, yicC, pyrE	DEL-3377068-21, MOB-2725207-IS1-9, SNP-3815823-A, DEL-2804648-38, SNP-2614996-G, SNP-3816848-T, MOB-889534-IS5-4
ADIP3-4	yeaR, kgtP, sspA, ybjL, yhiL, proV, yicC, mltD, pyrE	DEL-3377068-21, INS-233963-GT, MOB-2725207-IS1-9, SNP-3815823-A, MOB-3633911-IS5-4, DEL-2804648-38, MOB-1879829-Δ1-:, SNP-3816848-T, MOB-889534-IS5-4
ADIP3-8	sspA, kgtP, ybjL, proV, yicC, pyrE	DEL-3377068-21, MOB-2725207-IS1-9, SNP-3815823-A, DEL-2804648-38, SNP-3816848-T, MOB-889534-IS5-4
ADIP4-8	purL, kgtP, malQ, ybjL, yphC, pdxJ, srmB, nagA, rnt, metL	DEL-4130167-462, SNP-1728708-G, SNP-2713302-T, MOB-889488-IS1-9, SNP-2675452-C, SNP-2724590-T, SNP-3548179-T, SNP-2701175-C, SNP-2693818-G, INS-702444-GCATAACGCGCACGCCCTGTTTCATCAGCTCATCGC
ADIP6-3	spoT, kgtP, ubiE, proQ, nagC, ybjL, proV	SNP-3823700-T, SNP-700928-A, DEL-2804864-13, SNP-1915297-A, SNP-2725155-T, MOB-889534-IS5-4, SNP-4019173-G
ADIP6-9	spoT, kgtP, proQ, nagC, ybjL, proV, icd, ycjG	SNP-3823700-T, SNP-1196319-A, SNP-700928-A, SNP-1915297-A, SNP-2725155-T, MOB-889534-IS5-4, SNP-1389396-C, DEL-2804835-7

ADIP6-10	spoT, kgtP, proQ, nagC, ybjL, proV	SNP-2805493-T, SNP-3823700-T, SNP-700928-A, SNP-1915297-A, SNP-2725155-T, MOB-889534-IS5-4
ADIP7-2	kgtP, yagL, rpoS, yneO, hns, pstS	SNP-2725329-A, SNP-293574-G, MOB-1293038-IS1-9, MOB-1598223-IS5-4, DEL-2867359-9, INS-3911001-TTTC
ADIP7-5	ybjL, idnR, proV, sspA, kgtP	MOB-889540-IS5-4, SNP-3377240-G, DEL-2725643-1, MOB-4490689-IS1-9, DEL-2804864-13
ADIP8-3	pstS, yehD, hns, kgtP	MOB-1293015-IS1-8, SNP-2724588-T, DEL-2192452-1, MOB-3911563-IS1-9
ADIP8-7	pstS, yehD, hns, kgtP	MOB-1293015-IS1-8, SNP-2724588-T, MOB-3911563-IS1-9, DEL-2192452-1
ADIP8-10	pstS, insI1, yehD, hns, kgtP	MOB-1293015-IS1-8, MOB-280003-IS5-4, SNP-2724588-T, DEL-2192452-1, MOB-3911563-IS1-9
BUT1-2	tqsA, adeP, manY, rob, cspC, pyrE	DEL-3815810-1, SNP-3895843-C, DEL-1907330-2, SNP-1903497-C, SNP-4635114-C, MOB-1673883-IS5-4
BUT1-3	manY, pyrE, tqsA, cspC, rob	SNP-4635114-C, SNP-1903497-C, MOB-1673883-IS5-4, DEL-1907330-2, DEL-3815810-1
BUT1-5	tqsA, manY, yobF, ycaN, rob, pyrE	MOB-1907448-IS5-4, DEL-3815810-1, SNP-1674448-A, INS-4635196-G, SNP-1903497-C, SNP-949006-G
BUT2-9	hfq, marC, rob	SNP-1618698-A, SNP-4400407-G, DEL-3815859-82, INS-4634895-A
BUT3-3	manY, yobF, leuA, marC, pyrE	DEL-1618281-1, SNP-1903497-C, MOB-1907448-IS5-4, DEL-3815810-1, SNP-82594-G
BUT3-6	tqsA, manY, yobF, pheU, marC, pyrE	INS-4362600-C, MOB-1907448-IS5-4, DEL-3815810-1, SNP-1903497-C, MOB-1673883-IS5-4, DEL-1618281-1
BUT3-7	tqsA, manY, yobF, pheU, marC, pyrE	INS-4362600-C, MOB-1907448-IS5-4, DEL-3815810-1, SNP-1903497-C, MOB-1673883-IS5-4, DEL-1618281-1
BUT4-4	manY, marC, rob, glmU, cspC, pyrE	MOB-1907343-IS1-8, MOB-1618666-IS2-5, DEL-3815810-1, SNP-4635159-T, SNP-1903497-C, SNP-3915089-T
BUT4-7	manY, marC, rob, glmU, cspC, pyrE, sapA	MOB-1907343-IS1-8, MOB-1618666-IS2-5, DEL-3815810-1, SNP-4635159-T, SNP-1356672-G, SNP-1903497-C, SNP-3915089-T
BUT4-9	manY, marC, rob, glmU, cspC, pyrE	MOB-1907343-IS1-8, MOB-1618666-IS2-5, DEL-3815810-1, SNP-4635159-T, SNP-1903497-C, SNP-3915089-T
BUT5-2	manY, marC, mppA, rob, glmU, cspC, pyrE	MOB-1907343-IS1-8, DEL-3815810-1, SNP-4635159-T, DEL-1394081-2, SNP-1903497-C, MOB-1618850-IS5-4, SNP-3915089-T
BUT5-3	manY, marC, rob, glmU, cspC, pyrE	MOB-1907343-IS1-8, MOB-1618666-IS2-5, DEL-3815810-1, SNP-4635159-T, SNP-1903497-C, SNP-3915089-T
BUT6-1	manY, yobF, marC, pyrE, rob	SNP-4635243-T, SNP-1903497-C, MOB-1907448-IS5-4, DEL-3815810-1, DEL-1606886-11558
BUT6-3	manY, yobF, marC, pyrE, rob	DEL-1606886-11558, SNP-1903497-C, MOB-1907448-IS5-4, SNP-4635243-T, DEL-3815810-1
BUT6-8	manY, yobF, marC, pyrE, rob	SNP-4635243-T, SNP-1903497-C, MOB-1907448-IS5-4, DEL-3815810-1, DEL-1606886-11558
BUT7-6	manY, yobF, pyrE, rob, mppA	MOB-1907611-IS5-4, SNP-4635203-T, SNP-1903497-C, DEL-3815810-1, DEL-1392752-3292
BUT7-7	manY, yobF, pyrE, rob, mppA	MOB-1907611-IS5-4, SNP-4635203-T, SNP-1903497-C, DEL-3815810-1, DEL-1392752-3292
BUT7-9	manY, yobF, pyrE, rob, mppA	MOB-1907611-IS5-4, SNP-4635203-T, SNP-1903497-C, DEL-3815810-1, DEL-1392752-3292
BUT9-7	pyrE, manY, rob, marC, rraA	DEL-4119238-18, INS-1618379-C, SNP-4635048-C, DEL-3815810-1, SNP-1903497-C
BUT9-10	rraA, manY, marC, rob, pyrE, otsB	INS-1618379-C, SNP-4635048-C, DEL-3815810-1, SNP-1903497-C, SNP-1981720-A, DEL-4119238-18
COUM1-2	rho, fimD, ycfQ, sapC, rpoC, polB, nadR	SNP-3966727-T, SNP-4627958-T, DEL-4546637-1, SNP-1168483-T, SNP-4185540-T, SNP-1354284-A, SNP-64352-C
COUM2-3	rho, atpI, murC, sapF, rpoC, nadR	SNP-1352163-A, DEL-102228-1, MOB-3922629-IS5-4, DEL-4627451-124, SNP-3966751-T, SNP-4185540-T
COUM2-4	rho, atpI, murC, ccmA, sapF, rhaT, rpoC, nadR, yecT	SNP-3966751-T, DEL-102228-1, MOB-2297586-IS5-4, DEL-4627451-124, SNP-4185540-T, SNP-4099695-A, SNP-1352163-A, MOB-1961829-IS5-4, MOB-3922629-IS5-4
COUM2-7	rho, atpI, murC, sapF, rpoC, nadR	SNP-3966751-T, DEL-102228-1, DEL-4627451-124, SNP-4185540-T, SNP-1352163-A, MOB-3922629-IS5-4
COUM3-1	rho, atpI, mprA, dacA, manY, rpoB, hns, pyrE	SNP-663746-T, DEL-3815810-1, DEL-2810080-1165, MOB-1293196-IS5-4, SNP-3966727-T, DEL-260217-13738, SNP-3922483-A, SNP-4183802-G, SNP-1903497-C
COUM3-9	rho, atpI, mprA, dacA, manY, rpoB, hns, pyrE	SNP-663746-T, DEL-3815810-1, DEL-2810080-1165, MOB-1293196-IS5-4, SNP-3966727-T, SNP-4183802-G, SNP-3922483-A, SNP-1903497-C
COUM3-10	rho, atpI, mprA, dacA, manY, rpoB, hns, pyrE	SNP-663746-T, DEL-3815810-1, DEL-2810080-1165, MOB-1293196-IS5-4, SNP-3966727-T, SNP-4183802-G, SNP-3922483-A, SNP-1903497-C
COUM4-2	epmB, rpoA, rpsG, nadR, dcd	SNP-4375431-C, SNP-3473615-T, SNP-2141832-T, SNP-3440924-G, SNP-4627567-T
COUM4-5	rpsG, dcd, yfiN, ompN, nadR, rpoA	SNP-3473615-T, SNP-2141832-T, SNP-3440924-G, SNP-2743181-G, SNP-4627567-T, SNP-1436746-C
COUM4-10	rpoA, rpsG, nadR, dcd	SNP-3473615-T, SNP-2141832-T, SNP-3440924-G, SNP-4627567-T
COUM5-3	rho, atpI, sapF, yphF, ypjC, glnG, rpoC, mrdA, nadR	SNP-3966751-T, MOB-2784452-IS5-4, MOB-2678755-IS5-4, DEL-4054531-104, SNP-667158-T, SNP-4185540-T, SNP-1352163-A, DEL-4628232-1, MOB-3922629-IS5-4

COUM5-5	rho, sapF, ypjC, rpoC, mrdA, nadR	SNP-3966751-T, MOB-2784452-IS5-4, SNP-667158-T, SNP-4185540-T, DEL-4628214-1, SNP-1352163-A
COUM5-8	focA, rho, atpI, sapF, ypjC, tufA, rpoC, mrdA, ydiJ	SNP-3966751-T, MOB-2784452-IS5-4, SNP-954638-T, SNP-1768309-T, SNP-667158-T, SNP-4185540-T, DEL-3471319-1, SNP-1352163-A, INS-3922570-TAG
COUM6-2	rho, yjiP, manY, rnb, yhgE, nusA, pyrE	MOB-1347892-IS5-4, DEL-3815810-1, SNP-3966727-T, SNP-4569172-A, SNP-3317438-A, SNP-1903497-C, SNP-3530902-G
COUM6-5	rho, yjiP, manY, rnb, yhgE, nusA, pyrE	MOB-1347892-IS5-4, DEL-3815810-1, SNP-3966727-T, SNP-4569172-A, SNP-3317438-A, SNP-1903497-C, SNP-3530902-G
COUM6-9	rho, yjiP, manY, rnb, yhgE, nusA, fimC, pyrE	DEL-3815810-1, SNP-3530902-G, MOB-4544671-+G-S5, MOB-1347892-IS5-4, SNP-3966727-T, SNP-4569172-A, SNP-3317438-A, SNP-1903497-C
COUM7-5	rho, mprA, ypjA, manY, prlF, rpoB, ydjH, pyrE	SNP-4183814-A, DEL-3815810-1, SNP-3966727-T, DEL-2810804-1, MOB-1856052-IS5-4, SNP-1903497-C, INS-3277273-TTCAACA, MOB-2782626-IS5-4
COUM7-6	rho, mprA, ypjA, manY, mgrB, rpoB, pyrE	MOB-1908812-IS5-4, SNP-4183814-A, DEL-3815810-1, SNP-3966727-T, DEL-2810804-1, SNP-1903497-C, MOB-2782626-IS5-4
COUM8-1	manY, thrA, pyrE, mprA, yhjK	DEL-3815810-1, DEL-3683736-1, SNP-1903497-C, SNP-2374-T, DEL-2801966-11843
COUM8-6	manY, rho, pyrE, mprA, yhjK	INS-3966718-GAT, SNP-1903497-C, DEL-3685181-273, DEL-3815810-1, DEL-2801966-11843
GLUT1-3	spoT, kgtP, rnb, nagC, rpoC, ydfI	SNP-4186605-C, SNP-1630841-A, SNP-3823664-C, MOB-700614-IS1-9, DEL-2725672-1, SNP-1347104-T
GLUT1-9	rpoC, rnb, spoT, nagC, kgtP	SNP-3823664-C, MOB-700614-IS1-9, DEL-2725672-1, SNP-4186605-C, SNP-1347104-T
GLUT1-10	yiaT, hofM, spoT, insG, sspA, kgtP, proV, greA	SNP-3522182-A, INS-3377241-AGCTCACGATCCACCAGGGTC, INS-2805532-T, MOB-3328463-IS4-11, SNP-3823664-C, MOB-3751884-IS5-4, DEL-2725672-1
GLUT2-1	spoT, kgtP, tomB, ygjP, proV, nagA	SNP-3823751-A, MOB-701614-IS1-9, DEL-2725643-1, SNP-3236414-C, DEL-2804864-13, SNP-481075-G
GLUT2-9	nagA, spoT, rnb, kgtP	SNP-3823751-A, MOB-701614-IS1-9, DEL-2725643-1, DEL-1347882-1
GLUT2-10	rspA, spoT, kgtP, rpoC, proV, nagA	SNP-1654069-C, SNP-4186605-C, SNP-3823751-A, MOB-701614-IS1-9, DEL-2725643-1, DEL-2804864-13
GLUT3-5	rpoC, spoT, kgtP	SNP-3823770-T, SNP-2724971-C, SNP-4186605-C
GLUT3-7	rpoC, spoT, kgtP	SNP-3823770-T, SNP-2724971-C, SNP-4186605-C
GLUT3-9	spoT, kgtP, wzzE, ssuA, rclB, rnt	SNP-318484-T, SNP-996768-A, SNP-1728882-C, INS-2725518-C, INS-3969051-G, SNP-3823759-C
GLUT4-1	nagC, proX, spoT, kgtP	SNP-3824137-T, SNP-2724611-A, DEL-2807199-8, MOB-701188-IS1-9
GLUT4-4	proX, spoT, nagC, kgtP	SNP-2390019-A, MOB-3195220-IS186-4, DEL-2807199-8, MOB-701188-IS1-9, SNP-3824137-T, SNP-2724611-A
GLUT4-10	csiD, rpoC, spoT, kgtP	MOB-2788702-IS5-4, SNP-2724971-C, SNP-4186605-C, SNP-3823751-T
GLUT5-4	ytfR, spoT, sspA, kgtP, yagU, rpoB	DEL-3377359-18, DEL-2725375-1, SNP-3823106-T, DEL-303121-1, SNP-4451123-A, SNP-4181852-C
GLUT5-5	ytfR, spoT, rpoB, sspA, kgtP	MOB-3377491-IS2-5, SNP-4451123-A, DEL-2725375-1, SNP-3823106-T, SNP-4181852-C
GLUT5-9	ytfR, spoT, rpoB, sspA, kgtP	MOB-3377491-IS2-5, SNP-4451123-A, DEL-2725375-1, SNP-3823106-T, SNP-4181852-C
GLUT6-4	kgtP, spoT, yfjL, nagC, cspE	SNP-3823105-A, DEL-657215-25, MOB-700680-IS1-9, DEL-2765456-8, SNP-2725370-C
GLUT6-5	nagC, spoT, yfjL, kgtP, cspE	SNP-2725370-C, SNP-3823105-A, DEL-657215-25, DEL-2765456-8, MOB-700680-IS1-9
GLUT6-10	hcaD, nagA, spoT, rnt, kgtP	INS-2724732-AAAAGC, MOB-701889-IS1-9, SNP-3823139-A, SNP-1728425-A, DEL-2672981-6
GLUT7-2	spoT, rnt, nagC, kgtP	SNP-701396-A, SNP-1728926-C, SNP-2724848-A, DEL-3824201-6
GLUT7-6	nohQ, spoT, rnt, kgtP	SNP-2724848-A, SNP-1636300-G, SNP-1728926-C, DEL-3824201-6
GLUT7-7	kgtP, rlmI, yhfA, ravA, spoT, dkgA, rplM, nagC, rrlA, rrlC, uvrD, ybeF, rsmC, fruB, yhiL, tdcD, yfdC, lldR, yliE, rnt, aceK, roxA, yhfX	SNP-443040-T, DEL-3943892-1, DEL-1029739-1, SNP-3823724-T, SNP-2262665-A, DEL-2465722-1, SNP-3263200-A, DEL-701381-1, SNP-660573-C, SNP-4219696-T, SNP-3779384-G, SNP-4037513-C, INS-3931183-G, DEL-2725672-1, SNP-3510180-C, SNP-874067-A, SNP-1728884-A, SNP-3378539-G, SNP-3485967-G, SNP-3634152-C, SNP-3156603-C, SNP-4607712-T, SNP-1187352-A, DEL-3999387-1
GLUT8-5	rpoC, polB, proV, mprA, kgtP	SNP-2725818-G, DEL-2804864-13, MOB-2810987-IS1-9, SNP-4185540-T, SNP-64352-C
GLUT8-6	kgtP, sapC, rpoC, polB, proV, nagA	DEL-2804864-13, SNP-2725232-A, SNP-1354284-A, SNP-4185540-T, INS-702338-T, SNP-64352-C
GLUT8-9	kgtP, yobF, sapC, sdaC, rpoC, proV, polB, lit	MOB-1907448-IS5-4, DEL-2804926-1, INS-1198505-AATGATGA, DEL-2725209-9, SNP-4185540-T, SNP-2927703-A, SNP-1354284-A, SNP-64352-C
HEXA1-1	ptrA, rpoA, rpoC, bioB, sapB	SNP-809340-G, SNP-3440378-T, SNP-3440212-A, SNP-4185540-T, MOB-2957831-IS5-4, SNP-1354687-A
HEXA1-4	opgH, rpoA, rpoC, bioB, sapB	SNP-809340-G, SNP-3440378-T, DEL-1112435-5, SNP-3440212-A, SNP-4185540-T, SNP-1354687-A
HEXA1-5	sapB, rpoA, rpoC, bioB	SNP-809340-G, SNP-3440378-T, SNP-1354687-A, SNP-4185540-T, SNP-3440212-A
HEXA2-3	pykF, ompR, mdtK, prpE	SNP-353944-A, SNP-1743611-A, DEL-3536285-1, SNP-1756622-A

HEXA2-9	ompR, mdtK, prpE	SNP-1743611-A, SNP-353944-A, DEL-3536285-1
HEXA2-10	rpoA, mdtK	SNP-3440212-A, SNP-3440929-A, DEL-1744016-757
HEXA3-1	rpoC, rpoA, yfjL, mdtK, sapA	SNP-1356317-T, SNP-3440378-T, MOB-1743880-IS1-9, SNP-3440212-A, SNP-2764096-T, SNP-4185540-T
HEXA3-7	mdtK, rpoA, rpoC, yfjL	SNP-3440212-A, SNP-3440378-T, SNP-2764096-T, MOB-1743880-IS1-9, SNP-4185540-T
HEXA3-9	mdtK, rpoA, rpoC, yfjL	SNP-3440212-A, SNP-3440378-T, SNP-2764096-T, MOB-1743880-IS1-9, SNP-4185540-T
HEXA4-4	rpoA, ompR, proQ, glxK, hns	MOB-1293196-IS5-4, MOB-542938-IS5-4, DEL-1915293-5, INS-3536332-T, SNP-3440923-T
HEXA4-7	dosP, rpoA, ompR, proQ, hns	MOB-1293196-IS5-4, INS-3536332-T, DEL-1915293-5, SNP-1564102-G, SNP-3440923-T
HEXA4-10	rpoA, ompR, proQ, hns	MOB-1293196-IS5-4, INS-3536332-T, SNP-1915353-C, SNP-3440923-T
HEXA6-5	sapB, rpoA, mdtK	SNP-3440212-C, DEL-1744675-1, SNP-1354687-A, INS-3440937-CGCTCT
HEXA6-6	rpoA, mdtK	SNP-3440212-C, DEL-1744675-1, INS-3440937-CGCTCT
HEXA6-7	rhmD, rpoA, mdtK, sapB	SNP-3440212-C, SNP-2360829-A, DEL-1744675-1, SNP-1354687-A, INS-3440937-CGCTCT
HEXA6-9	mdtK, rpoA, rsd, sapB	SNP-3440212-C, DEL-1744675-1, INS-3440937-CGCTCT, SNP-1354687-A
HEXA7-2	ompC, emrY, rsfS, sfmF, rpoB, hns, rpoA	MOB-563324-IS1-9, SNP-2481325-A, SNP-4182358-T, MOB-2312877-IS5-4, MOB-1293124-IS5-4, SNP-3440923-T, DEL-668970-1
HEXA8-1	ompC, yedP, sapB, cydA, barA, murG, rpoA	SNP-99891-T, SNP-1354761-T, INS-2025248-TC, MOB-771258-IS5-4, MOB-2312877-IS5-4, DEL-2916392-12, SNP-3440923-T
HEXA8-2	ompC, yedP, sapB, cydA, murG, rpoA	SNP-99891-T, MOB-771306-IS5-4, SNP-1354761-T, INS-2025248-TC, MOB-2312877-IS5-4, SNP-3440923-T
HEXA8-5	ompC, yedP, sapB, murG, rpoC, rpoA	SNP-99891-T, SNP-1354761-T, INS-2025248-TC, MOB-2312877-IS5-4, SNP-3440923-T, SNP-4187619-T
HMDA1-10	purL, rph, spoT, lexA, proV, rpoB, rpsA	SNP-2694102-A, SNP-962939-A, SNP-3816611-A, DEL-2804864-13, SNP-4257602-T, SNP-4181786-T, SNP-3823025-A
HMDA2-1	ptsP, proV, pyrE, rpsA	MOB-2804836-IS1-9, DEL-2968163-1, DEL-3815808-1, SUB-963273-
HMDA2-8	ptsP, proV, pyrE, rpsA	MOB-2804836-IS1-9, SUB-963273-, DEL-2968163-1, DEL-3815808-1
HMDA3-4	rpoC, nagA, pyrE, kup	SNP-3933122-A, INS-702597-G, DEL-3815810-1, SNP-4188767-T
HMDA3-5	nagC, ygeG, kup, ygbT, pyrE, ybeX	SNP-3933122-A, SNP-2879763-A, DEL-3815810-1, DEL-691774-12, SNP-701405-A, SNP-2991218-G
HMDA3-6	gatY, rpoC, nagA, pyrE, kup	SNP-3933122-A, DEL-3815810-1, MOB-2177307-IS1-9, INS-702597-G, SNP-4188767-T
HMDA5-4	ptsP, ampC, pnp, pyrE, nagC	SNP-2966573-G, DEL-3815810-1, SNP-3310266-A, SNP-4378331-G, MOB-700602-IS1-9
HMDA5-5	ptsP, pyrE, nagC, ybeX	SNP-2966573-G, DEL-3815810-1, MOB-700602-IS1-9, SNP-691321-T
HMDA5-10	ptsP, pstB, pyrE, pepA, stpA	SNP-2966573-G, DEL-3815810-1, MOB-2798597-IS1-9, SNP-4485639-C, SNP-3908248-T
HMDA7-1	rpsG, wbbK, sspA, nusA	SNP-3377173-C, DEL-2104077-1, SNP-3473612-C, SNP-3317072-C
HMDA7-7	rpsG, sspA, nusA	SNP-3377173-C, SNP-3473612-C, SNP-3317072-C
HMDA7-10	rpsG, wbbK, sspA, nusA	SNP-3377173-C, DEL-2104077-1, SNP-3473612-C, SNP-3317072-C
HMDA8-5	mdtK, xapR, nagC, proV, cynR, pyrE, lhr, rnt	SNP-1728512-C, DEL-3815808-1, SNP-1732811-T, DEL-2804864-13, SNP-2522653-A, SNP-358399-G, SNP-700980-C, SNP-1744313-A
HMDA8-9	mdtK, nagC, proV, pyrE, lhr, rnt	SNP-1728512-C, DEL-3815808-1, SNP-1732811-T, DEL-2804864-13, SNP-700980-C, SNP-1744313-A
HMDA8-10	mpl, mdtK, nagC, proV, pyrE, lhr, rnt	SNP-1728512-C, DEL-3815808-1, SNP-1732811-T, DEL-2804864-13, DEL-4457113-4, SNP-700980-C, SNP-1744313-A
IBUA1-7	ptsP, pykF, insA, rpoB	SNP-20771-A, MOB-1755755-IS5-4, MOB-2967576-IS5-4, SNP-4183097-T
IBUA1-9	yedV, pykF, rlmE, rpoB, cheR	DEL-255591-18364, SNP-4182938-C, SNP-1969313-A, SNP-2037332-T, MOB-3327665-IS5-4, SNP-1756637-C
IBUA2-1	rpsC, yobF, yijD, bglF, sapD, rpoC, pykF	SNP-4187619-A, DEL-3905639-1, MOB-1907448-IS5-4, SNP-4161966-A, SNP-1352926-T, SNP-3449388-T, MOB-1755687-IS5-4
IBUA2-6	rpsC, yobF, yijD, bglF, sapD, rpoC, pykF	SNP-4187619-A, DEL-3905639-1, MOB-1907448-IS5-4, INS-3449508-GAACATAACGCGACG, SNP-4161966-A, SNP-1352926-T, MOB-1755687-IS5-4
IBUA2-9	rpsC, yobF, yijD, bglF, sapD, rpoC, pykF	SNP-4187619-A, DEL-3905639-1, MOB-1907448-IS5-4, SNP-4161966-A, SNP-1352926-T, SNP-3449388-T, MOB-1755687-IS5-4
IBUA3-10	pykF, sapF, ydbA, rpoB	SNP-4182820-T, SNP-1352163-A, MOB-1472662-IS5-4, MOB-1757082-+G-S5
IBUA4-1	yjjQ, pykF, sapB, rpoB	SNP-4182820-T, SNP-4603494-A, SNP-1354686-C, INS-1756894-TG
IBUA4-8	rpsD, pykF, rpoB	SNP-3441417-A, SNP-4182820-T, INS-1756894-TG
IBUA4-9	yaiP, speA, infA, pykF, rpoB, bglG	SNP-383289-T, SNP-4182820-T, DEL-3084357-1, SNP-926293-T, SNP-3906597-A, INS-1756894-TG

IBUA5-2	rpoS, pykF, prfA, rpoB	SNP-2866767-T, SNP-4182820-T, SNP-1265009-A, SNP-1756217-T
IBUA5-6	rpoS, pykF, prfA, rpoB	SNP-1265009-A, SNP-1756217-T, SNP-4182820-T, DEL-2867337-96
IBUA6-7	glyQ, rpoS, pykF, rpoB, infB, pyrE	SNP-3315513-G, DEL-3815808-1, INS-1756495-A, SNP-3725175-G, DEL-2867356-1, SNP-4184792-T
IBUA6-9	glyQ, rne, prfA, rpoC, pykF, ybbW	MOB-538086-IS5-4, INS-1756495-A, SNP-3725175-G, SNP-1143323-T, MOB-4281707-IS5-4, SNP-1265009-A, SNP-4187214-C
IBUA7-6	sapC, pykF, rpoB	SNP-1756434-G, SNP-4182820-T, SNP-1354314-G
IBUA7-7	sapC, pykF, rpsL, rpoB, lysU	SNP-4182820-T, SNP-4354843-T, SNP-1756434-G, SNP-3474485-A, SNP-1354314-G
IBUA7-9	gadE, pykF, sapC, rpoB	SNP-1756434-G, SNP-4182820-T, SNP-1354314-G
IBUA8-3	pykF, glyQ, ilvH	DEL-3815859-82, SNP-87381-T, SNP-3725175-G, INS-1756495-A, DEL-1995819-40006
IBUA8-4	pykF, glyQ, ilvH	DEL-1995819-40006, SNP-87381-T, SNP-3725175-G, DEL-3815859-82, INS-1756495-A
IBUA8-10	rrsA, glyQ, ilvN, pykF, yffQ	SNP-3725175-G, INS-1756495-A, SNP-2563402-A, SNP-4037067-C, DEL-3815859-82, SNP-3851044-G
OCTA1-3	rpoA, mreB, arpA, sapB, lit	INS-1198505-AATGATGA, MOB-4222091-IS1-9, SNP-3400673-C, SNP-3440923-T, SNP-1354687-A
OCTA1-5	lit, mreB, rpoA, yejO, sapA	MOB-2290201-IS5-4, SNP-1356297-T, SNP-3400673-C, DEL-1198498-8, SNP-3440923-T
OCTA1-9	lit, rpoA, mreB, sapA	SNP-3440923-T, SNP-1356297-T, SNP-3400673-C, DEL-1198498-8
OCTA2-10	dusB, cydX, rpoC, rlmH, nrdE	SNP-2803042-A, INS-774243-T, SNP-668691-A, MOB-3410273-IS5-4, INS-4186115-TTCCGCTGG
OCTA2-14	dusB, rpoC, rlmH	SNP-668691-A, INS-4186115-TTCCGCTGG, MOB-3410273-IS5-4
OCTA2-16	dusB, rpoC, rlmH	SNP-668691-A, INS-4186115-TTCCGCTGG, MOB-3410273-IS5-4
OCTA4-9	rpoA, trkH, mrdB	SNP-665850-T, SNP-4033217-A, SNP-3440923-T
OCTA4-10	rpoA, trkH, mrdB	SNP-665850-T, SNP-4033217-A, SNP-3440923-T
OCTA4-13	sapD, rpoA, mreB	SNP-3440923-T, SNP-3400300-A, SNP-1353062-A
OCTA5-4	gtrS, rpoC, ydcI, yihQ	MOB-4069461-IS5-4, SNP-1495028-C, SNP-4186605-C, MOB-2469636-IS5-4
OCTA5-8	recE, ydcI, rpoC, hns, gtrS, yihQ	MOB-4069461-IS5-4, SNP-4186605-C, MOB-1293196-IS5-4, MOB-1416518-IS5-4, SNP-1495028-C, MOB-2469647-IS5-4
OCTA5-9	rpoC, ydcI, yihQ	MOB-4069461-IS5-4, SNP-4186605-C, SNP-1495028-C
OCTA7-2	dusB, rpoC, mreC, pyrE, ycfQ	DEL-3410240-1, DEL-3815808-1, SNP-1168895-T, SNP-4186605-C, SNP-3399666-A
OCTA7-9	mreC, yfcZ, ycfQ, rpoC, dusB, pyrE	DEL-3815808-1, SNP-4186605-C, SNP-2460805-A, DEL-3410240-1, SNP-1168895-T, SNP-3399666-A
OCTA7-10	dusB, rpoC, mreC, pyrE, ycfQ	DEL-3410240-1, DEL-3815808-1, SNP-1168895-T, SNP-4186605-C, SNP-3399666-A
OCTA8-5	gtrS, hfq	MOB-2469886-IS1-9, SNP-4400417-T
OCTA8-7	gtrS, yciA, hfq	SNP-1311924-C, MOB-2469886-IS1-9, SNP-4400417-T
PUTR2-4	rpoC, cspC, mreB	SNP-4186706-A, INS-1907273-CGTCCTG, SNP-3400986-C
PUTR2-6	rpoC, cspC, mreB	SNP-4186706-A, INS-1907273-CGTCCTG, SNP-3400986-C
PUTR3-1	rph, ygaC, spoT, iscR, lexA, edd, proV, nusG, fliK, icdC	SNP-2661793-A, SNP-2799867-A, INS-2018716-CGGTGGCTG, SNP-3816611-A, SNP-1211308-T, SNP-4257602-T, INS-2804946-T, SNP-3823025-A, SNP-1934806-T, SNP-4178239-T
PUTR3-9	rph, spoT, yphF, yfjW, lexA, pstS, mreB	MOB-2678755-IS5-4, SNP-3816611-A, SNP-3400453-G, SNP-4257602-T, DEL-2774809-1, SNP-3823025-A, INS-3911366-T
PUTR3-10	rph, ygaC, spoT, iscR, lexA, tyrB, proV, nusG, icdC	SNP-2661793-A, SNP-2799867-A, SNP-3816611-A, SNP-4267824-C, SNP-1211308-T, SNP-4257602-T, DEL-2904286-122, INS-2804946-T, SNP-3823025-A, SNP-4178239-T
PUTR4-3	mrdB, cspC, proV, clpX, rpoB	DEL-457406-7, INS-2805131-T, MOB-1907410-IS5-4, SNP-4183154-T, SNP-665554-T
PUTR4-7	mrdB, proV, cspC, rpoB, rpsA	MOB-1907410-IS5-4, INS-2805131-T, SNP-4183154-T, SNP-962473-T, SNP-665554-T
PUTR4-8	glyX, ycgB, proV, rpoB, rpsA, cspC, mrdB	DEL-4392446-1, SNP-4392456-G, SNP-4183154-T, SNP-962473-T, SNP-4392453-T, INS-2805131-T, MOB-1907410-IS5-4, DEL-1236007-50, SNP-665554-T
PUTR5-1	spoT, pykF, fliR, waaS, pstS, mreB, yjhG, ybcK	DEL-3910569-7, SNP-3401016-C, SNP-4522146-A, MOB-2023551-IS5-3, SNP-3823799-T, SNP-568660-T, SNP-1755770-A, DEL-3805056-1
PUTR5-6	ytfR, rpoC, rpoD	SNP-3214770-C, SNP-4186551-G, SNP-4452005-A
PUTR5-8	rpoC, rpoD	SNP-3214770-C, SNP-4186551-G
PUTR6-2	yieK, stpA, pstA, sspA, murA	DEL-3908805-2, SNP-3899249-G, SNP-3377150-A, SNP-3336073-G, MOB-2798597-IS1-9
PUTR6-7	yeaR, nmpC, rph, yobF, intE, rpoC, proV, rpsA, cmtB, glnE	MOB-1907448-IS5-4, SNP-4186186-C, DEL-2804864-13, MOB-1879829-Δ1-:, DEL-3815859-82, SNP-3079559-T, SNP-962933-G, SNP-576891-T, DEL-3197154-12, MOB-1199680-IS1-8

PUTR6-10	yeaR, nmpC, rph, tdcR, yobF, tolA, yjcF, proV, rpsA, cmtB, intE	MOB-1907448-IS5-4, SNP-3267294-T, DEL-777151-48, SNP-4282760-C, DEL-2804864-13, MOB-1879829-Δ1-:, DEL-3815859-82, SNP-3079559-T, SNP-962933-G, SNP-576891-T, MOB-1199680-IS1-8
PUTR7-1	rpsA, spoT, mreB, nusA	SNP-3823799-A, SNP-3316916-C, SNP-962922-T, SNP-3400811-T
PUTR7-7	rpoD, rpoB, murA	SNP-3214770-C, SNP-3335317-G, SNP-4183154-T
PUTR7-9	rpoD, mdtJ, rpoB, murA	SNP-4183154-T, SNP-3335317-G, DEL-1673532-181, SNP-3214770-C
PUTR8-3	spoT, rpsG, proX, mreB, pyrE, argG	SNP-3400195-A, SNP-3318960-A, DEL-3815808-1, INS-2807248-T, SNP-3473612-C, SNP-3823811-A
PUTR8-6	yedP, spoT, rpsG, nagC, proX, mreB, leuL, pyrE, argG	SNP-2025435-A, SNP-3400195-A, SNP-3318960-A, DEL-3815808-1, INS-2807248-T, DEL-83679-3, DEL-701233-1, SNP-3473612-C, SNP-3823811-A
PUTR8-10	spoT, rpsG, nagC, proX, mreB, sfmH, pyrE, argG	SNP-3400195-A, SNP-3318960-A, DEL-3815808-1, INS-2807248-T, DEL-700785-47, SNP-3473612-C, SNP-562667-C, SNP-3823811-A

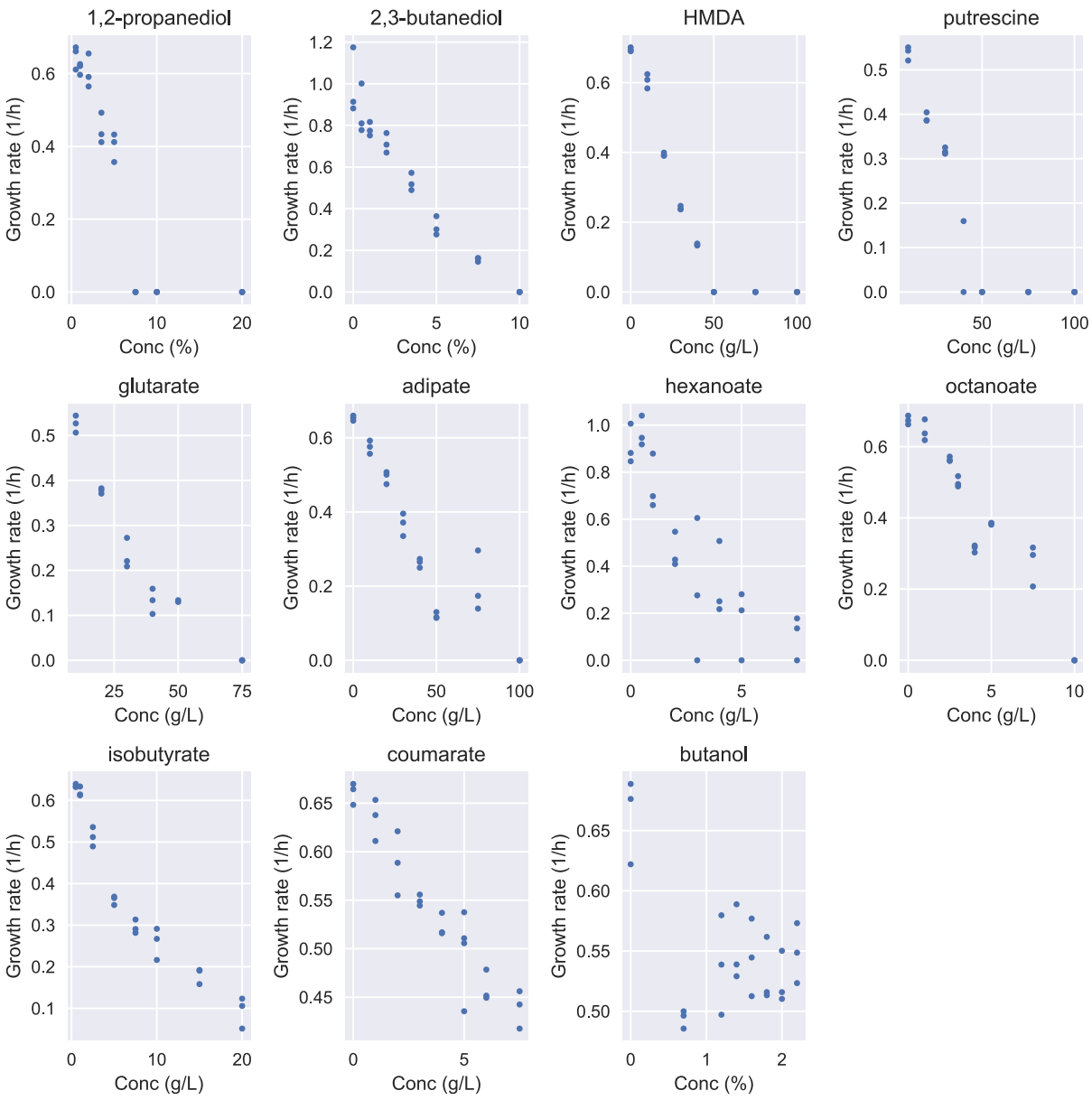

Supplementary Figure 1: *Compound toxicity screening. Growth rates of MG1655 for varying concentrations of the 11 selected compounds. Each individual concentration was tested in biological triplicates.*

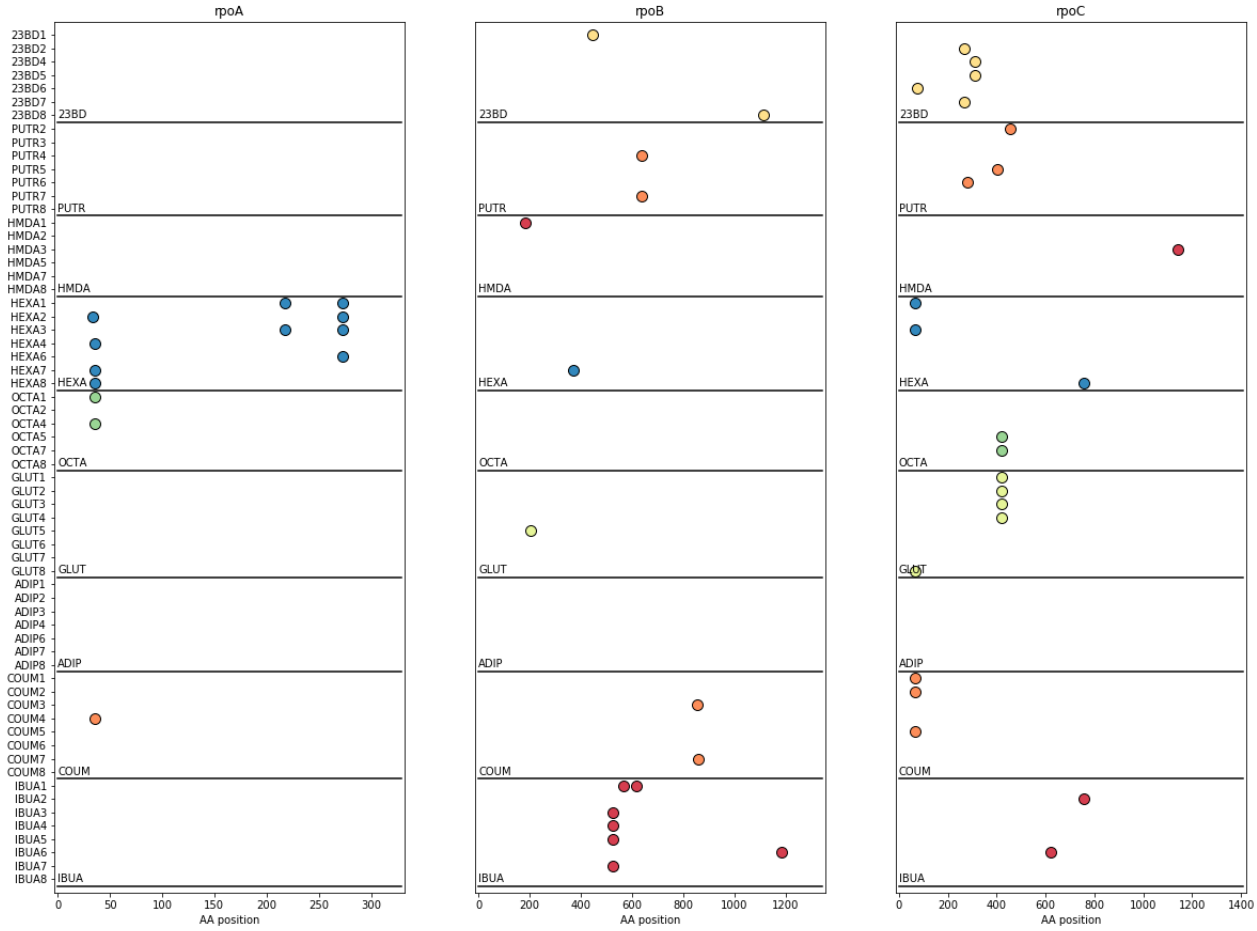

Supplementary Figure 2: *Overview of the locations of observed mutations in RNA polymerase genes. The mutations are shown per population. Mutations found in at least one isolate from a given population are included in the plot.*

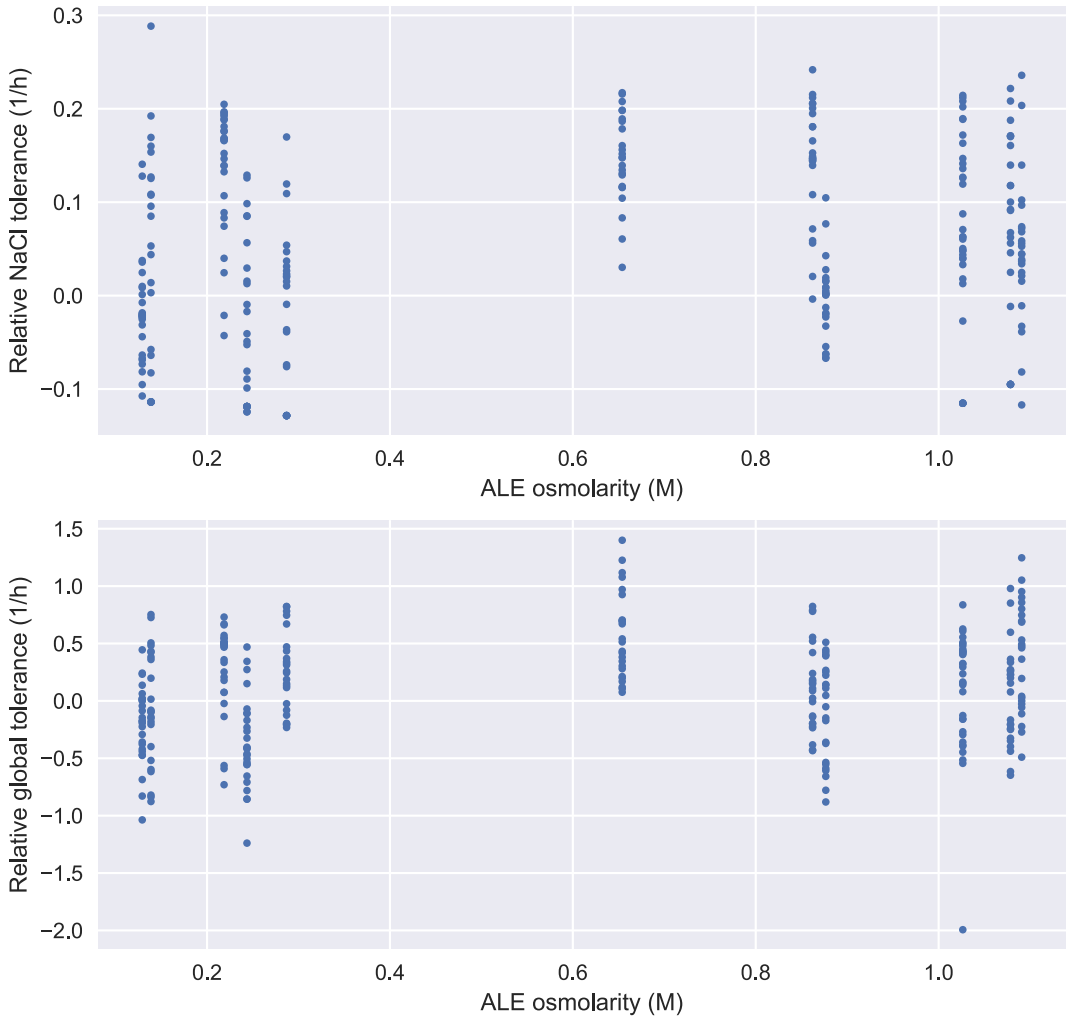

Supplementary Figure 3: *Relationship between final osmolarity of ALE and NaCl tolerance and global tolerance, respectively. Global tolerance is calculated as the mean tolerance to all the 11 chemicals. Each point represents a single evolved strain. The differences in osmotolerance and global tolerance between strains from different conditions does not seem to be caused by the differences in osmolarity between the conditions.*

Chapter 2: The metabolism of evolved tolerance

2.1 Introduction

As seen in the previous chapter, ALE can be used to quickly produce strains with improved characteristics for a target phenotype. Specifically, it was demonstrated that strain tolerance to several industrially relevant products could be improved significantly through ALE. Sequencing the evolved strains allows identification of the exact genetic changes that give rise to the improved phenotypes. Although such improvements can be very valuable in a strain engineering process, it is often desirable to also obtain a deeper understanding of the evolved strains and the observed mutations, i.e. what impact a mutation has on the cell, and why the presence of the mutation confers a growth advantage in the evolution condition. Elucidating such mechanisms of adaptation requires further characterization of the evolved strains in order to investigate how each strain differs from the unevolved parent strain. For instance, changes in regulation or metabolism can give indications of key cellular mechanisms that mediate the adaptive improvement of a desirable phenotype such as tolerance.

In metabolic engineering, where the ultimate objective is to reroute metabolic flux to production pathways, adaptive changes in metabolism are especially interesting. A key question to ask after successful strain optimization with ALE is thus whether the mutations have caused metabolic perturbations, and whether these perturbations are related to the observed growth adaptations. Metabolic changes are amenable to study using metabolomics methods, or other methods that derive from metabolomics such as fluxomics. While fluxomics would be the most informative way to examine metabolic flux rerouting, this approach primarily gives information on central carbon metabolism and is also challenging to apply to large numbers of strains due to the experimental and computational efforts required (Niedenführ et al., 2015). Metabolomics on the other hand can be performed relatively quickly and cheaply and also provides insight into the functioning of the strain's metabolism. Data obtained with different metabolomics methods differ with regard to both quality, e.g. the precision of the measurements and whether the data is absolute or relative; and quantity, e.g. how many metabolites are covered and how quickly a sample can be run (Griffiths and Wang, 2010). Since there is usually a trade-off between quality and quantity, the choice of method depends on the requirements for the specific use case.

In this chapter a metabolomic characterisation of the ALE strains obtained from the study in Chapter 1 will be described. For this analysis a high-throughput, high-coverage untargeted metabolomics method (Fuhrer et al., 2011) was chosen, sacrificing some data quality in exchange for the ability to characterize a larger number of strains. The chosen method is a direct-injection mass-spectrometry method, meaning that the samples are injected into a mass spectrometer without any prior chromatography. Whereas more traditional chromatography-coupled mass-spectrometry methods provide a list of ions annotated with mass-charge ratio and column retention time, a direct-injection method only provides mass-to-charge ratio (Fuhrer and Zamboni, 2015). This makes the subsequent metabolite annotation less accurate and prevents discrimination of isomers but increases throughput dramatically. The method does not use any standards, which limits measurements to relative ion intensities but allows a high coverage of known metabolites to be obtained. Objectives of the metabolomic characterization of the tolerant ALE strains were to:

1. Determine the metabolic similarity between strains evolved to tolerate the same or different chemicals
2. Investigate to which extent metabolism is involved in the evolution of chemical tolerance
3. Use the metabolomics information to elucidate in more detail the effect of each mutation observed in the evolved trains.

In addition to the metabolomic characterization of the ALE strains, metabolomics was also used to try to characterize the toxic effects of each chemical to a wild type strain from a metabolic perspective.

2.2 Methods

2.2.1 Strains

The strains used in this study were isolates from a series of evolution experiments designed to evolve chemical tolerance to industrially relevant compounds (See Chapter 1). All these strains were derived from *E. coli* K12 MG1655, which was also used as the reference strain for all analyses. As almost all strains evolved on 1,2-propanediol were hypermutators, no strains from this condition were included in this study. Due to problems with evaporation during the butanol evolutions, the evolved strains did not have significant increases butanol tolerance and were also not included in

this study. The strains that were used were evolved on 2,3-butanediol (23BD), hexamethylene-diamine (HMDA), putrescine (PUTR), glutarate (GLUT), adipate (ADIP), hexanoate (HEXA), octanoate (OCTA), isobutyrate (IBUA) and coumarate (COUM).

2.2.2 Mass spectrometry

All metabolomics data was obtained from an Agilent qTOF 6550 instrument, using a direct injection method with no prior chromatography step (Fuhrer et al., 2011).

2.2.3 Cultivations

All cultures were grown in triplicates in 96-deep well plates with sandwich cover lids at 37 deg.C with shaking at 300 rpm. The growth medium was M9 (6.8 g/L Na_2HPO, 3 g/L $KH2PO_4$, 1 g/L NH_4Cl, 0.5 g/L NaCl, 1 mM $MgSO_4$, 0.1 mM $CaCl_2$) with 1% glucose. Additionally, the medium contained the following trace elements: 22.17 µM ethylenediaminetetraacetate, 7.82 µM ZnSO, 1.77 µM $MnCl_2$, 0.63 µM $CoCl_2$, 0.51 µM $CuSO_4$, 0.83 µM Na_2MoO_4, 5.40 µM $FeSO_4$, 8.09 µM H_3BO_3, 0.30 µM KI.

2.2.4 Metabolic profile characterization

2.2.4.1 Sampling

The strains were cultivated overnight and reinoculated in fresh medium. In each cultivation plate the MG1655 reference strain was inoculated to 12 different starting densities over a 15-fold range in order to obtain a large number of reference metabolite measurements at different densities. When the cultures were at densities between OD600 of 0.5 and 1.5 they were sampled at three to four timepoints with approximately 1-hour intervals. The samples (30 µL of each culture) were immediately quenched in 120 µL cold extraction solution (50% methanol, 50% acetonitrile). The densities of the cultures were measured on a Tecan Sunrise plate reader at each sampling.

The quenched samples were incubated at -18 deg.C for 2 hours and centrifuged at 3000x g for 10 minutes. The supernatants were transferred to clean plates, which were sealed and kept at -80 deg.C until the time of mass spectrometry measurements.

2.2.4.2 Data processing

All detected ions were matched to deprotonation products of native *E. coli* metabolites by mass/charge ratio with a tolerance of 0.003 Dalton/charge. The list of native *E. coli* metabolites was obtained from the *i*JO1366 genome-scale reconstruction (Orth et al., 2011). Ion intensities were normalized by OD and compared to the MG1655 reference. This was done by fitting a linear relation between $\log_2$(OD) and $\log_2$(intensity) for the MG1655 reference samples for each ion

$$\log\left(intensity_{ref}\right) = \alpha \cdot \log\left(OD_{ref}\right) + \beta \tag{1}$$

For each sample a log Fold Change (logFC) for each ion was calculated by the deviation from the linear relation for MG1655, as shown in Figure 1.

$$logFC = \log(intensity_{mut}) - \alpha \cdot \log(OD_{mut}) - \beta \tag{2}$$

Evolved strain logFC's were calculated as the mean logFC for all the corresponding samples taken at a culture density between 0.5 and 1.5.

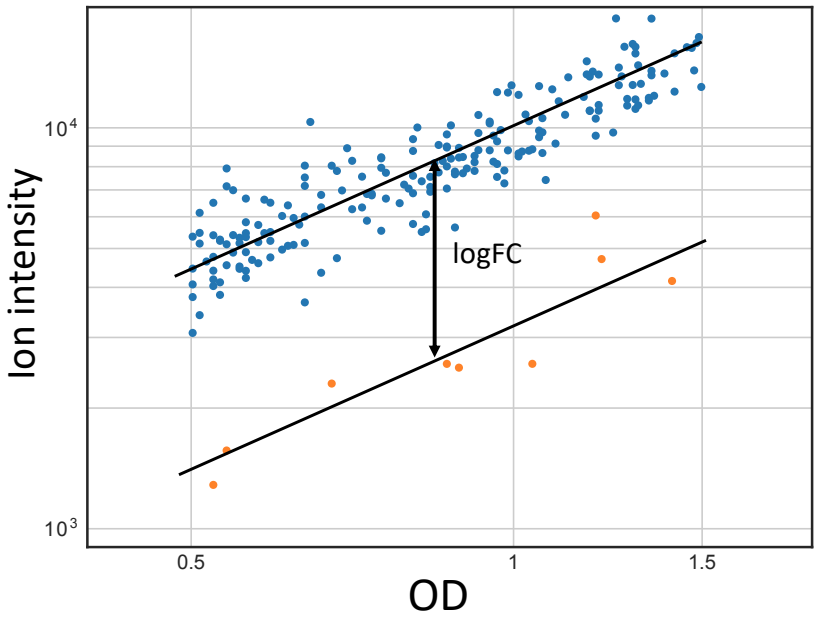

Figure 1: *Illustration of the calculation of logFC from the correlations of log(OD) and log(intensity) for the reference strain and a mutant strain. The blue points show OD and ion intensities for samples from the reference strain, while the orange points are samples from the mutant. The parallel linear trends between log(OD) and log(intensity) for the two strains show that the ion is systematically less abundant in the mutant strain compared to the reference strain.*

2.2.5 Chemical perturbation

2.2.5.1 Sampling

Cultures of MG1655 were grown in M9 medium with 1% glucose overnight and reinoculated in fresh medium inside a 37 deg.C climate chamber where all the chemical perturbation experiments were carried out using temperature-equilibrated equipment and materials. When the cultures reached OD 1, a sample of 20 µL was transferred to 80 µL cold extraction mix, as a baseline measurement. 390 µL of culture was then transferred to a well containing 10 µL of a solution of the given chemical and quickly mixed by pipetting. Immediately after, 200 µL of the perturbed culture was aspirated in an electronic pipette. At each sampling time 20 µL was dispensed into 80 µL of cold extraction mix. Sampling times were 10, 20, 30, 45, 60, 80, 100, 120, 180 and 300 seconds after perturbation. This was replicated for three separate cultures per perturbation chemical, and nine cultures for perturbation with water. The used perturbation concentrations are shown in Table 1.

2.2.5.2 Data processing

All detected ions were matched to deprotonation products of native *E. coli* metabolites by mass/charge ratio with a tolerance of 0.003 Dalton/charge. The list of native *E. coli* metabolites was obtained from the *i*JO1366 genome-scale reconstruction (Orth et al., 2011). For each annotated ion, the response to each chemical perturbation was compared to the response to the water perturbation. A linear model was used to identify significant interactions between metabolites and chemical perturbations, i.e. metabolites that responded differently to perturbation with the chemical compared to water. The linear model was given as:

$$\log(y_i) = \alpha + \beta_{condition_i} + \beta_{time_i} + \beta_{condition_i:time_i} + \epsilon_i \quad (3)$$

The left-hand term is the logarithm of the intensity of the ion in question for a sample i, while the right-hand side contains the intercept and the parameters associated with the condition and time point of sample i, as well as the residual, ϵ_i. The significance of the interaction term was tested using analysis of variance. For each condition the interaction p-values for each ion were corrected for multiple comparisons using the Benjamini-Hochberg False Discovery Rate (Benjamini and Hochberg, 1995). A corrected p-value less than 0.05 was considered evidence that the time-dependent response of the ion was different between the perturbation condition and the water

control. Additional control samples containing each one of the perturbation compounds and no cells were used to exclude ions that are associated with the perturbation compounds themselves.

2.3 Results and discussion

2.3.1 Metabolic characterization of evolved strains

All 169 evolved strains from the nine selected evolution conditions (2,3-butanediol (23BD), hexamethylenediamine (HMDA), putrescine (PUTR), glutarate (GLUT), adipate (ADIP), hexanoate (HEXA), octanoate (OCTA), isobutyrate (IBUA), and coumarate (COUM)) as well as the reference strain were subjected to metabolic characterization. Including biological replicates and multiple samplings, this resulted in a total of 2103 samples being analysed. Of the detected ions, 544 could be matched to metabolites found in the iJO1366 genome-scale metabolic model of *E. coli*. For each evolved strain, a metabolic profile was constructed, defined as the calculated logFC of each of these 544 ions compared to the reference strain.

The first question to be addressed was that of metabolic similarity between strains evolved in the same and different selective conditions, respectively. This was done by comparing the metabolic profiles of all evolved strains measured in a standard reference condition (M9 with 1 % glucose). Metabolic similarity can be defined as a function of the Euclidean distance between two metabolic profiles in the N-dimensional metabolic space, with N being the number of measured metabolites. All metabolic similarities were visualized simultaneously using the nonlinear dimensionality reduction method *t-distributed Stochastic Neighbour Embedding* (t-SNE) (van der Maaten and Hinton, 2008). Since the metabolic similarities between independently evolved populations in particular were of interest, metabolic profiles for each independent population were calculated as a simple mean of all isolates from that population. A t-SNE visualization of the metabolic similarities between independently evolved populations is shown in Figure 2. The t-SNE plot shows a very clear trend of high similarity between populations evolved in the same condition compared to populations evolved in different conditions. This suggests that each evolutionary condition has conferred a characteristic metabolic fingerprint that distinguishes the strains evolved in a given condition from strains evolved in other conditions. The existence of such a characteristic metabolic phenotype in all strains from a given conditions is evidence of some degree of convergent evolution,

i.e. parallel populations finding genetically distinct paths towards similar phenotypes, as opposed to parallel populations evolving to metabolically distinct phenotypes with similar fitness.

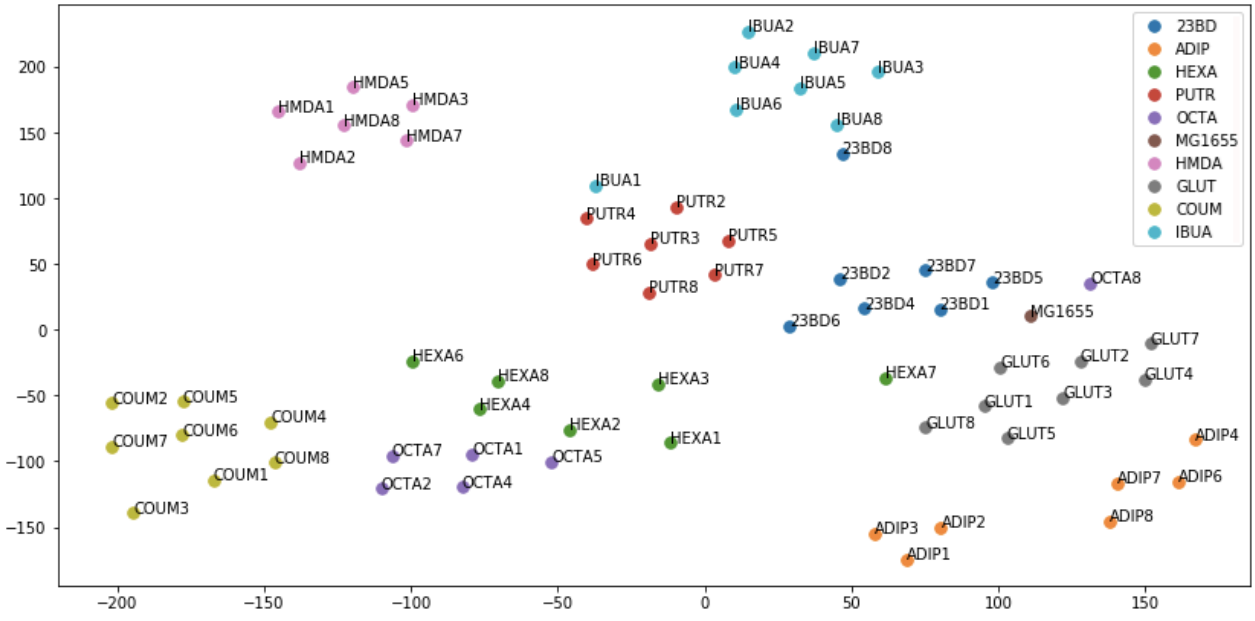

***Figure 2**: t-SNE plot of all evolution populations and MG1655 based on the mean metabolic profile of strains from each population. Each point represents a single independent population and is coloured by the condition it was evolved in.*

Given that each evolution condition seems to be associated with a characteristic metabolic profile, a relevant question was to which degree these metabolic profiles correlated with the tolerance phenotypes that the strains were evolved for. If the characteristic metabolic profiles are associated with tolerance phenotypes, it would be expected that evolution conditions with similar characteristic metabolic profiles would also result in strains with similar tolerance profiles, as measured by tolerance to each of the toxic chemicals (see Chapter 1, Figure 3a). To investigate this, each condition's characteristic metabolic profile was calculated as the centroid of the metabolic profiles of all isolates from that condition. Similarly, the mean tolerance profile for each condition was calculated as the centroid of tolerance profiles of all isolates from that condition. For each of the 36 pairs of evolution conditions, the cosine similarity between their metabolic and tolerance profiles, respectively, were compared. A scatter plot of this comparison is shown in Figure 3, showing a positive correlation (Pearson's r = 0.44, p = 0.0001) between metabolic similarity and tolerance similarity. This could indicate that the metabolic state plays a role in chemical tolerance,

even though non-metabolic factors are clearly also involved, given the modest correlation coefficient.

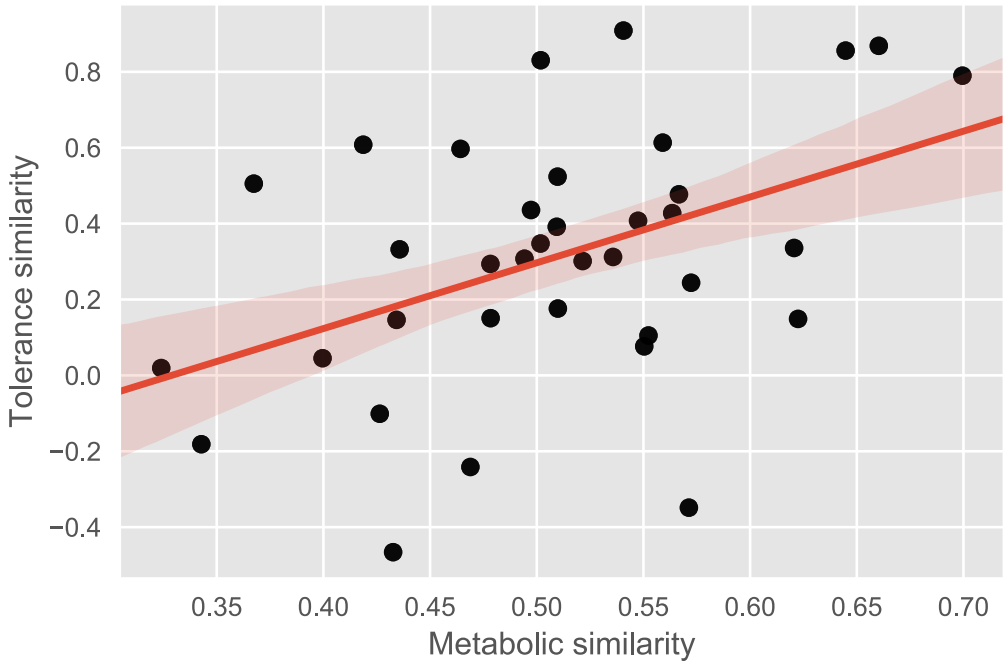

Figure 3: *Comparison of the metabolic similarity and phenotypic similarity between all 36 pairs of evolution conditions.*

Since independent populations evolved in the same condition seem to have reached similar metabolic phenotypes, a reasonable hypothesis would be that the metabolic phenotype in question is involved in the mechanism of tolerance. The reasoning in this argument is identical to the one used in Chapter 1 to hypothesize that a mutation arising independently in several parallel populations is likely to be directly related to tolerance. To investigate this hypothesis, the first step is to elucidate the details of the characteristic metabolic profile for each condition – in other words, which specific metabolic changes are characteristic for strains from a single condition?

While the t-SNE algorithm is a powerful method for identifying complex structures in large datasets, it partly sacrifices interpretability compared to simpler methods. While structure found by Principal Components Analysis can be investigated by analyzing the individual component vectors, no similar strategy can be applied with t-SNE, as the dimensionality reduction is not based on a linear transformation but on a complex non-linear mapping (Gisbrecht and Hammer, 2015). Instead an approach based on decision trees was used (Tan et al., 2005). For each evolution condition a decision tree was used to predict whether a strain was evolved in this condition or not based on the

measured metabolites. Because the rules of a fitted decision tree can be easily inspected, this allowed identification of metabolites that are important for distinguishing strains from a given condition from the remaining strains. Important metabolites were found by inspecting the nodes near the root of the tree. The usefulness of each single metabolite for distinguishing strains could then be visualized by showing the distribution of relative concentrations of this metabolite within each group of strains (Figure 4). Each panel of Figure 4 displays the logFC values for a metabolite that was found to be important for distinguishing strains from at least one of the evolution conditions. The points represent strains, separated by the conditions they were evolved in. This analysis shows that there are indeed metabolites in all conditions, that have consistently either increased or decreased concentrations in most strains. This confirms the pattern seen from Figure 2 of strains from the same condition being metabolically similar.

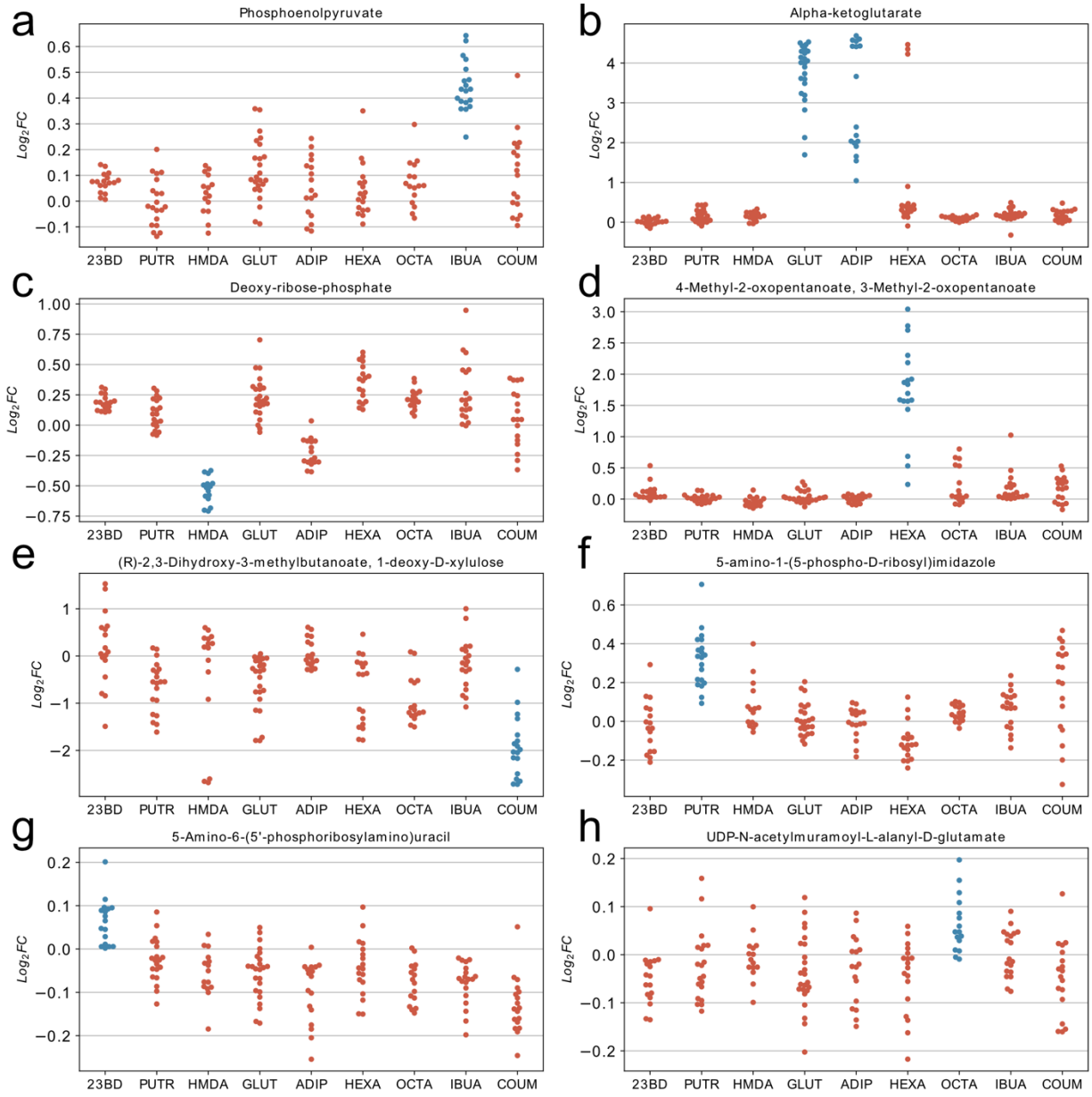

Figure 4: *The distributions of relative metabolite concentration for eight different metabolites that were found to be important for distinguishing strains from at least one condition. The points represent strains split by the condition they were evolved in. The conditions where the given metabolite was found to be important for distinguishing strains are highlighted in blue.*

In some cases, the consistently perturbed metabolites correspond to similar mutations seen in all strains from a given condition. More specifically these cases are the strains evolved on isobutyrate, glutarate and adipate. The strains evolved on isobutyrate all had mutations in the *pykF* gene and also had increased phosphoenolpyruvate (PEP) levels (Figure 4a). A disruptive mutation in the pyruvate kinase encoded by *pykF* could well be expected to create a bottleneck at this step, causing the substrate PEP to accumulate (Chapter 1, Figure 5d). While the presence of high PEP levels in the

isobutyrate strains is not surprising, it can help understand the effect of *pykF* mutations in these strains. PEP is a known regulator of upper glycolysis, specifically by inhibiting phosphofructokinase activity (Uyeda, 2006), and thus the isobutyrate strains presumably have decreased flux through the Embden-Meyerhof-Parnas pathway and increased flux through the Entner-Doudoroff or pentose phosphate pathways instead. The strains evolved on glutarate and adipate all had mutations in the *kgtP* gene, and also had very high levels of alpha-ketoglutarate (AKG) (Figure 4b). Since *kgtP* encodes an active AKG importer (Seol and Shatkin, 1991) this might seem unintuitive. This result can however be explained by AKG leaking out through the cell membrane, which has previously been documented (Yan et al., 2011). In the absence of a transporter to bring AKG back in, it will accumulate extracellularly resulting in high concentrations in the whole-culture sample being injected into the mass spectrometer.

The above cases are examples of convergent evolution on the genetic level, as all the independent populations have mutations in the same gene, which can explain the corresponding metabolic feature (high PEP or AKG levels respectively). In other conditions there is evidence of convergent evolution on the metabolic level, as all isolated strains share certain metabolic characteristics despite not having specific mutations in common. Examples of such conditions are HMDA and hexanoate. All the strains evolved on HMDA had decreased levels of deoxy-ribose-phosphate (Figure 4c). This cannot be explained by a common genetic change, as no single gene was mutated in all these strains. Indeed, one population did not have any mutational overlap with any one of the remaining populations. Likewise, all strains evolved on hexanoate had increased levels of methyl-2-oxopentanoate (Figure 4d) even if these strains do not share any universal mutations. The presence of characteristic phenotypic (e.g. metabolic) commonalities between strains with little or no genetic overlap might provide insight into the mechanisms with which individual genes contribute to tolerance. If gene A is mutated in some strains while gene B is mutated in other strains, it is likely that tolerance arises mechanistically from an effect that genes A and B have in common. In trivial cases genes A and B might simply be analogous, e.g. subunits of the same complex or different steps in a linear pathway, whereas if A and B have diverse sets of effects, such as transcriptional regulators, overlaying the two sets of effects with each other might indicate which effects are important for tolerance. While this method can be used for many different types of phenotypic

effects, the effects of each mutation must generally first be characterized, and thus, depending on the effect phenotype in question, a significant amount of work is required.

Further analyses were performed to elucidate the relationship between mutations and metabolic profiles in the evolved strains. A simple statistical model with a specific metabolite as dependent variable and mutations as independent variables could be used, but due to the very high degree of collinearity between the mutations (because of common ancestry as well as shared evolution conditions), fitting such a model was not considered feasible. Instead, previously published data on the relationship between genes and metabolites was used, in the form of metabolomics data for all single-gene knockout *E. coli* strains in the Keio collection (Fuhrer et al., 2017). This data provides information on the associations between genes and metabolites and can help estimate the impact on gene function of the individual mutations observed in the evolved strains, which is generally not known. A statistical model was used having the full metabolite profile as dependent variable and the impact of each mutation on the affected gene(s) as independent variable, given the gene knockout metabolite data from Fuhrer et al. (2017). To keep the model complexity reasonable some simplifying assumptions were made. First, the impact of a mutation on the function of a gene was quantified as a continuous univariate variable ranging from loss-of-function through neutral to gain-of-function. Second, the combined effect of several mutations on the metabolic profile was assumed to simply be the sum of each individual mutation effects on the metabolic profile. The resulting model is a multivariate linear model given by

$$Y = X \cdot W \cdot M \cdot K + \epsilon \tag{4}$$

Y is the matrix of relative metabolite concentrations in the evolved strains and has shape $N_{strains}$ x $N_{metabolites}$. *X* is a binary design matrix encoding the mutations found in each strain and has shape $N_{strains}$ x $N_{mutations}$, where $N_{mutations}$ is the number of unique mutations identified in the evolved strains. *W* is the parameter to be fitted and is a diagonal $N_{mutations}$ x $N_{mutations}$ matrix, where the diagonal contains the estimated impact score of each mutation (loss-of-function, neutral or gain-of-function). *M* is a second binary design matrix encoding which genes each mutation affects, and has shape $N_{mutations}$ x N_{genes}, where N_{genes} is the number of unique mutated genes in the evolved strains. Finally, *K* is a N_{genes} x $N_{metabolites}$ matrix containing the relative metabolite concentrations in each single-gene knockout strain. The parameter matrix *W* was fitted through gradient descent by

minimizing the sum of squares of the error term, ϵ. The fitted model can be used to get estimated impact scores, predicting whether each mutation has a loss-of-function or gain-of-function effect. A positive estimated impact score was interpreted as loss-of-function, while a negative estimated impact score was interpreted as gain-of-function.

Validating the estimated mutation impacts is difficult since, as mentioned earlier, it is not known what the real impacts of most mutations are. However, a rough classification into expected deleterious and non-deleterious mutations can be made based on their type and location in the genome alone. For deletions, insertions and mobile element insertions, a mutation was expected to be deleterious if it was within the coding sequence of a gene, while the majority of mutations located outside of coding sequences were not expected to be deleterious. For SNP's only nonsense (stop codon inducing) polymorphisms would be expected to be highly deleterious. Comparing the impacts estimated from mutation location to the impacts estimated by the model using metabolomics data showed that mutations expected to be deleterious were significantly more often estimated to have loss-of-function impacts (83 out of 156) compared to mutations not expected to be deleterious based on location (111 out of 305) (Fisher's exact test, $p < 0.001$). This pattern of association between impact estimated from mutation location and impact estimated from metabolomics data is apparent in all four types of mutations, as seen from Figure 5, which shows the fraction of mutations of different types being estimated to have loss-of-function impacts. This supports the validity of interpreting the impact scores estimated with the model using metabolomics data as an indicator of whether the mutation has a gain-of-function or loss-of-function effect. It is worth noting however, that the location-estimated impact of a mutation cannot be regarded as a classification of the true impact, and thus the predictive performance of the model-estimates cannot be accurately assessed. Particularly the assumption that all missense SNP's are non-deleterious is dubious, given the knowledge that many proteins are indeed sensitive to amino-acid substitutions in active sites.

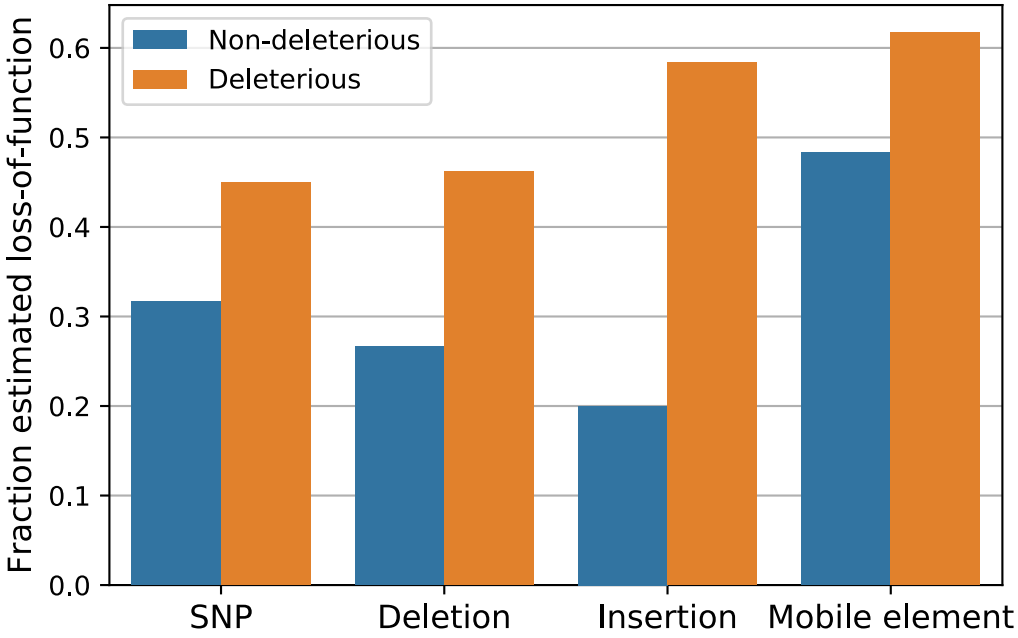

Figure 5: *Overview of the fraction of mutations estimated to be deleterious for each mutation types. The classification between Deleterious (orange) and Non-deleterious (Blue) is based on the nature and position of each mutation. The "fraction estimated deleterious" is calculated as the fraction of mutations having estimated impact scores larger than 0.*

Even though it is not generally possible to predict the impact of missense mutations, the ALE data does allow inferences to be drawn in certain cases. With available genetic data from populations evolved in parallel in the same condition, it is possible to assess whether a missense mutation is likely to be deleterious by considering other mutations in the same gene, within strains from the same condition. For instance, the *pykF* gene was, as previously mentioned, mutated in all strains from the isobutyrate condition. Seven distinct *pykF* mutations were observed in the isobutyrate strains, of which four were clearly deleterious (frameshift mutations and mobile element insertions), while the remaining three were missense SNP's. Since all these mutations were selected under the same condition, it is reasonable to assume that they have the same effect on the function of the *pykF* gene, i.e. inducing loss-of-function. Looking at the estimated impact scores, all seven mutations do indeed have positive scores (Figure 6), indicating loss-of-function impacts. The same can be done for other genes that were mutated in several populations from the same condition. In the 2,3-butanediol condition the genes *metJ* and *purT* were mutated in seven and five populations, respectively, out of seven. A single *metJ* mutation was a mobile element insertion, while seven were

missense SNP's of which five have putative loss-of-function effects based on the estimated impact score (Figure 6). The *purT* gene was mutated by a mobile element and three missense SNP's, all of which had putative loss-of-function effects (Figure 6).

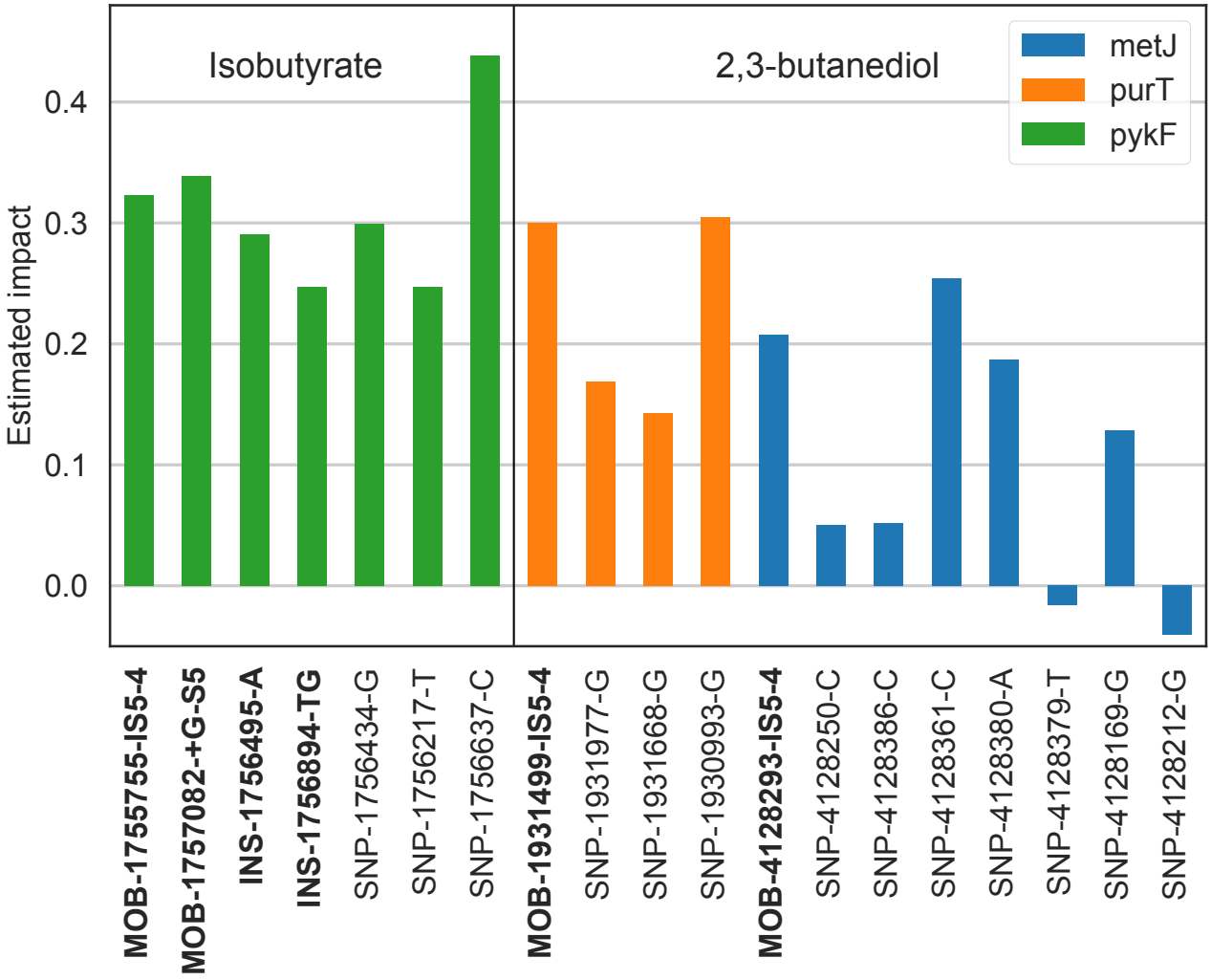

Figure 6: *Estimated impact scores for pykF mutations found in the isobutyrate strains and for purT and metJ mutations found in the 2,3-butanediol strains. The mutations that are expected to be deleterious based on their location are highlighted in bold. Almost all of the missense SNP's are estimated to be deleterious, consistent with the expectation that mutations in the same gene in the same condition will have the same effect. The mutation names indicate whether they are mobile elements (MOB), SNP's or insertions (INS), as well as the genome location of the mutation.*

Several mutations, predominantly missense SNP's, are also predicted to have a strong gain-of-function impact. One of these is a mutation in the *ilvH* gene, which was identified in two strains evolved on isobutyrate. The *ilvH* gene encodes an acetolactate synthase which converts two pyruvate molecules to acetolactate as part of the branched-chain amino acid biosynthesis. The mutation causes a substitution near the N-terminal of the protein, which contains an ACT domain

responsible for feedback inhibition by valine. The strains harboring the mutation had increased levels of valine (see Supplementary Figure 1), consistent with a disruption of feedback regulation of valine biosynthesis. Such a deregulation of an enzyme would indeed be an example of a gain-of-function mutation, as the catalytic activity would be expected to increase. The enzymatic conversion of pyruvate into acetolactate is also the first step of the isobutyrate biosynthesis pathway that was inserted into the evolved strains (Zhang et al., 2011). Interestingly, the strains with the mutation in *ilvH* or an equivalent mutation in the ACT domain mutation of the isozyme *ilvN* seemed to be able to produce isobutyrate significantly better than the other evolved strains (Chapter 1, Figure 6b (IBUA8-3 and IBUA8-10)). This could indicate that conversion of pyruvate into acetolactate is a limiting step in the production pathway due to allosteric inhibition by valine. Since valine and isobutyrate are chemically similar, it is also possible that the acetolactate synthase is inhibited by isobutyrate, resulting in deficient production of branched-chain amino acids.

Another example of a mutation predicted to have a gain-of-function effect is a nonsense mutation in the *rpoS* gene, found in the isobutyrate strains, which encodes the stress-associated sigma factor, σ^S. Although the induced stop codon truncates the protein by 54 amino acids, removing the sigma factor's domain 4 in its entirety, the estimated impact score of the mutation suggests that it confers a gain-of-function. *In vitro* experiments have shown that the deletion of domain 4, does not abolish the activity of σ^S (Gowrishankar et al., 2003). If deletion of domain 4 affects the regulation of σ^S it is possible that this will have a positive effect on σ^S activity.

Overall, the linear model based on metabolic profiles of the evolved strains and knockout strains shows predictive value in estimating the impact a given mutation has on the gene(s) it affects, although the accuracy is hard to assess due to the true impact of most of the observed mutations being unknown. Since the data for the knockout strains need only be collected once for a given organism, metabolic profiling of evolved strains can be an easy way to gain some insight into the nature of the observed mutations. A drawback of the method is that the metabolic effects of knockouts can only be measured for non-essential genes. Thus, the method is unable to provide information on mutations that affect essential genes. A potential solution to this challenge would be to use a library of over- or underexpression strains as references either for all genes or just for the essential genes.

2.3.2 Perturbation time-course metabolomics

The results presented above allow some insight to be gained into how the evolved strains have achieved tolerance, but in order to completely describe this process, the mechanisms of toxicity for the ALE conditions must be known. The nature of the toxic effects of the ALE compounds were investigated by perturbing wild-type MG1655 with each of nine chemicals and measuring the short-term metabolic responses. This approach allows detection of direct interactions between metabolism and the perturbing chemical, and thus quantification of the degree to which the toxic effects are related to metabolism. To avoid major problems with ion suppression in the mass spectrometry measurements, perturbation concentrations in the 160-180 µM range were used. Even though this was significantly below the concentrations used in the ALE experiments as well as the minimal inhibitory concentrations (Chapter 1, Supplementary Figure 1), it was hypothesized that direct metabolic effects, e.g. from allosteric inhibition might still be observed. In addition to the nine ALE chemicals, a range of control perturbations were also carried out. The control compounds included antibiotics, amino acids, a synthetic uncoupler of the proton gradient and an oxidative stressor (Table 1). The purpose of the control compounds was to validate that the experimental method can be used to detect known metabolic responses. Furthermore, in case such responses could be detected, it might be possible to compare the response to a chemical with unknown mechanism of toxicity to the responses to the control compounds, for which the effects are largely known.

Table 1: *Overview of the compounds used for perturbations and their concentrations. The antibiotics were used at the recommended concentrations for selective media.*

Compound	Concentration
2,3-butanediol	166 µM
HMDA	172 µM
Putrescine	170 µM
Glutarate	174 µM
Adipate	171 µM
Hexanoate	172 µM
Octanoate	173 µM
Isobutyrate	172 µM
Coumarate	152 µM

Compound		Concentration
Antibiotics	Ampicillin	130 µM
	Kanamycin	100 µM
	Chloramphenicol	130 µM
Uncoupler	Dinitrophenol	170 µM
Oxidative	H_2O_2	180 µM
Amino acids	Serine	171 µM
	Valine	160 µM
Control	Water	

For each perturbation condition, a list of significantly responding metabolites was identified. Significantly responding metabolites were defined as metabolites whose time-dependent response to a perturbation was significantly different compared to the control (water) condition.

As an example, in the chloramphenicol condition, the amino acids glutamate, lysine and leucine/isoleucine were among the metabolites found to significantly accumulate over time (Figure 7a). This is consistent with the mechanism of action for chloramphenicol, which is to prevent growth by inhibiting protein synthesis. Perturbation with either serine or valine resulted in high numbers of significantly responding metabolites, which is consistent with the fact that both are known to inhibit growth through allosteric inhibition of enzymes (De Felice et al., 1979; Hama et al., 1990). For perturbation with valine, several intermediates of branched-chain amino acid metabolism showed a fast negative response (Figure 7b), consistent with valine's known inhibition of acetolactate synthase, which catalyzes the first step of branch-chain amino acid synthesis.

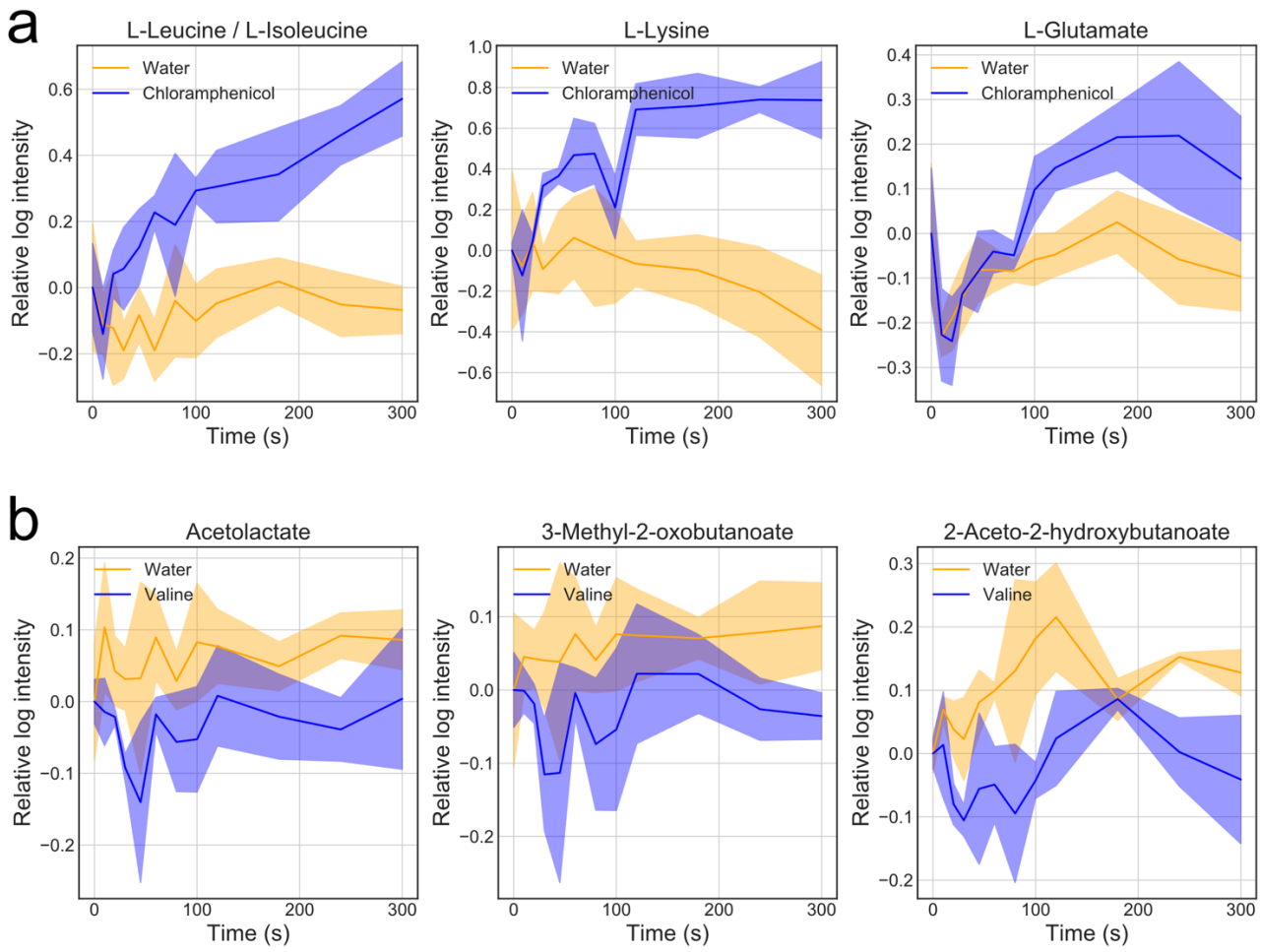

***Figure 7**: a) Time profiles for the amino acids leucine/isoleucine, lysine and glutamate following perturbation with water or chloramphenicol. b) Time profiles for branched-chain amino acid intermediates following perturbation with water or valine. The lines show the mean relative log intensities of biological replicates (three for chloramphenicol and valine, nine for water), while the shaded areas show the ± 1 standard deviation range.*

A summary of the number of significantly responding metabolites for each perturbation is shown in Figure 8. It is evident that perturbation with eight of the nine ALE compounds results in very weak or no metabolic effects compared to most of the control perturbations. In contrast to the rest of the ALE compounds, perturbation with coumarate does seem to elicit a metabolic response. One reason for this difference could be that coumarate is one of the more toxic compounds, in that relatively low concentrations were needed to inhibit growth (Chapter 1, Supplementary Figure 1). However, the same approximate levels of toxicity were observed for the compounds hexanoate, octanoate and isobutyrate , for which, in comparison to coumarate, only very little metabolic response to the perturbations was seen. Additionally, the perturbation concentration for coumarate is still several orders of magnitude lower than the concentrations used during ALE. It seems

therefore, that the toxic effects of coumarate are significantly more metabolic in nature than the other aforementioned compounds. The compounds 2,3-butanediol HMDA, putrescine, glutarate and adipate, on the other hand, might have toxic effects that are not related to metabolism, or alternatively the lack of a metabolic response could be explained by the relatively lower toxicity of these compounds, which were tolerated at concentrations approximately five times higher than coumarate. The considerable metabolic response to coumarate compared to the other ALE compounds might also be explained by the natural origin of coumarate. As a precursor in plants to the monolignol *p*-coumaryl alcohol, coumarate is involved in the formation of lignin and lignans, both of which are implicated in plant defenses against pathogens (Bagniewska-Zadworna et al., 2014; Qin et al., 2016). It is likely that the constituents of lignin and lignans, including coumarate, have been selected through evolution because of their potential for specific inhibitory bioactivity. For compounds that are never or very rarely found in nature, such bioactivity would be entirely accidental, and the affinity of interactions with metabolic enzymes would likely be much lower.

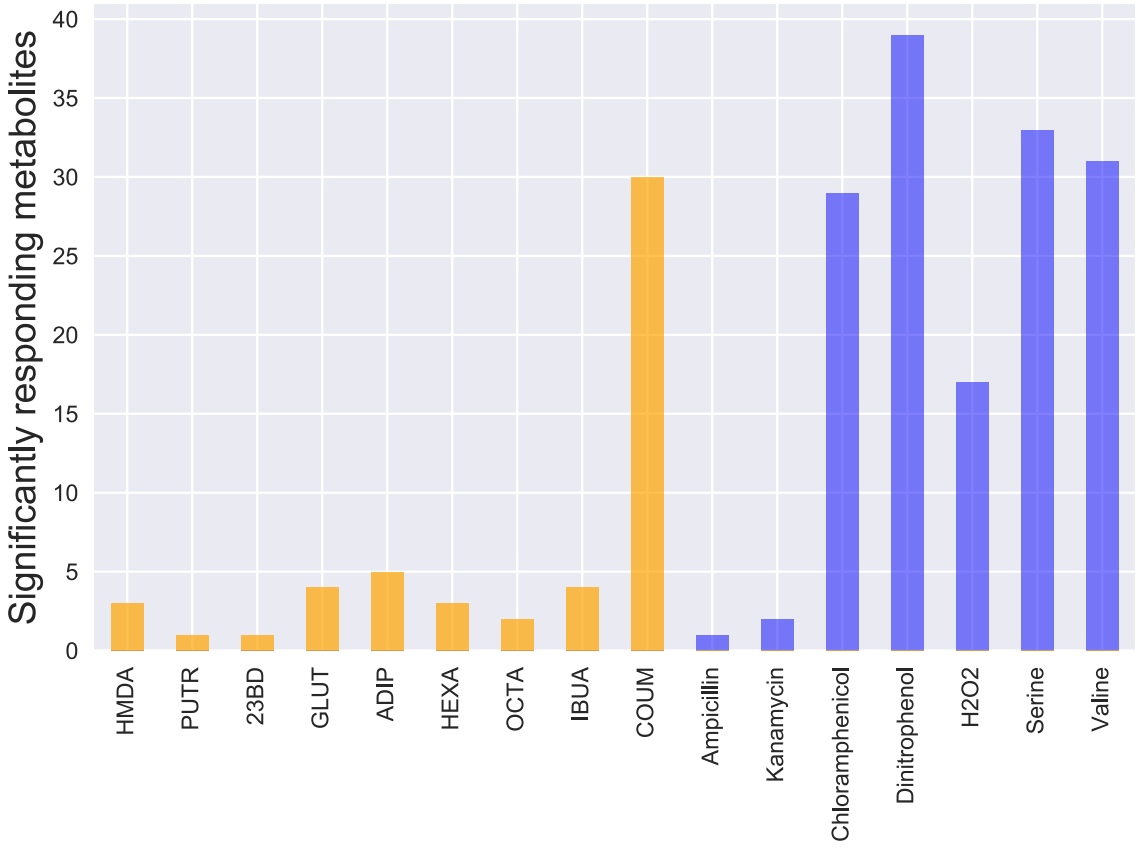

Figure 8: *The number of significantly responding metabolites for each perturbation condition. Data for the nine perturbations using the ALE compounds are colored orange, while the data for the control perturbations are colored blue.*

While the results from the control perturbations show that metabolic responses to a chemical perturbation can be detected using time-course metabolomics, only little information could be gained on the ALE compounds. Since a likely reason for the limited metabolic response to eight out of nine ALE compounds is that the perturbation concentrations were too low, the method might be better suited for investigating chemicals that are toxic at such low concentrations. On the contrary, the results for ampicillin and kanamycin, which were used at concentrations at which growth is inhibited, show that a metabolic response will not necessarily be seen just because the compound is toxic at the perturbation concentration. The lack of metabolic responses for these two antibiotics can be explained by their mechanisms of action: Ampicillin inhibits the synthesis of cell wall (Tomasz, 1979), while kanamycin causes mistranslation (Davies and Wright, 1971), both of which will likely only have a modest effect on cell metabolism within the time-frame of the experiment.

In cases where a metabolic response is detected, it would in principle be possible to use the responses of each metabolite to identify the specific mechanism of toxicity of a given chemical, e.g. targets for allosteric inhibition. As this would allow rapid identification of chemical-metabolism interactions, future work focusing on this aspect would be of value.

2.4 Conclusions

In this study high-throughput metabolomics was used to metabolically characterize a group of strains evolved to tolerate nine different chemicals, and to investigate the mechanisms of action for these chemicals. The metabolic profile characterizations of the evolved tolerant strains showed a strong association between metabolic profile and the condition each strain was evolved under. Additionally, a characteristic metabolic phenotype for a given evolution condition was often observed across strains with very little or no genetic commonality. This indicates that the metabolic phenotype is representative of the phenotypic changes that lead to improved tolerance, and that tolerance against a given chemical is achieved through very similar phenotypic mechanisms even though different strains have found different mutational paths to this phenotype. Taking advantage of previously published data on the metabolic effects of single-gene knockouts in *E. coli*, it was possible to use the metabolic profiles of the evolved strains to infer the impact of individual mutations on the functionality of the affected gene. Although the method showed promising

potential for differentiating between deleterious and non-deleterious mutations, additional validation is needed on mutations with known effects.

Using time-course metabolomics in perturbation experiments to elucidate details of chemical toxicity proved to be difficult due to technical limitations on perturbation concentrations in combination with the relatively low toxicity of some chemicals. However, results for a set of control perturbations suggested that the metabolomics approach can be used to quantify the degree of metabolic response to a chemical perturbation. Specific metabolite responses consistent with the known effects of two different control perturbations could be identified, demonstrating that the method might be used to infer mechanisms of action from the observed responses.

2.5 References

Bagniewska-Zadworna, A., Barakat, A., Łakomy, P., Smoliński, D.J., Zadworny, M., 2014. Lignin and lignans in plant defence: Insight from expression profiling of cinnamyl alcohol dehydrogenase genes during development and following fungal infection in Populus. Plant Sci. 229, 111–121. https://doi.org/10.1016/j.plantsci.2014.08.015

Benjamini, Y., Hochberg, Y., 1995. Controlling the False Discovery Rate: a Practical and Powerful Approach to Multiple Testing. J. R. Stat. Soc. Ser. B 57, 289–300.

Davies, J., Wright, G.D., 1971. Bacterial resistance to aminoglycoside antibiotics. J. Infect. Dis. 124, S7–S10. https://doi.org/10.1093/infdis/124.Supplement_1.S7

De Felice, M., Levinthal, M., Iaccarino, M., Guardiola, J., 1979. Growth inhibition as a consequence of antagonism between related amino acids: Effect of valine in Escherichia coli K-12. Microbiol. Rev. 43, 42–58.

Fuhrer, T., Heer, D., Begemann, B., Zamboni, N., 2011. High-throughput, accurate mass metabolome profiling of cellular extracts by flow injection-time-of-flight mass spectrometry. Anal. Chem. 83, 7074–7080. https://doi.org/10.1021/ac201267k

Fuhrer, T., Zamboni, N., 2015. High-throughput discovery metabolomics. Curr. Opin. Biotechnol.

31, 73–78. https://doi.org/10.1016/j.copbio.2014.08.006

Fuhrer, T., Zampieri, M., Sévin, D.C., Sauer, U., Zamboni, N., 2017. Genomewide landscape of gene–metabolome associations in *Escherichia coli*. Mol. Syst. Biol. 13, 907. https://doi.org/10.15252/msb.20167150

Gisbrecht, A., Hammer, B., 2015. Data visualization by nonlinear dimensionality reduction. Wiley Interdiscip. Rev. Data Min. Knowl. Discov. 5, 51–73. https://doi.org/10.1002/widm.1147

Gowrishankar, J., Yamamoto, K., Subbarayan, P.R., Ishimana, A., 2003. In Vitro Properties of RpoS Mutants of Escherichia coli with Postulated N-Terminal Subregion 1.1 or C-Terminal Region 4 Deleted. J. Bacteriol. 185, 2673–2679. https://doi.org/10.1128/JB.185.8.2673

Griffiths, W.J., Wang, Y., 2010. Mass Spectrometry in Metabolomics, in: Molecular Analysis and Genome Discovery: Second Edition. John Wiley and Sons, pp. 271–298.

Hama, H., Sumita, Y., Kakutani, Y., Tsuda, M., Tsuchiya, T., 1990. Target of serine inhibition in Escherichia coli. Biochem. Biophys. Res. Commun. 168, 1–6.

Niedenführ, S., Wiechert, W., Nöh, K., 2015. How to measure metabolic fluxes: A taxonomic guide for 13C fluxomics. Curr. Opin. Biotechnol. 34, 82–90. https://doi.org/10.1016/j.copbio.2014.12.003

Orth, J.D., Conrad, T.M., Na, J., Lerman, J. a, Nam, H., Feist, A.M., Palsson, B.Ø., 2011. A comprehensive genome-scale reconstruction of Escherichia coli metabolism. Mol. Syst. Biol. 7, 1–9. https://doi.org/10.1038/msb.2011.65

Qin, L., Li, W.C., Liu, L., Zhu, J.Q., Li, X., Li, B.Z., Yuan, Y.J., 2016. Inhibition of lignin-derived phenolic compounds to cellulase. Biotechnol. Biofuels 9, 1–10. https://doi.org/10.1186/s13068-016-0485-2

Seol, W., Shatkin, A.J., 1991. Escherichia coli kgtP encodes an alpha-ketoglutarate transporter. Proc. Natl. Acad. Sci. 88, 3802–3806.

Tan, P.-N., Steinbach, M., Kumar, V., 2005. Introduction to data mining, 1st ed. Pearson Addison

Wesley, Boston.

Tomasz, A., 1979. The Mechanism of the Irreversible Antimicrobial Effects of Penicillins: How the Beta-Lactam Antibiotics Kill and Lyse Bacteria. Annu. Rev. Microbiol. 33, 113–137. https://doi.org/10.1146/annurev.mi.33.100179.000553

Uyeda, K., 2006. Phosphofructokinase, in: Advances in Enzymology and Related Areas of Molecular Biology. John Wiley & Sons, Ltd, pp. 193–244. https://doi.org/10.1002/9780470122938.ch4

van der Maaten, L., Hinton, G., 2008. Visualizing Data using t-SNE. J. Mach. Learn. Res. 9, 2579–2605.

Yan, D., Lenz, P., Hwa, T., 2011. Overcoming fluctuation and leakage problems in the quantification of intracellular 2-oxoglutarate levels in Escherichia coli. Appl. Environ. Microbiol. 77, 6763–6771. https://doi.org/10.1128/AEM.05257-11

Zhang, K., Woodruff, A.P., Xiong, M., Zhou, J., Dhande, Y.K., 2011. A synthetic metabolic pathway for production of the platform chemical isobutyric acid. ChemSusChem 4, 1068–1070. https://doi.org/10.1002/cssc.201100045

2.6 Supplementary Materials

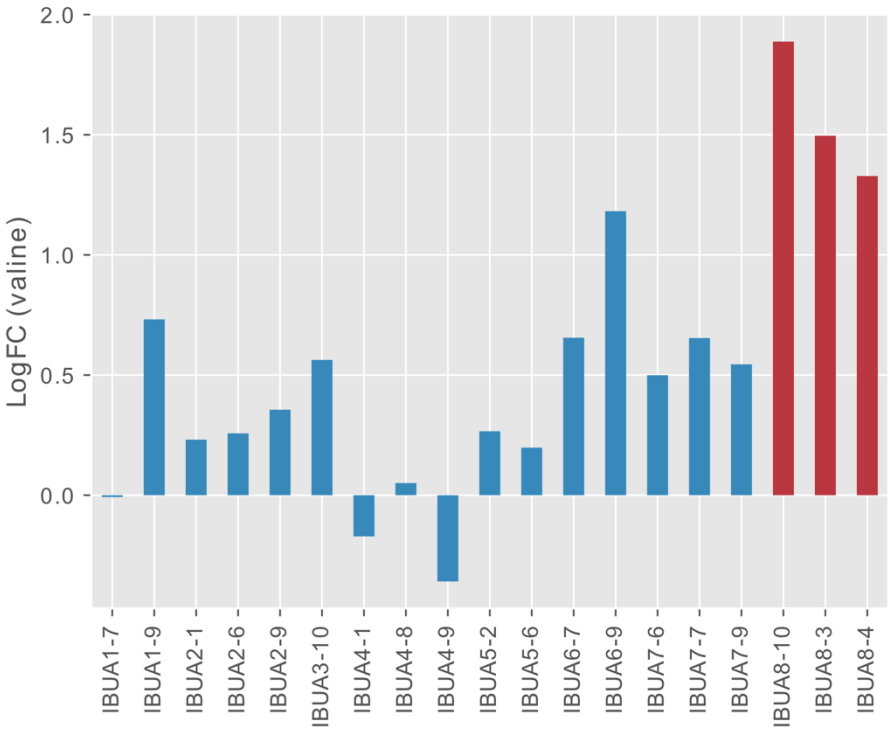

Supplementary Figure 1: *Log fold-change values for the strains evolved on isobutyrate. The strains that have mutations in ilvH/N are highlighted in red. These strains have increased levels of valine consistent with the hypothesized removal of valine feedback inhibition by these mutations.*

Chapter 3: A deep neural network for propagation of signals through a metabolic network

3.1 Introduction

In recent years there has been a rapid increase in the performance of machine learning algorithms on a variety of problems. The main factor in this trend has been the advent of deep neural networks (LeCun, Bengio, & Hinton, 2015). Traditional neural networks, also known as multilayer perceptrons (MLP), have been in use since the 1980's (Hopfield, 1988), but had started to lose popularity in the 2000's in favor of other algorithms such as support vector machines and other kernel-based methods (Hofmann, Schölkopf, & Smola, 2008).

One of the features that has allowed modern deep neural networks to outperform most other machine learning algorithms is the introduction of specialized layer architectures in addition to the fully connected hidden layers found in MLP's (LeCun et al., 2015). The most widespread specialized architectures are convolutional layers, which have successfully been used to process image, tomogram, and video data (Bernal et al., 2018; Karpathy et al., 2014; Krizhevsky, Sutskever, & Hinton, 2012), and recurrent layers which have allowed advances in analysis of sequence data, particularly in natural language processing (Bahdanau, Cho, & Bengio, 2015; Lipton, Berkowitz, & Elkan, 2015). Whereas traditional MLP's and other machine learning algorithms usually require that each data point is described by a vector of features, a large advantage of convolutional layers and recurrent layers is that they can take input without or with only minimal processing, e.g. raw pixel or text data. They can thus function as trainable feature extractors, that can learn to derive characteristics from the data with predictive value for the given problem.

Various problems within biology have benefited from the use of convolutional as well as recurrent neural networks. Convolutional networks have for example been used to identifying binding motifs for DNA- and RNA-binding proteins using a convolutional layer as trainable position weight matrices (Alipanahi, Delong, Weirauch, & Frey, 2015) and automated detection of subcellular protein localization in yeast from microscopy images (Pärnamaa & Parts, 2017). Recurrent neural networks in turn have been used among other things to predict protein secondary structure from amino acid

sequences (Sønderby & Winther, 2014) and predict RNA splice junctions from DNA sequences (Lee, Lee, Na, & Yoon, 2015).

However, problems that can be formulated as image or sequence analysis problems are only a small subset of possible biological prediction tasks. A more general type of datasets is what could be described as graph-structured data, or network-related data. Biology in general and systems biology in particular is known for its large number of networks ranging from genetic interaction networks through regulatory networks and protein interaction networks to metabolic reaction networks (Bader, Kühner, & Gavin, 2008; Kitano, 2002). Datasets of measurements related to e.g. genes, proteins or metabolites can thus be structured in a graph according to available information of the relevant networks, and including information on how different data points are related to each other can potentially allow statistical models to better describe the data. However, it is rarely obvious how network structure affects the relationship between data points, and it most likely depends on the type of network as well as the nature of the prediction problem. A potential solution to this problem is to use a trainable machine learning model to infer the significance of the network structure directly from the data (Bronstein, Bruna, Lecun, Szlam, & Vandergheynst, 2017).

The data used in traditional machine learning models such as MLP's, support vector machines or decision trees is inherently unstructured, and such models are thus poorly suited for operating on graph-structured data. Deep neural architectures such as recurrent and convolutional networks derive part of their power from the ability to take advantage of structure in the data, in the form of sequences or grids, respectively. Neither can however be applied to the more general structures that can be represented by graphs.

The challenge of combining machine learning and graphs such as biological networks has been addressed in numerous studies. This includes machine learning algorithms to infer network structure, e.g. in the form of protein interaction networks (Ballester & Mitchell, 2010) or transcriptional regulatory networks (Marbach et al., 2012), as well as algorithms that cluster or classify networks structures directly (Yanardag & Vishwanathan, 2015), e.g. to identify disease states from changes in biological networks (Mall, Cerulo, Bensmail, Iavarone, & Ceccarelli, 2017). In comparison, less work has focused on using prior knowledge about biological network structures to improve predictions based on data embedded in the network.

In this work a novel deep learning framework is developed to allow supervised prediction problems to take advantage of graph-structure between features in the input data. This framework is based on the concept of graph convolutional networks (GCN) developed by Kipf & Welling (2017) to do semi-supervised learning on datasets where observations are related to each other. The prediction problem used to test this deep learning framework involves using stoichiometric and regulatory networks of *Escherichia coli* metabolism to predict how a gene knockout will affect the levels of metabolites. The prediction problem including the types of input data, output data and graph structures are shown in Figure 1.

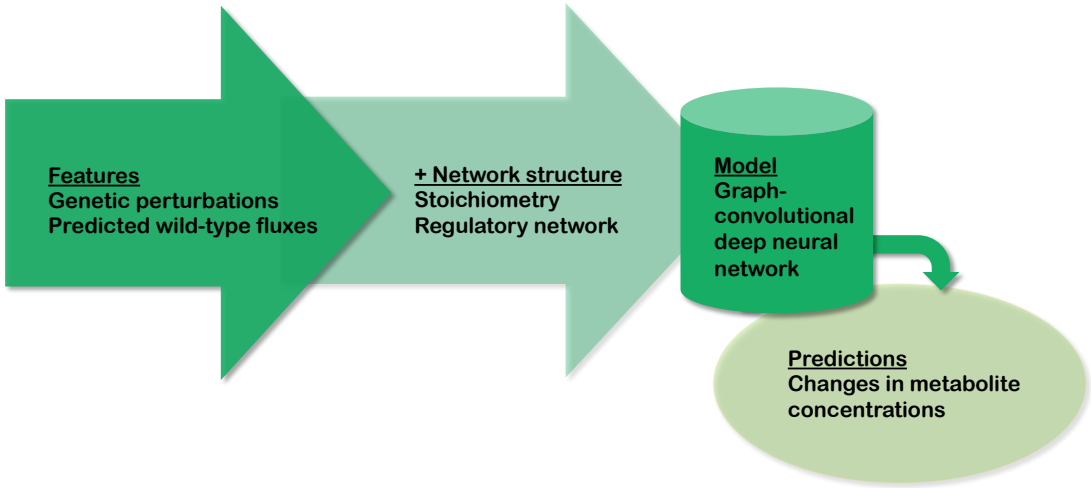

Figure 1: *Overview of the prediction problem used in this study. Changes in metabolite concentrations are predicted from predicted fluxes and genetic perturbation, using the graph structures of stoichiometric and regulatory networks.*

3.2 Methods

3.2.1 Neural network architecture

The deep neural network model used in this study consisted of a combination of graph convolutional layers (Kipf & Welling, 2017) and fully connected layers. A graph convolutional layer takes as input the normalized adjacency matrix, $\hat{A}$, for a graph, and a N x M data matrix, X, where N is the number of nodes in the graph and M is the number of data features per node. The trainable parameter of a graph convolutional layers is an M x K weight matrix, W, where K is the number of features per node in the output data. The activations of a graph convolutional layer are calculated as

$$Z = \sigma\left(\hat{\mathrm{A}}\, X\, W\right) \tag{1}$$

where σ is the chosen non-linearity function (Kipf & Welling, 2017). The adjacency matrix is normalized using its degree matrix, D

$$\hat{\mathrm{A}} = D^{-\frac{1}{2}} A\, D^{-\frac{1}{2}} \tag{2}$$

which preserves symmetry in the adjacency matrix and ensures that all rows sum to one (Kipf & Welling, 2017).

The graph convolutional layers used here were extended to allow the simultaneous use of several graph structures of a given set of nodes. The activations were instead calculated as

$$Z = \sigma(\sum_{i=1}^{L} \hat{\mathrm{A}}_i\, X\, W_i) \tag{3}$$

with *i* denoting the index of each graph structure and the corresponding weight matrix. During training this was implemented by letting $\hat{A}$ be an L x N x N tensor and *W* be an L x M x K tensor and summing over the dimension corresponding to L.

Four consecutive graph convolutional layers were used with the output of one feeding into the next. The activations from each of the four graph convolutional layers were concatenated into a single layer, yielding an N X K_{sum} matrix, with K_{sum} being the sum of K in each respective layer. This corresponds to an individual feature vector of length K_{sum} for each node in the graph. Finally, these feature vectors were fed into an MLP with a single hidden layer ending with a softmax output layer. The weights of this MLP were shared between all graph nodes.

All layers except the output layer used the leaky rectified nonlinearity (Maas, Hannun, & Ng, 2013):

$$f(x) = \begin{cases} x & if\ x > 0 \\ 0.01 \cdot x & if\ x \leq 0 \end{cases} \tag{4}$$

3.2.2 Training data

The dataset used for training was obtained from the online supplementary material of Fuhrer, Zampieri, Sévin, Sauer, & Zamboni (2017).

The input data consisted of genetic perturbations and predicted wild-type steady state fluxes. Genetic perturbations were encoded in a binary format, such that reactions impacted by a given gene knockout, had 1-inputs and the rest had 0-inputs. The flux data was input as the raw flux values for each reaction, predicted using parsimonious flux balance analysis, which minimizes the total sum of fluxes, subject to optimal biomass production (Lewis et al., 2010). The *i*JO1366 genome-scale reconstruction of *E. coli* (Orth et al., 2011) was used to determine the reactions impacted by a knockout and to predict fluxes.

The prediction targets were binary variables encoding whether a given metabolite level was either increased or decreased in the mutant strain (1) or the same as in the wild-type strain (0). Significant changes were defined at $\alpha = 0.05$ (two-tailed) using *z*-values calculated by Fuhrer et al. (2017). The mass spectrometry data from Fuhrer et al. (2017) was mapped to 310 *E. coli* metabolites (Supplementary Table 1), which were used as targets for all knockout strains.

3.2.3 Adjacency matrix

3.2.3.1 Stoichiometric network

A metabolic reaction network is often represented as metabolite nodes connected by reactions. This, however, is not a true graph as some reactions connect more than two metabolites. Such a structure can be represented as a hypergraph, a generalization of a graph where edges can connect arbitrary sets of nodes instead of only pairs. The metabolic hypergraph can be reformulated as a graph by conversion into a bipartite graph, where both metabolites and reactions are nodes and participation of a metabolite in a reaction is represented by an edge between the respective pair of nodes with a weight corresponding to the stoichiometric coefficient. Such a representation was used to create an adjacency matrix for the *E. coli* metabolic reaction network. To avoid division-by-zero problems when normalizing the adjacency matrix, all nodes were given self-connections (Kipf & Welling, 2017). If the nodes in the bipartite metabolic graph are ordered such that all metabolites precede all reactions, the adjacency matrix thus becomes the block matrix

$$A_{Stoic} = \begin{bmatrix} 0 & S \\ S^T & 0 \end{bmatrix} + I \tag{4}$$

where *S* is the usual stoichiometric matrix and *I* is the identity matrix. The stoichiometric structure was obtained from the *i*JO1366 genome-scale reconstruction of *E. coli* (Orth et al., 2011).

3.2.3.2 Small molecule regulatory network

In addition to the stoichiometric network, regulatory metabolite-reaction interactions were also included in the model in the form of a second graph structure. These interactions were embedded in a similar bipartite graph form as the stoichiometric network. The data for these interactions were obtained from Reznik et al. (2017). A regulatory matrix, *R*, was constructed with element r_{ij} describing the interaction between metabolite *i* and reaction *j*. A value of 1 was used for indicating activating interactions, -1 for inhibiting interactions and 0 for no interaction. The corresponding adjacency matrix was then calculated as

$$A_{SMRN} = \begin{bmatrix} 0 & R \\ R^T & 0 \end{bmatrix} + I \tag{5}$$

3.2.4 Implementation and training

The neural network including the graph convolutions were implemented in Python 3.5 using the Theano package (Al-Rfou et al., 2016). The training was carried out on nodes of an HPC cluster equipped with Tesla K40c graphics processing units.

3.3 Results and discussion

The neural network used to predict changes in metabolite levels contained four consecutive graph-convolution layers, where the input data could be propagated through the metabolic network. This was followed by fully connected layers applied independently to every node. Between the graph-convolution and fully connected layers was a concatenation layer, combining the outputs from all four graph-convolution layers. As each consecutive graph convolution enables more distant interactions in the graph, the concatenation allows the network to learn which combination of proximal and distal information provides the most predictive output. Since the graph-convolution layers conserve the graph structure of the input data, and the fully connected layers operate on individual nodes, the output has the same graph-structure as the input data. This allows the network to make predictions on every individual node, i.e. metabolite. Figure 2 shows a sketch of the neural network architecture.

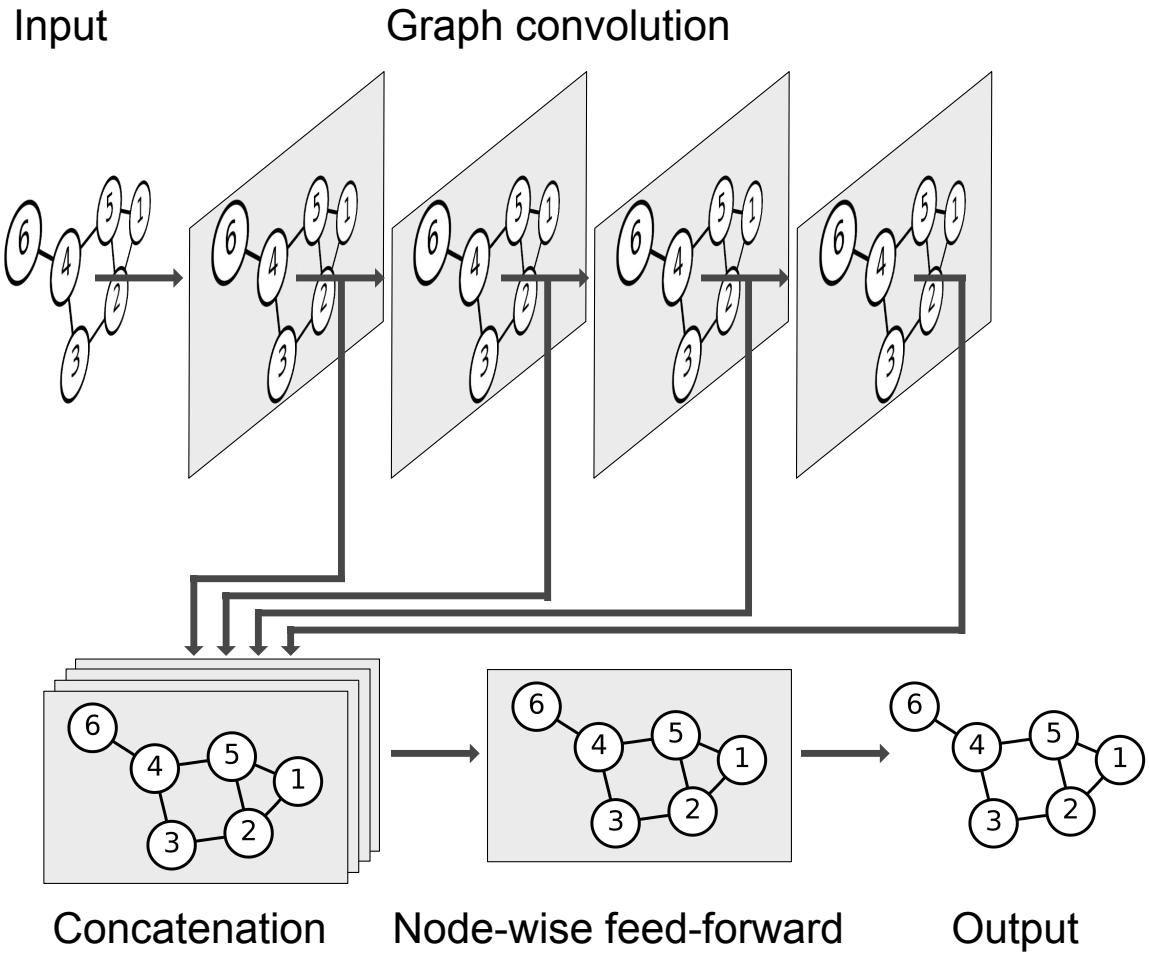

Figure 2: *Overview of the architecture of the neural network. Throughout the entire network the data maintains the network structure, allowing predictions on the level of individual nodes.*

The neural network was trained on the single-gene knockout metabolomics data for 1000 epochs, minimizing the cross-entropy between the predictions and targets. To simplify the prediction task, the chosen prediction target was whether a metabolite concentration was significantly changed or not in the knockout strain, regardless of the direction of change. To reduce overfitting, the dataset was randomly split into a training set (80 %) and a test set (20 %), which was used to evaluate the training progress after each epoch. The values of the cross-entropy loss function evaluated on the training and test sets throughout the training process are shown in Figure 3. As would be expected both the training and test losses decrease rapidly at first, after which the progress slows considerably. The training loss continues to slowly decrease, however the test loss stabilizes, indicating that further training does not generalize to new data.

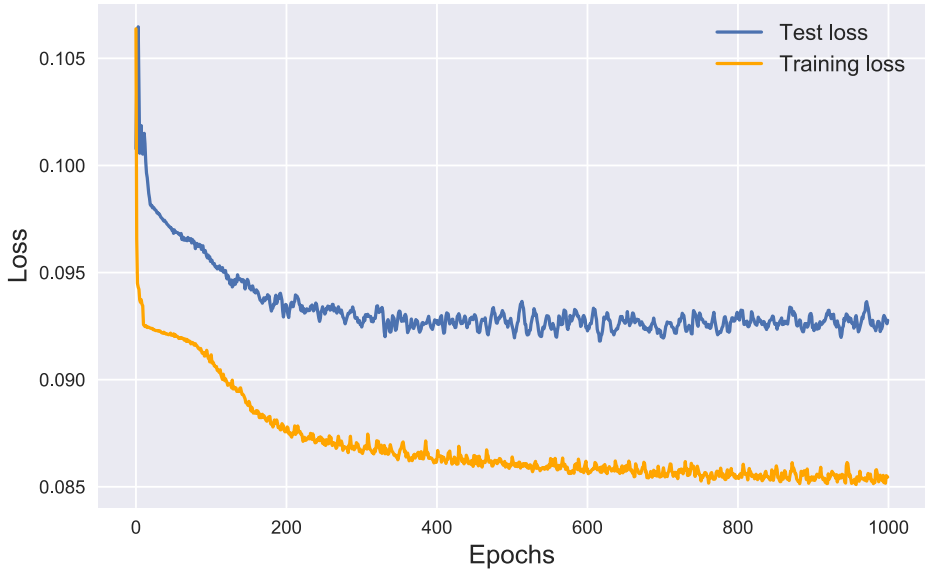

Figure 3: *The values of the cross-entropy loss function evaluated on the training and test sets, respectively, following each training epoch.*

The network weights from the epoch with the best test performance were chosen for further evaluation. The overall balanced accuracy of the predictions on the test set was 0.58. Figure 4 shows summary plots of the prediction results. Figure 4a shows the positive prediction rates for the actual negatives (no change) and actual positives (change) respectively, while Figure 4b shows the distributions of output scores and Figure 4c shows the receiver operating characteristic. These results suggest that the neural network has derived some predictive value from the input data and the graph structure, although the predictive performance is only slightly better than random guessing. The plots in Figure 4 also indicate that the predictions show a clear bias towards positive predictions, despite the dataset containing only around 5 % positive examples.

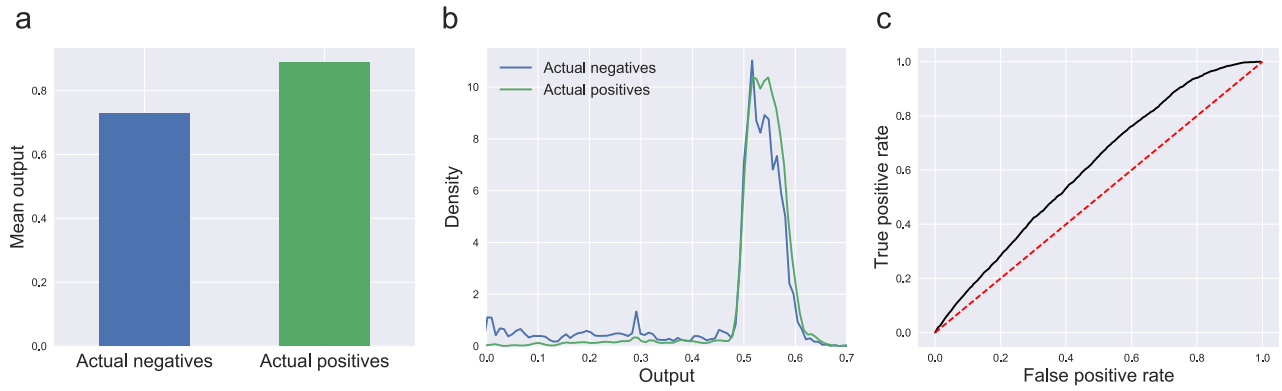

Figure 4: *Summary of the predictive results of the trained neural network. a) The positive prediction rates for actual negatives and actual positives. b) Distributions of the outputs for actual negatives and actual positives. c) Receiver operating characteristic of the predictive performance.*

Although the results of the trained neural network show that predictions are better than chance, this does not necessarily mean that the network has learned to propagate the input through the supplied graph structure. Training machine learning models on datasets with complex structure can sometimes lead to spuriously high prediction accuracies, as the model can learn to identify hidden but trivial patterns in the data (Chuang & Keiser, 2018). To test whether this was the case for the above results, the model was retrained on a control dataset. The control dataset was identical to the original dataset, except that the input data was randomly shuffled so that the target data (whether a metabolite concentration had changed) no longer corresponded to the input data (which reactions were affected by a knockout). If the neural network trained on the control dataset achieved predictive performance similar to the originally trained network, it would indicate that the predictive performance was a product of patterns that are not related to the input data. Conversely, if the originally trained network had actually learned to propagate the input data through the graph, the control dataset should yield a lower predictive performance. The neural network was trained on the control dataset using the same hyperparameters as the original training and reached a balanced accuracy of 0.52. This indicates that the originally trained neural network (with a balanced accuracy of 0.58) had indeed learned to propagate signals through the metabolic and regulatory networks, rather than just finding trivial patterns in the dataset.

To investigate in more detail what the neural network had learned, the predictions were summarized for each individual metabolite. This allows insight into whether the 0.58 accuracy was

obtained by predicting all metabolites equally well, or whether a few metabolites were predicted at high accuracy while others were predicted near chance levels. Figure 5 shows the true positive rate and false positive rate for each metabolite. This shows that most metabolites are predicted to be either almost universally negative (lower left corner) or almost universally positive (upper right corner), while relatively few metabolites are predicted to sometimes be negative and sometimes positive. Of these few metabolites, most are predicted at near-chance levels, with only a handful predicted at high accuracies (upper left corner). This shows that the achieved predictive accuracy is based on distinguishing changing and non-changing concentrations of just a few metabolites, while the majority of metabolites are predicted at accuracies close to random chance.

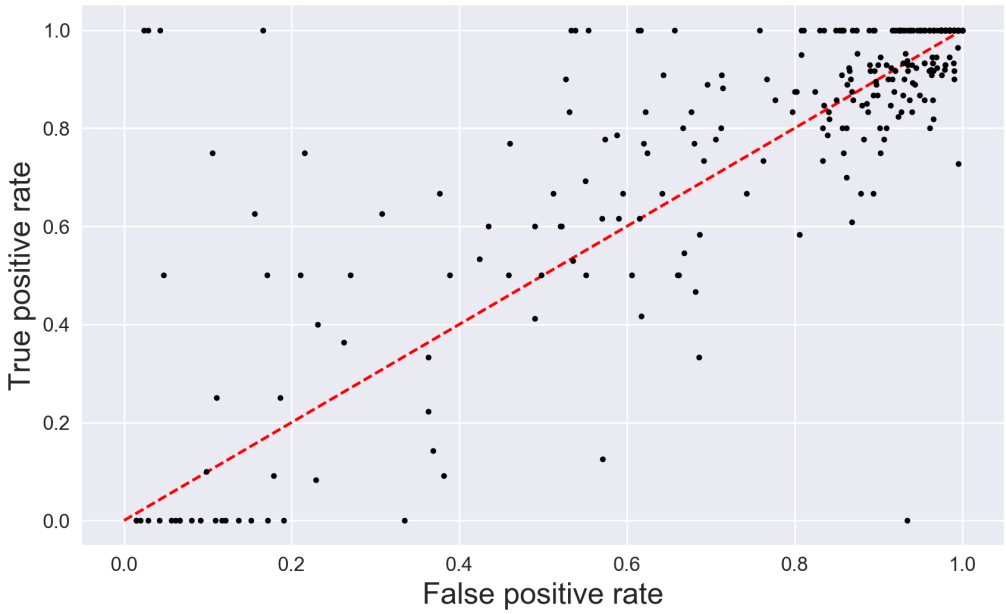

Figure 5: *Predictive performance of individual metabolites. Each point shows the false positive rate and true positive rate for a given metabolite.*

While the predictions obtained using the deep neural network with graph-structured data did not reach performance levels where they would be practically useful, they still represent an interesting and potentially valuable step forward within machine learning in metabolic engineering. Prediction problems like the one attempted here are hard if not impossible to solve without including either graph-structures or other representations of preexisting domain knowledge in the model, and the results obtained here suggest that propagation of signals through a graph using deep neural networks is possible, even if currently not with impressive accuracy. It is also worth noting that the present prediction problem is inherently difficult, given the nature of the input and output data.

Most machine learning problems use a rich set of input features to predict one or a few outputs, while the prediction of metabolic changes from genetic perturbations uses a sparse input vector to predict a rich set of output features. Future work on graph-structured deep learning might focus on amending the input data with further informative features and experimenting with additional graph relationships between the nodes.

3.4 Conclusion

In this study a novel deep neural network was presented for propagating input signals through graph-structured stoichiometric and regulatory networks of metabolites and reactions. The network was tested by using genetic knockouts to predict changes in metabolite levels throughout the metabolic network. The obtained balanced accuracy of 0.58 showed that the network could learn some rules for relating genetic perturbations to metabolite levels, but further investigation showed that the performance was driven by good predictions on a few metabolites and near-chance predictions on most metabolites. Training the network on a control dataset showed that the predictive performance can indeed largely be ascribed to propagation of the input signals through the supplied graph-structures.

3.5 References

Al-Rfou, R., Alain, G., Almahairi, A., Angermueller, C., Bahdanau, D., Ballas, N., … Zhang, Y. (2016). Theano: A Python framework for fast computation of mathematical expressions. *ArXiv*, *abs/1605.0*. Retrieved from http://arxiv.org/abs/1605.02688

Alipanahi, B., Delong, A., Weirauch, M. T., & Frey, B. J. (2015). Predicting the sequence specificities of DnA- and RnA-binding proteins by deep learning. *Nature Biotechnology*, *33*(8), 831–838. https://doi.org/10.1038/nbt.3300

Bader, S., Kühner, S., & Gavin, A. (2008). Interaction networks for systems biology. *FEBS Letters*, *582*, 1220–1224. https://doi.org/10.1016/j.febslet.2008.02.015

Bahdanau, D., Cho, K., & Bengio, Y. (2015). Neural Machine Translation by Jointly Learning to Align and Translate. *ArXiv*.

Ballester, P. J., & Mitchell, J. B. O. (2010). A machine learning approach to predicting protein-ligand binding affinity with applications to molecular docking. *Bioinformatics*, *26*(9), 1169–1175. https://doi.org/10.1093/bioinformatics/btq112

Bernal, J., Kushibar, K., Asfaw, D. S., Valverde, S., Oliver, A., Martí, R., & Lladó, X. (2018). Deep convolutional neural networks for brain image analysis on magnetic resonance imaging: a review. *Artificial Intelligence In Medicine*, 1–18. https://doi.org/10.1016/j.artmed.2018.08.008

Bronstein, M. M., Bruna, J., Lecun, Y., Szlam, A., & Vandergheynst, P. (2017). Geometric Deep Learning: Going beyond Euclidean data. *IEEE Signal Processing Magazine*, *34*(4), 18–42. https://doi.org/10.1109/MSP.2017.2693418

Chuang, K. V, & Keiser, M. J. (2018). Comment on "Predicting reaction performance in C – N cross-coupling using machine learning." *Science*, *8603*, 1–3.

Fuhrer, T., Zampieri, M., Sévin, D. C., Sauer, U., & Zamboni, N. (2017). Genomewide landscape of gene–metabolome associations in *Escherichia coli*. *Molecular Systems Biology*, *13*(1), 907. https://doi.org/10.15252/msb.20167150

Hofmann, T., Schölkopf, B., & Smola, A. J. (2008). Kernel Methods in Machine Learning. *The Annals of Statistics*, *36*(3), 1171–1220. https://doi.org/10.1214/009053607000000677

Hopfield, J. J. (1988). Artificial Neural Networks. *IEEE Circuits and Devices Magazine*, *4*(5), 3–10.

Karpathy, A., Toderici, G., Shetty, S., Leung, T., Sukthankar, R., & Fei-Fei, L. (2014). Large-scale Video Classification with Convolutional Neural Networks. *IEEE Conference on Computer Vision and Pattern Recognition*, 1725–1732. https://doi.org/10.1109/CVPR.2014.223

Kipf, T. N., & Welling, M. (2017). Semi-Supervised Classification with Graph Convolutional Networks. In *ICLR 2017* (pp. 1–14). https://doi.org/10.1051/0004-6361/201527329

Kitano, H. (2002). Systems Biology: A Brief Overview. *Science*, *295*, 1662–1665.

Krizhevsky, A., Sutskever, I., & Hinton, G. E. (2012). ImageNet Classification with Deep Convolutional Neural Networks. *Proceedings of Advances in Neural Information Processing Systems*, *25*, 1090–10.

LeCun, Y., Bengio, Y., & Hinton, G. (2015). Deep learning. *Nature*, *521*, 436–444. https://doi.org/10.1038/nature14539

Lee, B., Lee, T., Na, B., & Yoon, S. (2015). DNA-Level Splice Junction Prediction using Deep Recurrent Neural Networks. *ArXiv*.

Lewis, N. E., Hixson, K. K., Conrad, T. M., Lerman, J. A., Charusanti, P., Polpitiya, A. D., … Palsson, B. (2010). Omic data from evolved E. coli are consistent with computed optimal growth from genome-scale models. *Molecular Systems Biology*, *6*(390).

https://doi.org/10.1038/msb.2010.47

Lipton, Z. C., Berkowitz, J., & Elkan, C. (2015). A Critical Review of Recurrent Neural Networks for Sequence Learning. *ArXiv*.

Maas, A. L., Hannun, A. Y., & Ng, A. Y. (2013). Rectifier Nonlinearities Improve Neural Network Acoustic Models. *ArXiv*. https://doi.org/10.1016/0010-0277(84)90022-2

Mall, R., Cerulo, L., Bensmail, H., Iavarone, A., & Ceccarelli, M. (2017). Detection of statistically significant network changes in complex biological networks. *BMC Systems Biology*, *11*(1), 1–17. https://doi.org/10.1186/s12918-017-0412-6

Marbach, D., Costello, J. C., Küffner, R., Vega, N. M., Prill, R. J., Camacho, D. M., … Zimmer, R. (2012). Wisdom of crowds for robust gene network inference. *Nature Methods*, *9*(8), 796–804. https://doi.org/10.1038/nmeth.2016

Orth, J. D., Conrad, T. M., Na, J., Lerman, J. a, Nam, H., Feist, A. M., & Palsson, B. Ø. (2011). A comprehensive genome-scale reconstruction of Escherichia coli metabolism. *Molecular Systems Biology*, *7*(535), 1–9. https://doi.org/10.1038/msb.2011.65

Pärnamaa, T., & Parts, L. (2017). Accurate Classification of Protein Subcellular Localization from High-Throughput Microscopy Images Using Deep Learning. *Genes, Genomes, Genetics*, *7*, 1385–1392. https://doi.org/10.1534/g3.116.033654/-/DC1

Reznik, E., Christodoulou, D., Goldford, J. E., Briars, E., Sauer, U., Segrè, D., & Noor, E. (2017). Genome-Scale Architecture of Small Molecule Regulatory Networks and the Fundamental Trade-Off between Regulation and Enzymatic Activity. *Cell Reports*, *20*(11), 2666–2677. https://doi.org/10.1016/j.celrep.2017.08.066

Sønderby, S. K., & Winther, O. (2014). Protein Secondary Structure Prediction with Long Short Term Memory Networks. *ArXiv*.

Yanardag, P., & Vishwanathan, S. V. N. (2015). Deep Graph Kernels. *Proceedings of the 21th ACM SIGKDD International Conference on Knowledge Discovery and Data Mining - KDD '15*, 1365–1374. https://doi.org/10.1145/2783258.2783417

3.6 Supplementary Materials

Supplementary Table 1: *List of BiGG ID's for all the metabolites that a detected ion in the Fuhrer et al. (2017) dataset was mapped to.*

1pyr5c	4mop	but	gal1p	lald__D	pyr
23camp	4pasp	camp	galctn__D	lald__L	quin
23ccmp	4ppan	cbasp	galctn__L	lcts	r1p
23cgmp	4r5au	cbi	galt	leu__L	rbl__L
23cump	5aop	cdp	galt1p	lgt__S	rib__D
23dhb	5dh4dglc	cechddd	gcald	lipoate	rml1p
23dhmb	6pgl	cenchddd	gdp	lys__L	ru5p__D
23dhmp	8aonn	chor	gdptp	lyx__L	ru5p__L
23doguln	aact	cinnm	gg4abut	mal__D	s17bp
26dap_LL	ac	cit	ggbutal	mal__L	s7p
26dap__M	acac	citr__L	ggptrc	malt	sarcs
2ahbut	accoa	cmp	ghb	man	sbt6p
2aobut	acetol	cpmp	glc__D	man1p	sbt__D
2ddg6p	acgal	csn	glcn	man6p	ser__L
2ddglcn	acgam	cys__D	glu1sa	mana	skm
2dh3dgal	acgam6p	cys__L	glu5sa	manglyc	skm5p
2dh3dgal6p	acglu	cytd	glu__D	melib	sl2a6o
2dhp	acmana	dca	glu__L	met__D	so3
2dr1p	acmanap	ddca	glucys	met__L	succ
2dr5p	acmum	dgdp	glx	mi1p__D	sucglu
2mcacn	acmum6p	dgmp	gly	micit	sucorn
2mcit	acnam	dgsn	glyald	mnl	sucr
2me4p	acon_C	dgtp	glyb	mnl1p	sucsal
2mecdp	acser	dha	glyc	msa	tag6p__D
2obut	actp	dhap	glyc__R	mthgxl	tagdp__D
2oph	ade	dhor__S	gmhep1p	nac	tartr__L
2p4c2me	adn	dhpppn	gmhep7p	no3	thdp
2pg	adp	dhpt	gmp	ocdca	thr__L
35cgmp	agm	dimp	gsn	ocdcea	thymd
3amp	ahcys	dmlz	gthox	octa	tre
3c2hmp	ahdt	dpcoa	gthrd	op4en	trp__L
3c3hmp	air	dtbt	gua	orn	ttdca
3c4mop	akg	dtdpglu	h2mb4p	orot	tyr__L
3cmp	ala_B	dtdprmn	hco3	pac	uacgam

3dhq	ala__D	dtmp	hdca	pant__R	uacmam
3dhsk	ala__L	dxyl5p	hdcea	pap	udp
3gmp	alaala	e4p	his__L	paps	udpacgal
3hcinnm	all__D	enter	histd	phe__L	udpg
3hpp	altrn	f1p	hom__L	phpyr	udpgal
3hpppn	ametam	f6p	hqn	pi	ump
3mob	amp	fc1p	hxan	pnto__R	ura
3mop	ara5p	fdp	ichor	ppal	uri
3pg	arbt	fgam	icit	ppbng	val__L
3ump	arbt6p	fpram	ile__L	ppgpp	xan
4abut	arg__L	fprica	indole	pphn	xmp
4ahmmp	argsuc	fru	inost	ppi	xu5p__D
4ampm	asn__L	g1p	ins	pro__L	xu5p__L
4c2me	asp__L	g3p	itp	pser__L	xyl__D
4crsol	aspsa	g3pc	kdo	ptrc	xylu__D
4hbz	athr__L	g3pe	kdo8p	pyam5p	xylu__L
4hoxpacd	atp	g6p	lac__D	pydam	
4hthr	btal	gal	lac__L	pydx5p	

Part II: Model-based strain design

As previously mentioned, designing microbial strains for chemical production processes is a difficult and time-consuming task. The first part of this thesis explored how non-rational methods, particularly adaptive laboratory evolution (ALE), can be used to improve certain characteristics of production strains. Some traits, such as tolerance as shown in Chapter 1, can be easily improved in ALE experiments, but many production-related traits such as product yields or production rates that cannot be trivially selected for, are harder to optimize with evolutionary processes. For this reason, development of good production strains almost always also requires utilization of rational engineering methods. Because of the complexity of microbial metabolism, and physiology in general, genetically modifying a strain can sometimes have unintuitive effects on the functioning of the cell, which makes rational design difficult. To aid in the understanding of how genetic modifications impact cellular processes, mathematical models of the cell can therefore be a valuable tool, with mathematical models of metabolism being of particular relevance for metabolic engineering. Metabolic models can enable system-wide analysis of the cell and e.g. help predict genes that should be overexpressed in order to produce a target compound (Choi, Lee, Kim, & Woo, 2010) or construct novel pathways for synthesizing a product of interest (Pharkya, Burgard, & Maranas, 2004). Some models only require knowledge of the organism's metabolic capabilities, much of which can be inferred from the annotated genome (Faria, Rocha, Rocha, & Henry, 2018), while other models can integrate experimental data such as transcriptomics or proteomics in order to improve the predictive accuracy. Chapter 4 will provide an introduction to genome-scale models of metabolism and review different methods for integrating large-scale data into the models.

While genome-scale metabolic models can be utilized in rational computational strain design, they can also be used in combination with non-rational methods, e.g. ALE. It is possible to engineer microbial strains that must produce a given metabolite in order to grow, i.e. where production is growth-coupled (Feist et al., 2010). Since ALE is based on continuous selection of fast-growing mutant strains, in cases where production is growth-coupled, ALE will thus indirectly select mutants that have an increased production rate for the growth-coupled chemical. Growth-coupled strains can in principle be constructed without the use of computational tools, but due to the complex structure of metabolism, algorithms based on genome-scale metabolic models allow identification

of non-obvious growth-coupled designs (Klamt & Mahadevan, 2015). In Chapter 5 a novel algorithm for predicting growth-coupled designs is presented and validated by its ability to identify known experimentally validated growth-coupled designs as well as unknown designs that are growth-coupled *in silico*.

References

Choi, H. S., Lee, S. Y., Kim, T. Y., & Woo, H. M. (2010). In silico identification of gene amplification targets for improvement of lycopene production. *Applied and Environmental Microbiology*, *76*(10), 3097–3105. https://doi.org/10.1128/AEM.00115-10

Faria, J. P., Rocha, M., Rocha, I., & Henry, C. S. (2018). Methods for automated genome-scale metabolic model reconstruction. *Biochemical Society Transactions*, *46*, 931–936.

Feist, A. M., Zielinski, D. C., Orth, J. D., Schellenberger, J., Herrgard, M. J., & Palsson, B. O. (2010). Model-driven evaluation of the production potential for growth-coupled products of Escherichia coli. *Metabolic Engineering*, *12*(3), 173–186. https://doi.org/10.1016/j.ymben.2009.10.003

Klamt, S., & Mahadevan, R. (2015). On the feasibility of growth-coupled product synthesis in microbial strains. *Metabolic Engineering*, *30*, 166–178. https://doi.org/10.1016/j.ymben.2015.05.006

Pharkya, P., Burgard, A. P., & Maranas, C. D. (2004). OptStrain : A computational framework for redesign of microbial production systems OptStrain : A computational framework for redesign of microbial production systems. *Genome Research*, (814), 2367–2376. https://doi.org/10.1101/gr.2872004

Chapter 4: Enhancing metabolic models with genome-scale experimental data

Kristian Jensen*, Steinn Gudmundsson** & Markus J. Herrgård*

*The Novo Nordisk Foundation Center for Biosustainability, Technical University of Denmark, Building 220, Kemitorvet, 2800 Kgs. Lyngby, Denmark

**Center for Systems Biology, University of Iceland, Sturlugata 8, IS 101 Reykjavik, Iceland

Abstract

Genome-scale metabolic reconstructions have found widespread use in scientific research as structured representations of knowledge about an organism's metabolism and as starting points for metabolic simulations. With few simplifying assumptions, genome-scale models of metabolism can be used to estimate intra-cellular reaction rates in any organism for which a well-curated metabolic reconstruction is available. However, with the rapid increase in the availability of genome-scale data, there is ample opportunity to refine the predictions made by metabolic models by integrating experimental data. In this chapter, we review different methods for combining genome-scale metabolic models with genome-scale experimental data, such as transcriptomics, proteomics and metabolomics. Integrating experimental data into the models generally results in more precise and accurate simulations of cellular metabolism.

4.1 Reconstruction and analysis of metabolic networks

It is essential to study metabolism in order to describe and understand the functioning of living cells. The chemical conversion of nutrients into energy, biomass and secondary products is one of the main components of the cellular phenotype, and a defining characteristic of life. Since the metabolic capabilities of an organism are ultimately determined by its genotype, advances in genome sequencing technologies during the last two decades have had a substantial impact on our knowledge about metabolism. With a fully annotated whole genome sequence of an organism, it is feasible to compile a database of all the biochemical reactions that can be catalyzed inside the cell. Besides a list of reactions and their stoichiometries, such a database, called a genome-scale metabolic reconstruction, often includes information that links each reaction to the genes encoding the enzymes that catalyze it (Price et al. 2004). The earliest published genome-scale reconstructions were for organisms with small genomes such as *Haemophilus influenzae* (Schilling and Palsson 2000) and *Escherichia coli* (Edwards and Palsson 2000), but reconstructions for more complex organisms including *Saccharomyces cerevisiae* (Förster et al. 2003), *Arabidopsis thaliana* (de Oliveira Dal'Molin et al. 2010) and *Homo sapiens* (Duarte et al. 2007) have followed since. Revised versions of genome-scale metabolic reconstructions are often published when new genes are discovered or annotated functions of known genes are updated.

A genome-scale metabolic reconstruction allows systematic analysis of the metabolic network of an organism, and can even form a starting point for whole-cell simulations (Orth et al. 2010; Karr et al. 2012). In order to perform such analyses, the genome-scale reconstruction must be formulated as a mathematical model, e.g. in the form of a system of differential equations,

$$\frac{d\boldsymbol{x}}{dt} = \boldsymbol{S} \cdot \boldsymbol{v}(\boldsymbol{x}, \boldsymbol{k}) \qquad (1)$$

Here $\boldsymbol{S}$ denotes the stoichiometric matrix, derived from the genome-scale reconstruction with element s_{ij} denoting the stoichiometric coefficient of metabolite *i* in reaction *j*, and $\boldsymbol{x}$ is a vector of concentrations of all metabolites in the cell. Reaction rates, $\boldsymbol{v}$, are a function of current metabolite concentrations and kinetic parameters, $\boldsymbol{k}$. Given initial metabolite concentrations, the system of differential equations is readily solved numerically. While the formulation is conceptually simple, its

use on the genome-scale is impeded by limited knowledge of the many kinetic parameters (McCloskey et al. 2013).

To avoid the issue of unknown kinetic parameters, constraint-based metabolic modeling methods are often used instead. Constraint-based modeling imposes constraints on the system and finds metabolic reaction rates that are consistent with these constraints. The most central constraint is the assumption of steady-state, where the concentrations of internal metabolites are assumed to be constant. This corresponds to setting the left-hand side of Equation 1 to zero and results in a system of linear equations,

$$\boldsymbol{S} \cdot \boldsymbol{v} = \mathbf{0} \tag{2}$$

that can be solved for the reaction rates or metabolic fluxes, $\boldsymbol{v}$ (Orth et al. 2010). The kinetic parameters are not accounted for explicitly in constraint-based models, which only require the stoichiometric matrix to be known. For most genome-scale reconstructions, the system of equations is underdetermined, meaning that an infinite number of flux solutions exist. One way to address this issue is to identify a solution that optimizes a specific objective. This is based on an assumption that the cell has evolved to maximize some biological objective, e.g. production of ATP or production of biomass. Production of biomass is modeled through a bulk-reaction that consumes biomass constituents such as nucleotides and amino acids in empirically determined ratios (Orth et al. 2010). This method is known as flux balance analysis (FBA) and has become the foundation of most work in constraint-based metabolic modeling. Performing flux balance analysis requires the solution of a linear optimization problem. The result is a set of reaction rates that satisfy the constraints of the system and is consistent with the defined biological objective.

Despite the simple formulation and strong assumptions, FBA has proven useful in a number of metabolic modeling applications, to predict the rates of metabolic reactions, typically called the flux distribution (McCloskey et al. 2013). It can been used for instance to predict essential metabolic genes, i.e. genes that are required for the synthesis of one or more biomass constituents. This is done by simply removing corresponding reactions from the model and performing FBA. If the maximal biomass flux is zero in the knockout model, the gene is expected to be essential. Comparisons with experimental data from single-knockout studies have shown good

correspondence with the results of FBA-based essentiality predictions in *E. coli* and other bacteria such as *Pseudomonas aeruginosa* (Edwards and Palsson 2000; Oberhardt et al. 2008). In other organisms, e.g. *S. cerevisiae*, predictions of essentiality are less accurate, and for multiple knockouts in particular there is only a very low correlation between experimental data and FBA predictions (Heavner and Price 2015).

The assumption of maximization of biomass production as a metabolic objective is often reasonable for microorganisms during exponential growth, but it will clearly not hold for most mammalian cells or other multicellular organisms whose evolutionary pressure has selected for far more complex traits than simply growth at the cellular level. As replacement for FBA, Markov chain Monte Carlo (MCMC) methods can be used to uniformly sample the feasible steady-state flux space described by Equation 2. MCMC methods provide an estimate of the joint probability distribution of fluxes and do not depend on a pre-specified biological objective. The applications of random sampling methods include the analysis of red blood cells under storage conditions (Bordbar et al. 2016), aspirin resistance in platelets (Thomas et al. 2015), transcriptional regulation in human adipocytes (Mardinoglu et al. 2014) and in bacterial communities in the human gut (Shoaie et al. 2013), as well as the metabolic re-wiring that takes place in epithelial to mesenchymal transition during the development of breast cancer (Halldorsson et al. 2017).

4.2 Constraining metabolic models with transcriptomics and proteomics data

Although mass balance is an essential principle, metabolism is constrained by other factors and physical principles as well. FBA assumes that the cell can use all metabolic reactions at a given time in the combination that gives the highest biomass production. However, this is contradicted by the fact that only a proportion of an organism's genes will be transcriptionally active at the same time. Thus further constraints can be imposed on the model by leveraging information about the transcriptional state of the cell. This can be used to create context-specific models from generic models, such as the generic human reconstruction Recon1 (Duarte et al. 2007), as well as to improve the accuracy of flux predictions. The simplest realization of this idea utilizes the fact that an enzyme cannot catalyze any reaction flux if its encoding gene is not expressed. Reactions catalyzed by genes with transcript levels below a defined threshold can thus be forced to be inactive by removing them from the model. Flux distributions obtained with such a constrained model were found to be more

strongly correlated to experimentally measured fluxes in *S. cerevisiae* compared to an unconstrained model (Åkesson et al. 2004). More sophisticated algorithms minimize the difference between the predicted flux distribution and the gene expression data. The Gene Inactivity Moderated by Metabolism and Expression (GIMME) algorithm (Becker and Palsson 2008) finds flux values which minimize the utilization of reactions with low expression levels, in order to meet pre-specified metabolic requirements such as growth. The iMAT method developed by Shlomi and coworkers (Shlomi et al. 2008) alleviates the need for a pre-specified cellular objective and is therefore suitable for analyzing mammalian cells and tissues. The method partitions gene expression values into three groups, corresponding to high, moderate and low expression and then maximizes the number of reactions with flux levels in agreement with the expression states. This enabled identification of tissue-specific metabolic activities in different human tissues, and the construction of tissue-specific models of human metabolism. An extension of iMAT was used to construct a model of cancer metabolism from Recon1 and expression data from cancer cell lines in the NCI-60 collection. The cancer model was then used to identify several cytostatic drug targets, and generate a list of potential selective anti-cancer treatments (Folger et al. 2011).

Since Åkesson and coworkers first used gene-expression data to constrain metabolic models, a large number of methods that integrate expression data and flux predictions have been published. An evaluation of many of these methods, by their ability to predict flux distributions in *E.* coli and *S. cerevisiae*, showed that none of them performed significantly better than parsimonious FBA, an extension of FBA that finds the flux distribution with the smallest sum of fluxes that can support the optimal objective value (Machado and Herrgård 2014). This suggests that gene transcription levels do not correlate strongly with reaction fluxes, at least in microbial cells, which is not surprising considering that translational efficiency, post-translational modifications and allosteric regulation all have an effect on fluxes as well.

A step closer to the actual reactions than mRNA abundance is protein concentration. A certain correlation between mRNA and protein concentration is to be expected (Gry et al. 2009), and several methods for integrating gene expression data into metabolic models can indeed use protein abundance data with the same algorithms, simply by replacing gene expression thresholds with protein abundance thresholds (Becker and Palsson 2008; Machado and Herrgård 2014). However,

there have also been attempts to more explicitly incorporate proteomics data into the modeling frameworks. A central component of enzyme kinetics is the concept of the catalytic capacity of an enzyme. Each enzyme molecule can only perform a certain number of conversions per second; an increased flux will therefore require a larger number of enzymes at some point. The maximum possible flux, represented by the V_{max} parameter, can be calculated from the enzyme concentration and catalytic turnover number, k_{cat}

$$V_{max} = k_{cat} \cdot [E] \tag{3}$$

If the catalytic turnover parameters are known, this relationship can be used to constrain fluxes using protein concentration data. In the GECKO modeling framework (Sánchez et al. 2017), a constraint is added for each enzyme, representing the enzyme's degree of utilization, where the upper bound is set to the measured enzyme concentration. The utilization of an enzyme is obtained by summing v/k_{cat} for all reactions catalyzed by that enzyme. Using GECKO with a proteomics dataset for *S. cerevisiae*, Sanchez and coworkers showed that the space of possible fluxes was reduced considerably by excluding all flux distributions that were not consistent with the observed enzyme levels. On the other hand, the fluxes predicted for *S. cerevisiae* grown in glucose limited minimal medium did not have a significantly smaller error compared to experimentally measured fluxes than those predicted with FBA. It is possible however, that the advantage of using proteomics data will be larger in cases where the assumption of maximal growth is not valid, e.g. under stress conditions or in genetically perturbed strains. GECKO can also be used in the absence of proteomics data by imposing a single overall constraint on the total enzyme mass. This resulted in more accurate predictions of maximal growth rates on a wide range of different carbon sources, for which FBA tends to overestimate growth rate. Another interesting growth effect that was captured by including an overall protein constraint is the shift from respiration to fermentation at high growth rates. This overflow metabolism, also known as the Crabtree effect in yeast (Crabtree 1929) and the Warburg effect in cancer cells (Warburg et al. 1927), cannot be captured by FBA, where simply the flux distribution with the highest biomass yield is found, independently of growth rate. The overflow effect is most likely caused by respiratory enzymes having a higher proteome cost than fermentative enzymes (Basan et al. 2015), which means that at high growth rates protein allocation becomes limiting and fermentation becomes more efficient even though it has a lower energy/carbon yield.

Overflow metabolism has been modeled e.g. in *E. coli* (Basan et al. 2015), *S. cerevisiae* (Sánchez et al. 2017) and cancer cells (Shlomi et al. 2011), by different models with the common trait of somehow constraining the proteome.

The causes of the Warburg effect in cancer cells were studied using Recon1 by placing a constraint on total enzyme concentration to account for enzyme solvent capacity (Shlomi et al. 2011). To compute the contribution of each enzyme to the total concentration, an estimate of the enzyme turnover number was required. Estimates for 15% of the reactions could be obtained from biochemical databases, the rest was assigned a fixed value of 25/s. Using FBA and random sampling, the Warburg effect was shown to be a consequence of metabolic adaptations to increase biomass productivity. Further analysis revealed the preference of cancer cells to take up glutamine instead of other amino acids.

Resource allocation between cellular processes in *Bacillus subtilis* was recently analyzed using a method that incorporates genome-wide protein quantification data and extracellular nutrient concentrations with a metabolic reconstruction (Goelzer et al. 2015). The method, Resource Balance Analysis (RBA), links flux to enzyme abundance, assuming a relationship similar to Equation 3, while incorporating information on protein activity and protein localization. The use of RBA is fairly involved compared to the methods described earlier and requires specification of a large number of parameters. The parameters were partly obtained from Uniprot and partly inferred from data. RBA accurately predicted the allocation of resources in *B. subtilis* over a wide range of conditions. In vivo knockouts of enzymes which were expressed but predicted to have zero flux in the model resulted in significantly increased growth (Goelzer et al. 2015). This suggests that the method may be useful for constructing minimal cell factories, e.g. for protein production.

4.3 Models of metabolism and macromolecular expression

The previously described methods for combining *omics* data and metabolic models are mostly based on heuristically formulated constraints and/or objectives. When the measured quantities – such as mRNA and protein abundances – are not explicitly accounted for in the modeling framework, they cannot be seamlessly integrated into it. To address this problem, an extended modeling framework that explicitly models the expression of macromolecules, such as RNA and protein, has been

developed. Construction of such models of metabolism and expression (ME-models) began with the reconstruction of the macromolecular expression network of *E. coli*, analogously to the metabolic network (Thiele et al. 2009). Transcription of a given gene to produce mRNA is modeled as a reaction consuming nucleotides in proportions consistent with the specific sequence, and similarly translation is modeled as a reaction consuming charged tRNAs while producing protein and uncharged tRNAs. In order to model how metabolic catalysis is dependent on translation of a specific protein and how translation of a protein is dependent on transcription of its gene to mRNA, these different reactions must be coupled (Thiele et al. 2009; Lerman et al. 2012). A certain quantity of an enzyme can only catalyze a limited reaction flux and Equation 3 can be rearranged to enable calculation of the minimum amount of enzyme required to catalyze a given flux

$$[E] \geq \frac{v}{k_{cat}} \tag{4}$$

Equation 4 represents a constraint that can be used to couple metabolic reactions to the enzymes that catalyze them. Identical constraints can be formulated for ribosomes and mRNA in translation reactions and for RNA-polymerase in transcription reactions. A constraint-based modeling framework, however, does not model concentrations of metabolites (or enzymes) and is thus not directly compatible with such constraints. To circumvent this it is necessary to account for growth-related dilution. In a growing cell, metabolite pools are continuously diluted, because of the expanding intracellular volume, by a rate equal to the product of the growth rate and metabolite concentration. This means that in steady-state, catalysis of a reaction requires that the catalyzing enzyme be produced at a rate proportional to the growth rate. Enzymatic conversion of compound *A* into compound *B* by enzyme *E* thus becomes (Lloyd et al. 2017):

$$A + \frac{\mu}{k_{cat}} E \rightarrow B \tag{5}$$

In FBA the requirement of enzyme production is modeled through the composition of the biomass reaction, but since this reaction is determined *a priori*¸ FBA cannot model how biomass composition changes under different growth rates and conditions. With ME-models the empirical biomass reaction is replaced by explicitly modeling the relationship between metabolism and macromolecular expression. ME-models can thus directly predict the expression levels of different

proteins, which can be compared with *omics* datasets. A ME-model of the thermophilic bacterium *Thermotoga maritima* (Lerman et al. 2012), found moderate correlations between predicted and experimentally measured mRNA profiles (r= 0.54), protein expression profiles (r = 0.57), as well as proteome amino acid composition (r = 0.79). A ME-model of *E. coli* showed improved prediction of growth rates in different nutrient conditions compared to FBA (Thiele et al. 2012), and could accurately predict several internal fluxes (O'Brien et al. 2013). Additionally, since ME-models explicitly include the cost of producing the enzymes required for various pathways, they implicitly limit the total proteome size and thus also capture metabolic overflow effects, such as the acetate overflow metabolism in *E. coli* (O'Brien et al. 2013).

Whereas traditional constraint-based metabolic models include, and can thus directly predict, growth rate, uptake and secretion rates and internal fluxes, ME-models can additionally predict expression profiles and proteome composition, and thus they can also be directly constrained by expression and proteomics data. Because of this, ME-models represent an intuitive and theoretically justified method of integrating transcriptomics and proteomics data into metabolic models. They have not yet found broad usage in the metabolic modeling community, presumably because of the time it takes to run simulations (several orders of magnitude higher than with FBA), and the lack of related model and software infrastructure, but these issues are continuously being addressed (Yang et al. 2016; Lloyd et al. 2017).

4.4 Augmenting models with metabolomics data

In a discussion of data integration in metabolic models, it is impossible not to mention metabolomics. Different analytical methods, e.g. enzymatic assays, chromatography and mass spectrometry, can be used to take snapshots of the cellular metabolism with varying resolution, coverage, precision and throughput. However, they all provide useful information about the concentrations of metabolite pools in the cell. One of the earliest uses of metabolomics data to improve metabolic modeling was metabolic flux analysis (MFA), which utilizes time-course metabolite concentration data from cultures fed with isotopically labeled substrates to infer flux values in the metabolic network (Stephanopoulos 1999; Sauer 2006). This is done by monitoring how the isotopes, e.g. ^{13}C or ^{15}N, spread to downstream metabolite pools over time. The advantage of this method is that the resulting fluxes can be used directly to constrain metabolic models or to

compare the validity of different simulation methods. However, MFA is labor- and cost intensive and works best on a smaller subset of the entire metabolic network, typically just the central carbon metabolism (Antoniewicz 2015; Gopalakrishnan and Maranas 2015).

Changes in extracellular metabolite concentrations over time can be used to estimate uptake and secretion rates and constrain the flux space. However, since constraint-based modeling frameworks model fluxes under an assumption of steady-state, internal metabolite concentration data at a single time point without isotopic labeling cannot be directly utilized. Despite this, metabolomics data can still be used to either constrain the models or to provide new insights in combination with the simulation results. In order to model cells that are not in steady-state, such as human blood cells undergoing physiological changes during storage, Bordbar and coworkers devised a method called unsteady-state FBA (Bordbar et al. 2017). Using time-course metabolomics they determined the rate of accumulation or depletion for internal metabolites, which was then modeled by adding source and sink reactions to the metabolic model. These reactions were then constrained to have fluxes corresponding to the experimentally determined rates of concentration changes. Subsequent MFA revealed that the fluxes predicted with this method were more accurate than those obtained by regular FBA.

Aside from enforcing steady state, a commonly used constraint in constraint-based models is to force certain fluxes to only go in one direction. This is straightforward for some reactions whose thermodynamics make it practically irreversible under biological conditions. Other reactions are closer to equilibrium and can go in both directions depending on specific conditions. The spontaneous direction of a reaction can be calculated by the formula

$$\Delta_{\mathrm{r}}G = \Delta_{\mathrm{r}}G^{\circ} + RT\ log(Q) \qquad (6)$$

If the left-hand side (the reaction Gibbs free energy) is negative, the reaction will proceed spontaneously in the forward direction, while it will proceed spontaneously in the reverse direction if the reaction Gibbs free energy is positive. $\Delta_{\mathrm{r}}G^{\circ}$ is the reaction Gibbs free energy under standard conditions, *RT* is the gas constant times the absolute temperature and *Q* is the reaction quotient, containing the concentrations of the reaction products and substrates. The standard Gibbs free energy must in principle be determined experimentally, but in most cases it can be calculated from

the structure of the participating metabolites and already known reaction Gibbs free energies for other reactions (Noor et al. 2013). This means that a dataset of metabolite concentrations can be used to constrain reactions to a specific direction depending on the specific metabolic conditions, reducing the space of feasible fluxes significantly (Soh and Hatzimanikatis 2014). In many simulated growth conditions, it can be sufficient simply to constrain reaction directionalities according to the most common mode of operation without regard to actual metabolite concentrations. Some reactions however, occur in the unconventional direction under extreme conditions, such as very high CO_2 concentrations. In such cases using thermodynamics and metabolite data to inform reaction directionalities will be particularly beneficial and can lead to more accurate simulations (Soh et al. 2012).

Constraint-based simulations can also be combined with metabolomics data in another way. In addition to calculating a flux distribution, simulating a constraint-based model also provides so-called shadow prices. Each shadow price is linked to a metabolite and reflects how much the objective function, e.g. growth, could be improved if the model were allowed to get some of that metabolite "for free". In other words a shadow price is a measure of how limiting a given metabolite's mass balance is for the objective function. Depending on the algorithm used to solve the FBA problem, shadow prices are either a byproduct of the solution process or can be obtained with modest computational effort.

Zampieri and coworkers investigated the evolution of antibiotic resistance in *E. coli* using adaptive laboratory evolution (Zampieri et al. 2017). By maximizing and minimizing flux through each reaction in the model and calculating the shadow prices, the authors could identify reactions, which, when maximized or minimized, resulted in shadow prices that were consistent with the observed patterns of metabolite concentration changes. Those reactions were hypothesized as being targets of evolution, whose flux should be increased in order to increase antibiotic resistance.

Besides constraint-based modeling, the most common way to simulate cellular metabolism is with kinetic models. This involves the solution of the system of differential equations shown in Eq. 1 from given initial metabolite concentrations. As previously described, one of the challenges with this approach is the requirement of knowing the values of all the kinetic parameters of the system. For small biochemical systems, the kinetic parameters can sometimes be determined individually

through *in vitro* experiments, but for genome-scale models this is not feasible. Additionally there is no guarantee that the *in vitro* kinetic parameters are representative of how an enzyme functions *in vivo* (Teusink et al. 2000). Instead of the bottom-up approach of experimentally determining each parameter, a top-down approach may be used, where the model parameters might initially be estimated from prior information, such as *in vitro* data, but are predominantly selected by fitting simulation results to genome-scale experimental data. This has long been done for small-scale networks, using metabolomics and MFA data (Jamshidi and Palsson 2008; Srinivasan et al. 2015), however with continual increases in dataset sizes and computing power, it has also become feasible to do this for genome-scale networks. Recently a genome-scale kinetic model of *E. coli* was published along with estimated values for all kinetic parameters (Khodayari and Maranas 2016). The model parameters were fitted using experimental flux data and model predictions were validated against metabolomics data. In addition the model could quantitatively predict product yields of 24 different compound in 320 mutant strains, which was considerably better than the constraint-based simulation methods it was tested against. In another study kinetic models of human red blood cells were used to investigate individual variations in susceptibility to side effects of the hepatitis B drug Ribavirin (Bordbar et al. 2015). By measuring intracellular metabolite levels in red blood cells of 24 patients, they could determine individual kinetic parameter values for each of the patients, and show that those parameters were predictive of whether the patient was sensitive to side effects. Furthermore, the identified relationships between kinetic parameters and sensitivity to drug side-effect were consistent with known mechanisms of Ribavirin side effects. These results show that kinetic modeling frameworks have the potential to significantly outperform constraint-based simulations, and that with modern *omics* technologies and computer power, it is feasible to parametrize them sufficiently to predict metabolic behavior (Saa and Nielsen 2017).

4.5 Combining metabolic models and machine learning methods

The term machine learning covers a broad range of methods where large datasets are used to infer relationships between variables or to predict various outcomes from given input data. Often this is done without much consideration of specific mechanisms of the studied phenomena. Such data-driven methods can of course be applied to metabolic data, but with limited connection to biological mechanisms, the results are often difficult to interpret. Instead, machine learning methods can be

combined with domain-specific biological knowledge, such as the information encoded within a genome-scale reconstruction, to create hybrid methods that also take advantage of the metabolic network structure.

Plaimas and coworkers predicted gene essentiality in *E. coli* using a hybrid method (Plaimas et al. 2008). Instead of using FBA to predict essentiality as described previously, they defined a set of features for each reaction, including metrics of network topology, gene expression data and predicted FBA fluxes. These features were fed into a support vector machine classifier together with labels from experimental essentiality data (Baba et al. 2006). The predictive accuracy of gene essentiality was 92%, compared to 85% for FBA. Furthermore, the genes where essentiality was not correctly predicted were retested experimentally, and in several cases the authors identified errors in the original experimental dataset. By removing single features from the input data one at a time, the authors could also identify which features were most important for accurately predicting essentiality. Prediction with FBA suffers mainly from two problems, namely that the metabolic network might be incomplete, and that the assumption of growth optimality does not always hold (O'Brien et al. 2015). A hybrid method can instead learn from data, utilizing the biological context, e.g. in the form of a metabolic network, only when it improves prediction performance. A similar method was recently used to predict drug side effects (Shaked et al. 2016). A list of drugs known to inactivate one or more enzymatic reactions was used as training data, with features corresponding to the minimum and maximum possible FBA flux for each reaction after deactivating the drug's target reaction(s) in the Recon1 model. Support vector machine classifiers were then trained to predict which (if any) side effects the drug would have. Using a feature selection method it was also possible to find the features that were most strongly associated with a given side effect. Many of the results were found to be consistent with the published literature of these drug side effects.

A third example of a combination of machine learning with metabolic network data was used to predict novel drug-reaction interactions for cancer therapy (Li et al. 2010). The method requires the construction of a reaction flux similarity matrix. This matrix was obtained using the GIMME algorithm to predict reaction fluxes from gene expression data in 59 cancer cell lines. Reactions with the same flux profile across the cell lines were said to have a high similarity, while reactions with different flux profiles had a low similarity. The reaction flux similarity matrix was combined with

knowledge of existing drug-reaction interactions, using a K-nearest neighbors algorithm, to predict new interactions.

Where purely model-based algorithms may suffer from lack of biological knowledge such as kinetic parameters, the use of machine learning methods in biomedical research is often hampered by difficulties in interpreting the results. The examples above show that the two methodologies can be combined to achieve results that are informed by experimental data, while maintaining biologically relevant relationships between variables. Such hybrid methods can be used to build accurate predictive models, while also providing new biological insights and will without doubt find widespread use in the future.

4.6 Conclusions

Genome-scale models of metabolism have found applications ranging from industrial biotechnology to human health. These models can now be readily built for any organism to predict metabolic phenotypes such as the effect of a gene knock-out on cell growth. Advanced formulations of genome-scale models allow integrating diverse omics data types including transcriptomics, proteomics and metabolomics data to the modeling. Advanced genome-scale models make more accurate condition-dependent model predictions, and expand the range of predicted intracellular variables from metabolic fluxes to concentrations of metabolites and proteins. Genome-scale mechanistic models can also be combined with purely data-driven machine learning methods to obtain hybrid mechanistic/statistical models with the potential for improving predictive performance. With increasing amounts of different omics data types becoming available for all organisms, the modeling approaches described in this chapter can be further improved and extended to obtain highly predictive models of cellular processes.

4.7 References

Åkesson M, Förster J, Nielsen J (2004) Integration of gene expression data into genome-scale metabolic models. Metab Eng 6:285–293 . doi: 10.1016/j.ymben.2003.12.002

Antoniewicz MR (2015) Methods and advances in metabolic flux analysis: a mini-review. J Ind Microbiol Biotechnol 42:317–325 . doi: 10.1007/s10295-015-1585-x

Baba T, Ara T, Hasegawa M, Takai Y, Okumura Y, Baba M, Datsenko KA, Tomita M, Wanner BL, Mori H (2006) Construction of Escherichia coli K-12 in-frame, single-gene knockout mutants: the Keio collection. Mol Syst Biol 2: . doi: 10.1038/msb4100050

Basan M, Hui S, Okano H, Zhang Z, Shen Y, Williamson JR, Hwa T (2015) Overflow metabolism in Escherichia coli results from efficient proteome allocation. Nature 528:99–104 . doi: 10.1038/nature15765

Becker SA, Palsson BO (2008) Context-specific metabolic networks are consistent with experiments. PLoS Comput Biol 4: . doi: 10.1371/journal.pcbi.1000082

Bordbar A, Johansson PI, Paglia G, Harrison SJ, Wichuk K, Magnusdottir M, Valgeirsdottir S, Gybel-Brask M, Ostrowski SR, Palsson S, Rolfsson O, Sigurjónsson OE, Hansen MB, Gudmundsson S, Palsson BO (2016) Identified metabolic signature for assessing red blood cell unit quality is associated with endothelial damage markers and clinical outcomes. Transfusion 56:852–862 . doi: 10.1111/trf.13460

Bordbar A, McCloskey D, Zielinski DC, Sonnenschein N, Jamshidi N, Palsson BO (2015) Personalized Whole-Cell Kinetic Models of Metabolism for Discovery in Genomics and Pharmacodynamics. Cell Syst 1:283–292 . doi: 10.1016/j.cels.2015.10.003

Bordbar A, Yurkovich JT, Paglia G, Rolfsson O, Sigurjónsson ÓE, Palsson BO (2017) Elucidating dynamic metabolic physiology through network integration of quantitative time-course metabolomics. Sci Rep 7: . doi: 10.1038/srep46249

Crabtree HG (1929) Observations on the carbohydrate metabolism of tumours. Biochem J 23:536–45 . doi: 10.1042/bj0230536

de Oliveira Dal'Molin CG, Quek L-E, Palfreyman RW, Brumbley SM, Nielsen LK (2010) AraGEM, a Genome-Scale Reconstruction of the Primary Metabolic Network in Arabidopsis. Plant Physiol 152:579–589 . doi: 10.1104/pp.109.148817

Duarte NC, Becker SA, Jamshidi N, Thiele I, Mo ML, Vo TD, Srivas R, Palsson BO (2007) Global reconstruction of the human metabolic network based on genomic and bibliomic data. Proc

Natl Acad Sci 104:1777–1782 . doi: 10.1073/pnas.0610772104

Edwards JS, Palsson BO (2000) The Escherichia coli MG1655 in silico metabolic genotype: Its definition, characteristics, and capabilities. Proc Natl Acad Sci 97:5528–5533 . doi: 10.1073/pnas.97.10.5528

Folger O, Jerby L, Frezza C, Gottlieb E, Ruppin E, Shlomi T (2011) Predicting selective drug targets in cancer through metabolic networks. Mol Syst Biol 7:527–527 . doi: 10.1038/msb.2011.63

Förster J, Famili I, Palsson BO, Nielsen J (2003) Large-scale evaluation of in silico gene deletions in Saccharomyces cerevisiae. Omi A J Integr Biol 7:193–202 . doi: 10.1089/153623103322246584

Goelzer A, Muntel J, Chubukov V, Jules M, Prestel E, Nölker R, Mariadassou M, Aymerich S, Hecker M, Noirot P, Becher D, Fromion V (2015) Quantitative prediction of genome-wide resource allocation in bacteria. Metab Eng 32:232–243 . doi: 10.1016/j.ymben.2015.10.003

Gopalakrishnan S, Maranas CD (2015) 13C metabolic flux analysis at a genome-scale. Metab Eng 32:12–22 . doi: 10.1016/j.ymben.2015.08.006

Gry M, Rimini R, Strömberg S, Asplund A, Pontén F, Uhlén M, Nilsson P (2009) Correlations between RNA and protein expression profiles in 23 human cell lines. BMC Genomics 10:365 . doi: 10.1186/1471-2164-10-365

Halldorsson S, Rohatgi N, Magnusdottir M, Choudhary KS, Gudjonsson T, Knutsen E, Barkovskaya A, Hilmarsdottir B, Perander M, Mælandsmo GM, Gudmundsson S, Rolfsson Ó (2017) Metabolic re-wiring of isogenic breast epithelial cell lines following epithelial to mesenchymal transition. Cancer Lett 396:117–129 . doi: 10.1016/j.canlet.2017.03.019

Heavner BD, Price ND (2015) Comparative Analysis of Yeast Metabolic Network Models Highlights Progress, Opportunities for Metabolic Reconstruction. PLoS Comput Biol 11:1–26 . doi: 10.1371/journal.pcbi.1004530

Jamshidi N, Palsson BØ (2008) Formulating genome-scale kinetic models in the post-genome era.

Mol Syst Biol 4:171 . doi: 10.1038/msb.2008.8

Karr JR, Sanghvi JC, MacKlin DN, Gutschow M, Jacobs JM, Bolival B, Assad-Garcia N, Glass JI, Covert MW (2012) A whole-cell computational model predicts phenotype from genotype. Cell 150:389–401 . doi: 10.1016/j.cell.2012.05.044

Khodayari A, Maranas CD (2016) A genome-scale Escherichia coli kinetic metabolic model k-ecoli457 satisfying flux data for multiple mutant strains. Nat. Commun. 7:13806

Lerman JA, Hyduke DR, Latif H, Portnoy VA, Lewis NE, Orth JD, Schrimpe-Rutledge AC, Smith RD, Adkins JN, Zengler K, Palsson BO (2012) In silico method for modelling metabolism and gene product expression at genome scale. Nat Commun 3:929 . doi: 10.1038/ncomms1928

Li L, Zhou X, Ching W-K, Wang P (2010) Predicting enzyme targets for cancer drugs by profiling human metabolic reactions in NCI-60 cell lines. BMC Bioinformatics 11:501 . doi: 10.1186/1471-2105-11-501

Lloyd CJ, Ebrahim A, Yang L, King ZA, Catoiu E, O'Brien EJ, Liu JK, Palsson BO (2017) COBRAme: A Computational Framework for Building and Manipulating Models of Metabolism and Gene Expression. bioRxiv 106559 . doi: http://dx.doi.org/10.1101/106559

Machado D, Herrgård M (2014) Systematic Evaluation of Methods for Integration of Transcriptomic Data into Constraint-Based Models of Metabolism. PLoS Comput Biol 10: . doi: 10.1371/journal.pcbi.1003580

Mardinoglu A, Agren R, Kampf C, Asplund A, Nookaew I, Jacobson P, Walley AJ, Froguel P, Carlsson LM, Uhlen M, Nielsen J (2014) Integration of clinical data with a genome-scale metabolic model of the human adipocyte. Mol Syst Biol 9:649–649 . doi: 10.1038/msb.2013.5

McCloskey D, Palsson BØ, Feist AM (2013) Basic and applied uses of genome-scale metabolic network reconstructions of Escherichia coli. Mol Syst Biol 9:661 . doi: 10.1038/msb.2013.18

Noor E, Haraldsdóttir HS, Milo R, Fleming RMT (2013) Consistent Estimation of Gibbs Energy Using Component Contributions. PLoS Comput Biol 9: . doi: 10.1371/journal.pcbi.1003098

O'Brien EJ, Lerman JA, Chang RL, Hyduke DR, Palsson BO (2013) Genome-scale models of metabolism and gene expression extend and refine growth phenotype prediction. Mol Syst Biol 9:693–693 . doi: 10.1038/msb.2013.52

O'Brien EJ, Monk JM, Palsson BO (2015) Using genome-scale models to predict biological capabilities. Cell 161:971–987 . doi: 10.1016/j.cell.2015.05.019

Oberhardt MA, Puchałka J, Fryer KE, Martins Dos Santos VAP, Papin JA (2008) Genome-scale metabolic network analysis of the opportunistic pathogen Pseudomonas aeruginosa PAO1. J Bacteriol 190:2790–2803 . doi: 10.1128/JB.01583-07

Orth JD, Thiele I, Palsson BØ (2010) What is flux balance analysis? Nat Biotechnol 28:245–248 . doi: 10.1038/nbt.1614

Plaimas K, Mallm J-P, Oswald M, Svara F, Sourjik V, Eils R, Konig R (2008) Machine learning based analyses on metabolic networks supports high-throughput knockout screens. BMC Syst Biol 2:67 . doi: 10.1186/1752-0509-2-67

Price ND, Reed JL, Palsson BØ (2004) Genome-scale models of microbial cells: evaluating the consequences of constraints. Nat Rev Microbiol 2:886–897 . doi: 10.1038/nrmicro1023

Saa PA, Nielsen LK (2017) Formulation, construction and analysis of kinetic models of metabolism: A review of modelling frameworks. Biotechnol Adv 0–1 . doi: 10.1016/j.biotechadv.2017.09.005

Sánchez BJ, Zhang C, Nilsson A, Lahtvee P, Kerkhoven EJ, Nielsen J (2017) Improving the phenotype predictions of a yeast genome-scale metabolic model by incorporating enzymatic constraints. Mol Syst Biol 13:935 . doi: 10.15252/msb.20167411

Sauer U (2006) Metabolic networks in motion: 13C-based flux analysis. Mol Syst Biol 2:1–10 . doi: 10.1038/msb4100109

Schilling CH, Palsson BØ (2000) Assessment of the Metabolic Capabilities of Haemophilus influenzae Rd through a Genome-scale Pathway Analysis. J Theor Biol 203:249–283 . doi:

10.1006/jtbi.2000.1088

Shaked I, Oberhardt MA, Atias N, Sharan R, Ruppin E (2016) Metabolic Network Prediction of Drug Side Effects. Cell Syst 2:209–213 . doi: 10.1016/j.cels.2016.03.001

Shlomi T, Benyamini T, Gottlieb E, Sharan R, Ruppin E (2011) Genome-scale metabolic modeling elucidates the role of proliferative adaptation in causing the warburg effect. PLoS Comput Biol 7:1–8 . doi: 10.1371/journal.pcbi.1002018

Shlomi T, Cabili MN, Herrgård MJ, Palsson BØ, Ruppin E (2008) Network-based prediction of human tissue-specific metabolism. Nat Biotechnol 26:1003–1010 . doi: 10.1038/nbt.1487

Shoaie S, Karlsson F, Mardinoglu A, Nookaew I, Bordel S, Nielsen J (2013) Understanding the interactions between bacteria in the human gut through metabolic modeling. Sci Rep 3:2532 . doi: 10.1038/srep02532

Soh KC, Hatzimanikatis V (2014) Constraining the Flux Space Using Thermodynamics and Integration of Metabolomics Data. In: Krömer JO, Nielsen LK, Blank LM (eds) Metabolic Flux Analysis: Methods and Protocols. Springer New York, New York, NY, pp 49–63

Soh KC, Miskovic L, Hatzimanikatis V (2012) From network models to network responses: Integration of thermodynamic and kinetic properties of yeast genome-scale metabolic networks. FEMS Yeast Res 12:129–143 . doi: 10.1111/j.1567-1364.2011.00771.x

Srinivasan S, Cluett WR, Mahadevan R (2015) Constructing kinetic models of metabolism at genome-scales: A review. Biotechnol J 10:1345–1359 . doi: 10.1002/biot.201400522

Stephanopoulos G (1999) Metabolic Fluxes and Metabolic Engineering. Metab Eng 1:1–11 . doi: 10.1006/mben.1998.0101

Teusink B, Passarge J, Reijenga CA, Esgalhado E, Van Der Weijden CC, Schepper M, Walsh MC, Bakker BM, Van Dam K, Westerhoff H V., Snoep JL (2000) Can yeast glycolysis be understood terms of vitro kinetics of the constituent enzymes? Testing biochemistry. Eur J Biochem 267:5313–5329 . doi: 10.1046/j.1432-1327.2000.01527.x

Thiele I, Fleming RMT, Que R, Bordbar A, Diep D, Palsson BO (2012) Multiscale Modeling of Metabolism and Macromolecular Synthesis in E. coli and Its Application to the Evolution of Codon Usage. PLoS One 7: . doi: 10.1371/journal.pone.0045635

Thiele I, Jamshidi N, Fleming RMT, Palsson BO (2009) Genome-scale reconstruction of escherichia coli's transcriptional and translational machinery: A knowledge base, its mathematical formulation, and its functional characterization. PLoS Comput Biol 5: . doi: 10.1371/journal.pcbi.1000312

Thomas A, Rahmanian S, Bordbar A, Palsson BØ, Jamshidi N (2015) Network reconstruction of platelet metabolism identifies metabolic signature for aspirin resistance. Sci Rep 4:3925 . doi: 10.1038/srep03925

Warburg O, Wind F, Negelein E (1927) The metabolism of tumors in the body. J Gen Physiol 8:519–530 . doi: 10.1085/jgp.8.6.519

Yang L, Ma D, Ebrahim A, Lloyd CJ, Saunders MA, Palsson BO (2016) solveME: fast and reliable solution of nonlinear ME models. BMC Bioinformatics 17:391 . doi: 10.1186/s12859-016-1240-1

Zampieri M, Enke T, Chubukov V, Ricci V, Piddock L, Sauer U (2017) Metabolic constraints on the evolution of antibiotic resistance. Mol Syst Biol 13:917 . doi: 10.15252/msb.20167028

Chapter 5: OptCouple: joint simulation of gene knockouts, insertions and medium modifications for prediction of growth-coupled strain designs

Kristian Jensen[1], Valentijn Broeken[1], Anne Sofie Lærke Hansen[1], Nikolaus Sonnenschein[1], Markus J. Herrgård[1*]

[1] The Novo Nordisk Foundation Center for Biosustainability, Technical University of Denmark, Building 220, Kemitorvet, 2800 Kgs. Lyngby, Denmark

* Correspondence: herrgard@biosustain.dtu.dk

Abstract

Biological production of chemicals is an attractive alternative to petrochemical-based production, due to advantages in environmental impact and the spectrum of feasible targets. However, engineering microbial strains to overproduce a compound of interest can be a long, costly and painstaking process. If production can be coupled to cell growth it is possible to use adaptive laboratory evolution to increase the production rate. Strategies for coupling production to growth, however, are often not trivial to find. Here we present OptCouple, a constraint-based modeling algorithm to simultaneously identify combinations of gene knockouts, insertions and medium supplements that lead to growth-coupled production of a target compound. We validated the algorithm by showing that it can find novel strategies that are growth-coupled in silico for a compound that has not been coupled to growth previously, as well as reproduce known growth-coupled strain designs for two different target compounds. Furthermore, we used OptCouple to construct an alternative design with potential for higher production. We provide an efficient and easy-to-use implementation of the OptCouple algorithm in the cameo Python package for computational strain design.

5.1 Introduction

The use of microorganisms as cell factories offers the possibility of producing a wide range of chemicals from renewable sources, as well as manufacturing natural compounds too complicated for chemical synthesis in large amounts (Becker and Wittmann, 2015). However, successfully engineering microorganisms to produce a target compound most often requires trial-and-error experimentation with different possible pathways, and even when production is achieved, many iterations of subsequent optimization are usually necessary to increase production rate and yield to satisfy industrial needs (Lee and Kim, 2015).

One strategy for optimizing chemical production in microbial strains is to utilize the power of natural selection in adaptive laboratory evolution (ALE) experiments (Portnoy et al., 2011; Shepelin et al., 2018). This allows the identification of mutant strains with enhanced viability under the evolution conditions. The inherent selection for cells that are able to grow faster than the rest of the population makes it easy to optimize for characteristics such as product tolerance or substrate utilization, while directly improving production characteristics such as production rate, titer and yield is more difficult (Hansen et al., 2017; Shepelin et al., 2018). Indeed, with the advent of more and more methods, models, and databases for automated running and analysis of ALE experiments, such as eVOLVER (Wong et al., 2018), ALEsim (LaCroix et al., 2017), and ALEdb (Phaneuf et al., 2018), the need for new selective pressures by clever strain and experimental design becomes the primary challenge for evolutionary strain engineering.

Using evolution to improve biochemical production rates can be achieved by coupling production to growth, i.e. ensuring that production is a necessary by-product of cell growth, such that adaptations that increase the growth rate of the cells will also increase production. For a review of examples of successful growth-coupling for biochemical production, see e.g. Shepelin et al. (2018). A recent successful example is the growth-coupling of itaconic acid production in *Escherichia coli* by four gene deletions, a downregulation, and glutamate supplementation that ensure formation of itaconic acid to prevent accumulation of PEP inside the cell (Harder et al., 2016). The design was aided by the computation of minimal cut sets (MCS), which are sets of gene knockouts that will prevent all undesirable flux distributions while maintaining the ability to produce the target compound (Klamt and Gilles, 2004; von Kamp and Klamt, 2014).

Since growth-coupling strategies are not always obvious from looking at a metabolic map of the microorganism, it is beneficial to use genome-scale metabolic models together with computational methods like the MCS framework, to quickly search the design space for strain modifications that can potentially make production growth-coupled. One of the first computational methods for predicting strategies for improving bio-production was OptKnock (Burgard et al., 2003). OptKnock uses a mixed integer linear programming (MILP) formulation to predict gene knockouts that allow higher production under growth-optimal conditions. While the predictions made by OptKnock will allow for increased production, they will not necessarily make production growth-coupled, as alternative pathways can be used instead. The algorithm RobustKnock (Tepper and Shlomi, 2009) seeks to solve this problem by predicting knock-out combinations that maximize the minimal production under optimal growth. The more recent algorithm gcOpt (Alter et al., 2018) is similar to RobustKnock, but requires a fixed growth rate to be set, allowing the formulation to be simplified. In addition to finding gene knockouts, there are also algorithms, e.g. the RobOKoD algorithm (Stanford et al., 2015), that attempt to increase production rates by predicting native genes to under- and overexpress. However, growth-coupling a production pathway alleviates the need for such expression level perturbations, since these can be optimized subsequently by means of ALE (Shepelin et al., 2018).

It has been shown that almost all metabolites in *E. coli* can be growth-coupled through knockouts, but in many cases this would require deletion of an infeasible number of genes (von Kamp and Klamt, 2017). Growth coupling may be easier to achieve by inserting heterologous genes that alter host metabolism in addition to knocking out native genes. The algorithm OptStrain (Pharkya et al., 2004) predicts both knockouts and insertions for increasing production, but does so in a two-step process. First, heterologous reactions that enable or improve the production capabilities are identified from a database of known reactions. This can be a novel production pathway or stoichiometrically favourable alternate reactions. Subsequently, knockouts that increase the possible production yield at maximal growth are identified using the OptKnock algorithm. With a two-step procedure like OptStrain, it is only possible to find heterologous genes and knockouts that improve production independently of each other. To solve this problem the algorithm SimOptStrain (Kim et al., 2011) does simultaneous prediction of gene insertions and knockouts. This enables the identification of heterologous gene insertions that have beneficial effects, only in the presence of

specific knockouts. An example of a design where heterologous genes and knockouts are combined is the growth-coupling of product methylation in a cysteine auxotrophic *E. coli* strain described by Luo and Hansen (2018). Insertion of *CYS3* and *CYS4* from *Saccharomyces cerevisiae* enable cysteine synthesis from supplemented methionine through a pathway that requires flux through S-adenosylmethionine (SAM)-dependent methyltransferase reactions. As seen in this design as well as the previously mentioned itaconic acid production design, growth-coupling strategies can result in auxotrophies, such that the growth medium must be supplemented with additional nutrients, i.e. methionine and glutamate, respectively. Although auxotrophies are generally undesirable in production processes as the addition of a supplement can incur a significant extra cost, auxotrophic growth-coupled strains can still be very useful in the strain development phase, particularly in combination with ALE (Shepelin et al., 2018). The recent algorithm SelFi (Hassanpour et al., 2017) attempts to couple growth to the flux catalysed by a target enzyme by constructing a carbon supply pathway including the target reaction and disabling alternative carbon supply pathways. This is done using a combination of knockouts and heterologous gene insertions as well as medium supplements. However, similar to OptStrain this is done in a two-step process, potentially excluding some designs. Furthermore, since growth coupling is achieved by constructing a new carbon supply pathway, the scope of target reactions is limited to reactions that can feasibly be incorporated into such a pathway.

Here we introduce OptCouple, an algorithm that simultaneously finds gene knockouts, insertions and modifications to the growth medium that result in coupling the production of a target chemical to growth in microorganisms. We have validated OptCouple by showing that it can predict known successful growth-coupling designs for the common production host *E. coli* and have used it to predict novel growth-coupling strategies.

5.2 Materials and methods

All computations were carried out in Python 3.6.4. A list of installed packages and an implementation of the entire prediction workflow, and scripts for the described analyses can be found in the supplementary material. Simulations were done using the iJO1366 genome-scale reconstruction of *E. coli* (Orth et al., 2011) as well as the reduced EColiCore2 model (Hädicke and

Klamt, 2017). Simulations were performed with a maximum glucose uptake rate of 10 mmol/gDW/h and a maximum oxygen uptake of 1000 mmol/gDW/h.

5.2.1 MILP-based optimization of growth-coupling potential

The following section will go through the mathematical optimization problem forming the core of OptCouple. For the full mathematical formulation, see supplementary materials.

Growth-coupling potential can be defined as the increase in maximal growth rate obtained when allowing flux through the target reaction, i.e. the reaction producing the chemical of interest.

The symbol *M* is used to denote a full metabolic model with metabolites $m_i \forall\ i \in N$ and reactions $r_j\ \forall\ j \in R$, the target reaction, r_{target}, with the biomass reaction, $r_{biomass}$, as the objective function, while the symbol M^* is used to denote the metabolic model without the target reaction.

If we use *f* to denote objective function of a problem, the growth-coupling potential, *U*, can be mathematically described as:

$$U = \hat{f}(M) - \hat{f}(M^*) \quad (1)$$

where $\hat{f}$ is used to denote the optimal objective value of a problem.

Every linear optimization problem can be converted into a dual problem (Ignizio and Cavalier, 1994), which will be denoted by a *D*-subscript, i.e. M_D. One property of duality in linear optimization is that the dual problem will have the same optimal objective value as the primal, however if *M* is a maximization problem, M_D will be a minimization problem, and vice versa.

Each potential perturbation, i.e. gene knock-out, knock-in, as well as addition of a growth medium supplement, can be represented by a binary variable, $y_j \in Y\ \forall\ j \in R$, controlling the flux of the reaction associated with the given perturbation, i.e. native reactions, heterologous reactions and exchange reactions, for knockouts, knock-ins and medium supplements, respectively. Additional coupling constraints are added to ensure that a given reaction can only carry flux when its corresponding perturbation variable, y_j, has a value of 1 (see supplementary material).

The goal is to formulate an optimization problem that optimizes *U*, by finding an optimal combination of values for the control variables, *Y* and reaction fluxes, *v*:

$$Maximize_{Y,v}\ \hat{f}(M) - \hat{f}(M^*) \tag{2}$$

This can be formulated as a bi-level optimization problem:

(3)

$Maximise_Y\ f(M) - f(M^*)$

subject to:

$Maximise_v\ f(M)$

subject to:

$S \cdot v = 0$

$v_j = 0\ \forall\ j \in \{j \mid y_j = 0\}$

$Maximise_v\ f(M^*)$

subject to:

$S \cdot v = 0$

$v_j = 0\ \forall\ j \in \{j \mid y_j = 0\}$

$v_{target} = 0$

The bi-level formulation can be interpreted as finding the combination of control values that allows the highest growth-coupling potential, subject to the constraints that the fluxes (*v*) of *M* and M^* must be optimal for growth (under the given control variable values).

The bi-level formulation can be converted into a single optimization problem by replacing M^* with its dual form, M^*_D:

$$Maximize_{Y,v}\ f(M) - f(M_D^*) \tag{4}$$

Since *M* is a maximization problem and M^*_D is a minimization problem, maximizing this expression automatically ensures that $f(M) = \hat{f}(M)$ and $f(M_D^*) = \hat{f}(M_D^*)$, and since the optimal objective

value of a dual problem is the same as the optimal objective value of its primal, the expression $\hat{f}(M) - \hat{f}(M_D^*)$ still corresponds to the growth-coupling potential.

To maintain computational feasibility of the problem, maximum numbers of knock-outs, insertions and media modifications, respectively, can be set as constraints on the binary variables.

OptCouple is implemented in the *cameo* Python package (Cardoso et al., 2018) for computational strain design (https://github.com/biosustain/cameo), and an implementation can also be found in the supplementary material.

5.2.2 Selecting allowed gene insertions and medium supplements

The set of allowed heterologous gene insertions was obtained from metanetx (Moretti et al., 2016), through the universal model interface of the Python package *cameo* (Cardoso et al., 2018). Only reactions with a cross-reference to the BiGG database were used. To avoid drastically increasing running times due to the large pool of heterologous reactions, the list of allowed insertions was reduced according to the number of allowed simultaneous insertions. If a single insertion was allowed, only reactions with metabolites native to the host were allowed. For higher numbers of allowed insertions, the heterologous reaction network was pruned such that only reactions whose metabolites could be reached with the allowed number of inserted reactions were included. The list of allowed medium modifications is specified manually. For all predictions described in this work the list comprised fructose, lactate, acetate, and all 20 standard proteinogenic L-amino acids

5.2.3 Running MILP optimizations

The MILP problems were optimized using the Gurobi solver (ver 7.5.2) through the *optlang* interface (Jensen et al., 2017). The computations were run on nodes of an HPC cluster equipped with Intel Xeon 2660v3 processors and 128 GB memory. The problems were solved to optimality, and subsequently reoptimized using Gurobi's solution pool feature to collect additional optimal and sub-optimal integer solutions. The second optimization was run with a time-limit approximately ten times the running time of the first optimization, up to a maximum of 30 hours. For problems that could not be solved to optimality within 30 hours, only as many suboptimal solutions as possible were collected from the second run. Each problem was optimized multiple times and the identified solutions from each run were all pooled together to increase the number of obtained solutions.

Since the identification of integer solutions is not deterministic, and since multiple solutions from the same run tend to be similar, this allowed a more diverse sampling of the solution space.

5.2.4 Reducing solution redundancy

With other MILP-based algorithms like OptKnock (Burgard et al., 2003), a common practice is to gradually increase the number of allowed knockouts, to avoid getting solutions with unnecessary knockouts. With three different upper limits on modifications (for knockouts, gene insertions and medium supplements, respectively), such a strategy is significantly more time-consuming. Instead, a postprocessing workflow was used to identify the predicted modifications in each solution that do not contribute to growth-coupling. Each solution was simulated, and each modification was removed one at a time. If a modification could be excluded without eliminating growth-coupling, it was removed from the solution. Solutions that could be reduced to the same set of modifications were merged into a single solution. The remaining solutions were summarized by production and growth rates, as well as a production envelope plot.

5.3 Calculation

OptCouple is based on an MILP formulation, conceptually similar to the formulations used in existing algorithms like OptKnock, RobustKnock and SimOptStrain. MILP formulations are an efficient way of optimizing an objective function over a combinatorial space, such as the space of possible genetic modifications. The objective function of OptCouple is the growth-coupling potential (Figure 1), defined as the amount with which the maximal growth rate will be decreased by preventing the target compound from being produced. Using the broadest definition of growth-coupling, sometimes called weak growth-coupling, namely that optimal growth requires a non-zero production flux (Feist et al., 2010; Klamt and Mahadevan, 2015), production is growth-coupled if and only if the growth-coupling potential is strictly positive. Optimizing for the growth-coupling potential ensures that the predicted strain designs and medium conditions will be easy to evolve with ALE to increase production, as the producing strains will have a large advantage over the non-producing strains. The algorithm RobustKnock maximises the minimum production at optimal growth instead, which also ensures growth-coupling, however the difference in growth rate between producers and non-producers can sometimes be marginal.

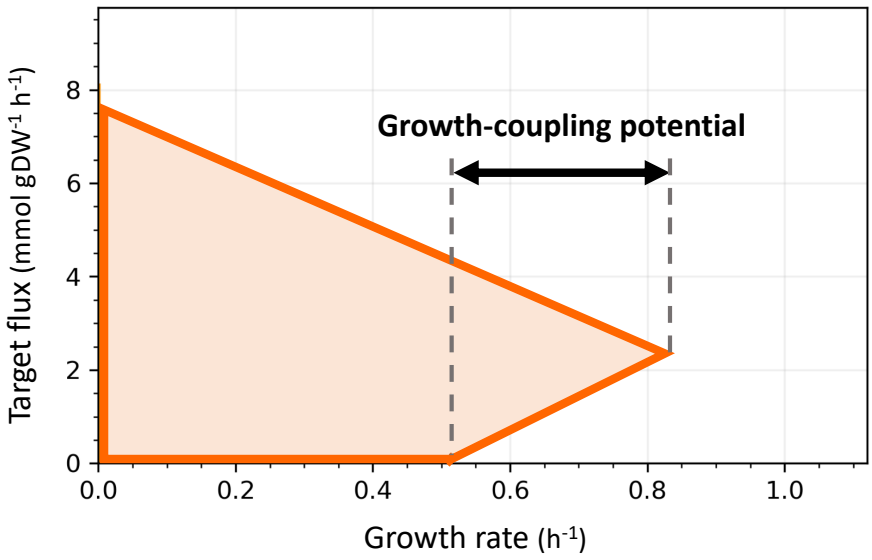

Figure 1: *Visual depiction of the growth-coupling potential on a production envelope.*

Most previous methods try to find the single most optimal solution based on the chosen objective function. Since the most optimal solution (regardless of the objective function) might not be practically feasible for a strain engineering project, OptCouple uses an alternate approach to generate a large pool of different growth-coupled designs. These solutions can then be evaluated based on multiple parameters in order to find candidate strategies to implement *in vivo*. The workflow of OptCouple is shown in Figure 2. In step 1, before running the MILP optimization, a metabolic model must be chosen, as well as the reaction to optimize. Furthermore, the universe of modifications must be defined. This includes deciding which native reactions may be knocked out, which heterologous reactions can be added, and which modifications to the medium are allowed. In step 2, the MILP problem is formulated, with binary variables to represent the allowed modifications. In step 3, the problem is solved using a dedicated MILP solver. Since the mathematically optimal solution is not necessarily the best strategy for a given metabolic engineering project, multiple solutions are identified in a single run, with high computational efficiency by using a solver with the capacity to find “solution pools”. Step 4 involves analysing the solutions found in step 3 and selecting one or more candidate strategies. Before manual inspection the number of solutions is automatically reduced by merging redundant solutions, i.e. separate solutions with only trivial differences, and ranking e.g. by growth-coupling potential or potential production rate.

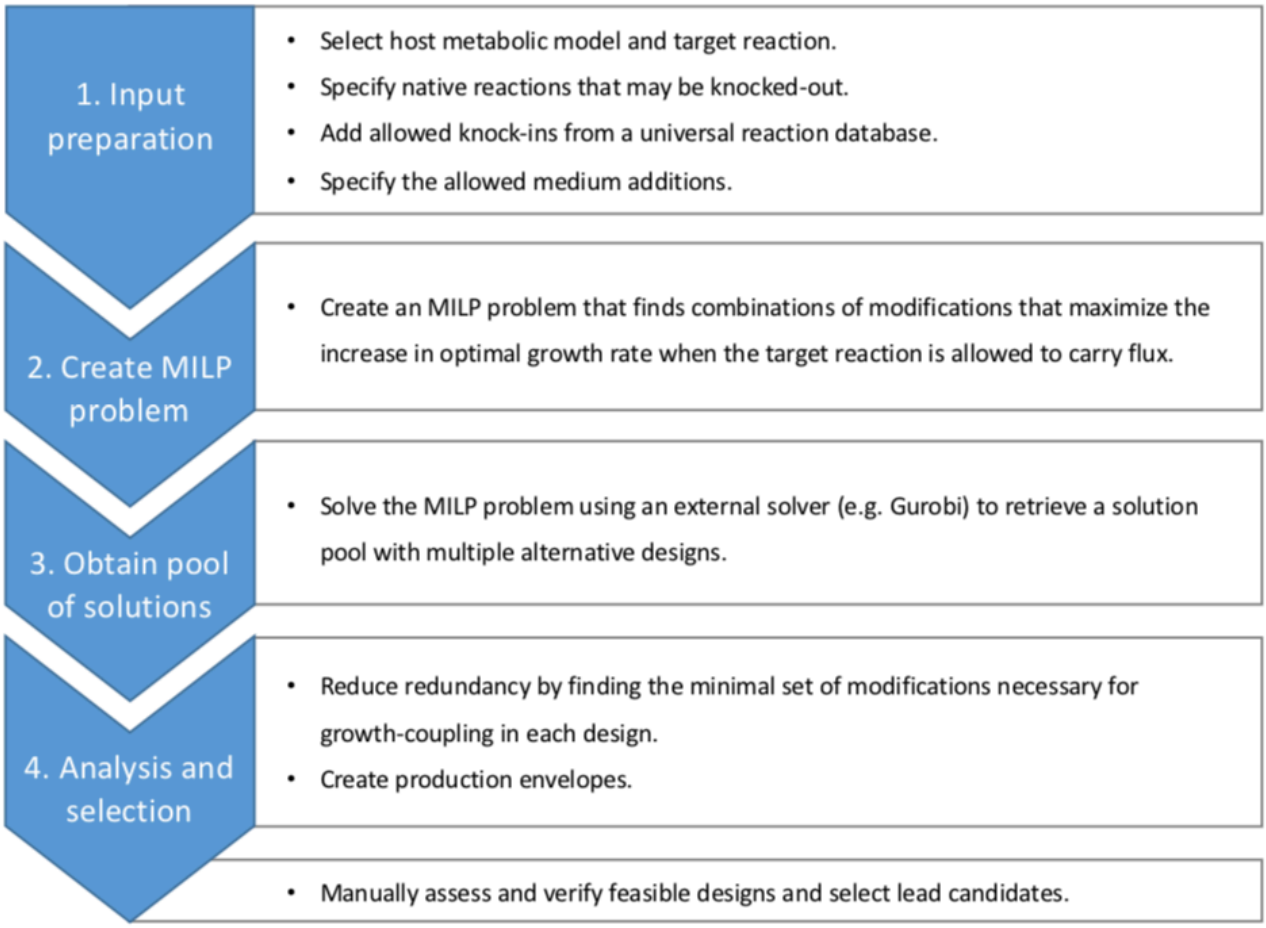

Figure 2: *Overview of the workflow used for predicting growth-coupling designs with OptCouple.*

5.4 Results and discussion

Initial testing of OptCouple was done to validate the novel objective function based on growth-coupling potential, and its ability to predict strain designs that are growth-coupled *in silico.* For this case, we chose propionic acid, which is an industrially relevant chemical that has not yet been produced biologically in economically viable amounts (Eş et al., 2017), and for which growth-coupling in *E. coli* has not been demonstrated. Furthermore, propionic acid is a native metabolite of *E. coli*, avoiding the necessity of first identifying or predicting a production pathway. OptCouple was run with a maximum of three knockouts, three insertions and one medium supplement, using a demand reaction for propionic acid as target. After removing redundancies in the predictions, two promising designs were identified, as seen in Table 1, which both produce propionic acid using the propionyl-CoA succinate CoA-transferase (PPCSCT) reaction. The first design, which is illustrated in

Figure 3, achieves growth-coupling by establishing propionic acid as a by-product of the supply of succinyl-CoA, which is a precursor for the biomass components methionine, lysine and murein. This is done by knocking out the native routes of producing succinyl-CoA (AKGDH and SUCOAS) as well as the recycling reaction for propionic acid (ACCOAL). The second design couples the PPCSCT reaction to the biosynthesis of NAD, establishing production of propionic acid as a by-product.

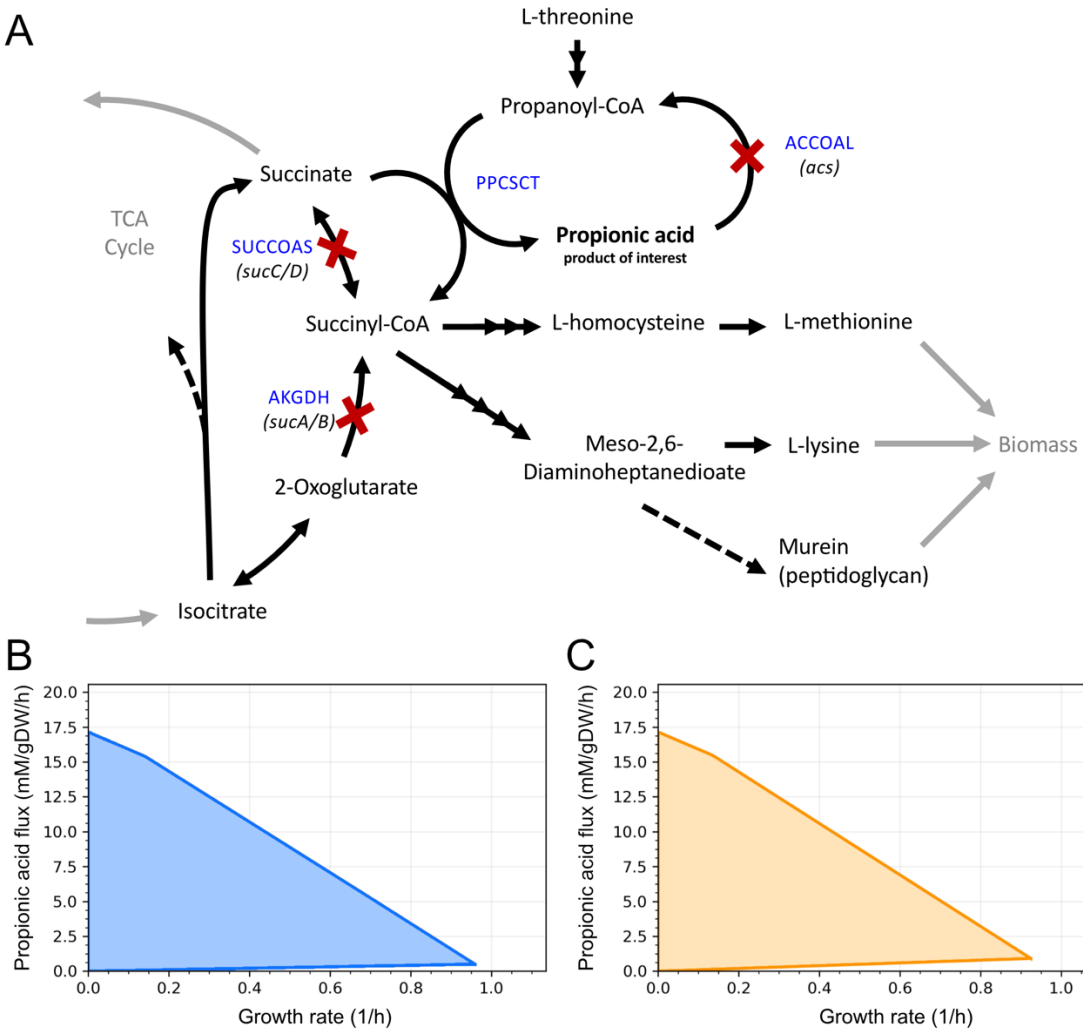

Figure 3: *Overview of the designs predicted with OptCouple for growth-coupling of propionic acid. A) Pathway map of one of the predictd designs. Propionic acid production is coupled to succinyl-CoA production through the propanoyl-CoA succinate CoA-transferase. Alternative routes to succinyl-CoA are knocked out. B) Production envelope for the design shown in A. C) Production envelope of the second growth-coupled design, which couples production of propionic acid to the biosynthesis of NAD.*

Both of the strain designs for propionic acid lead to growth-coupling through non-obvious combinations of knockouts, but only require knockouts. To demonstrate the full potential of

OptCouple and to test its ability to predict designs that are growth-coupled *in vivo*, we further evaluated the algorithm by its ability to identify known and experimentally validated growth-coupling strategies that require knockouts as well as medium supplements and gene insertions. We chose to use the itaconic acid growth-coupling of Harder et al. (2016) (requiring knockouts and medium supplement) as well as the product methylation growth-coupling of Luo & Hansen (2018) (requiring knockouts, medium supplement and gene insertions). Heterologous production of itaconic acid in *E. coli* can be achieved by the insertion of a single heterologous gene, *cadA* (*Aspergillus terreus*), encoding an enzyme that decarboxylates aconitic acid into itaconic acid (Harder et al., 2016). Growth-coupling has been realised by Harder et al. (2016) by knocking out the genes encoding isocitrate lyase, succinyl-CoA synthase, pyruvate kinase and phosphotransacetylase, as well as down-regulating isocitrate dehydrogenase. Additionally, Harder et al. (2016) inserted an orthologous citrate synthase to prevent allosteric regulation, but since the constraint-based modeling framework used here does not account for regulation, this modification was disregarded. When these modifications are applied to the iJO1366 genome-scale model of *E. coli* no growth-coupling is seen, as maximal growth does not allow for any production of itaconic acid. In order to attempt to reproduce the design, we chose to use the reduced metabolic model EColiCore2 (Hädicke and Klamt, 2017) instead. When the modifications from Harder et al. (2016) are introduced into this model, optimal growth does allow for production of itaconic acid, although it is not required.

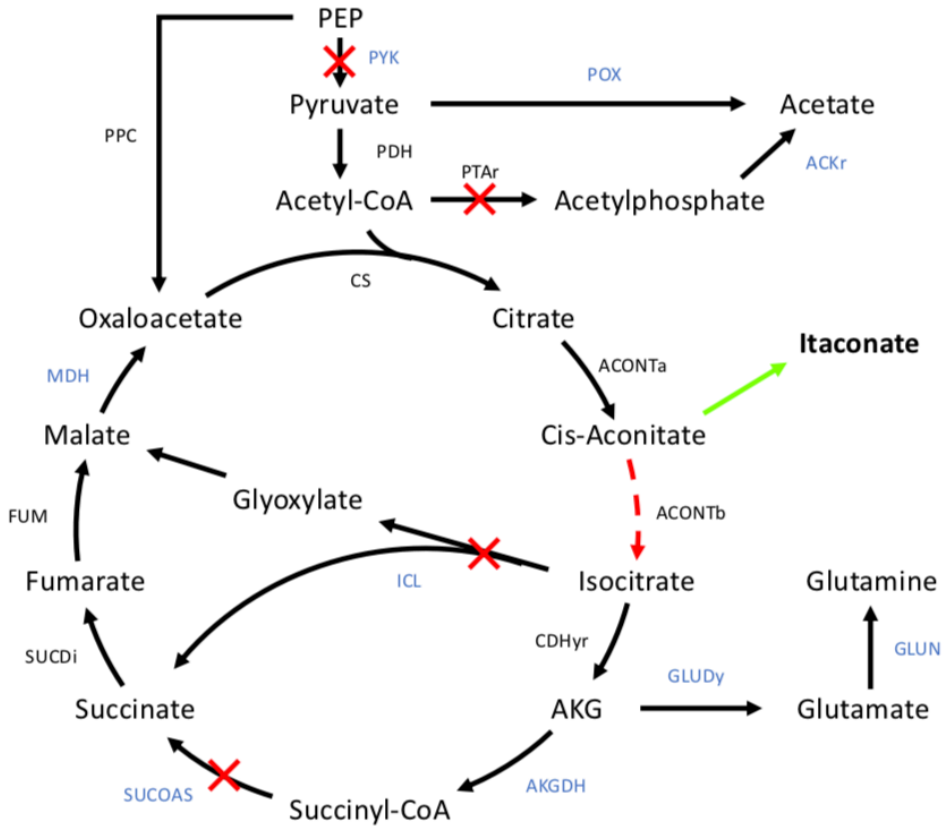

Figure 4: *Overview of the itaconic acid growth-coupling designs. The red crosses are reactions that were knocked out by Harder et al. (2016). The reactions whose names are written in blue are reactions that were commonly knocked out in the designs predicted by OptCouple.*

The itaconic acid-producing reaction was added to the model prior to running OptCouple, as the scope of this work was not to predict production pathways, but to identify growth-coupling strategies for an existing pathway. The algorithm was run, allowing up to six knockouts and a single medium supplement. A selection of the solutions is shown in Table 1. The majority of the identified designs contained modifications that are consistent with the design by Harder et al. (2016), as shown in Figure 4. This includes disrupting the TCA cycle downstream of aconitate, the glyoxylate shunt, as well as reactions that can act as a sink for pyruvate or acetyl-CoA. Additionally, the algorithm suggested the addition of glutamate or glutamine to the medium, as also required in the design by Harder et al. (2016). The similarities between these results and the design by Harder et al. (2016) provided an indication that OptCouple can be used to predict combinations of knockouts and medium supplements and create functional strategies for coupling chemical production to growth.

While the results obtained for growth-coupling of itaconic acid demonstrated the utility of the algorithm for predicting knockouts and medium modifications, they did not require prediction of gene insertions. To test the ability of OptCouple to predict such modifications, the product methylation growth-coupling design of Luo & Hansen (2018) was used. This time the iJO1366 genome-scale model was chosen, as the modifications suggested by Luo & Hansen (2018) do confer growth-coupling in this context. To predict designs for product methylation, a dummy reaction converting SAM into *S*-adenosylhomocysteine (SAH) and an exportable methyl group metabolite was created and used as target reaction. The algorithm was run with a single knockout, two insertions and one medium supplement allowed. Among the predicted strategies we found a design that consisted of the exact same combination of modifications as suggested by Luo & Hansen (2018), while designs with several minor variations were also predicted. These variations consisted of different knockouts or insertions but resulted in the same general mechanism of growth-coupling, by requiring product methylation to convert SAM into SAH as part of the conversion of supplemented methionine into cysteine required for biomass production. The ability to predict the exact design of the validated methylation growth-coupling, as well as alternative seemingly equivalent designs, indicates that OptCouple can reliably be used to predict new feasible growth-coupling strategies, requiring a combination of gene knockouts, insertions and medium supplements.

Table 1: *Overview of selected predicted growth-coupling strategies for the three test cases. For each design is shown the required modifications, the production rate and yield at optimal growth (mmol/gDW/h and mol/mol glucose) and the growth-coupling potential, U, i.e. the difference in maximal growth rate between producers and non-producers. The knocked out and inserted reactions are denoted by their BIGG identifiers. The supplemented are denoted by standard three-letter amino acid abbreviations.*

Knockouts	Insertions	Supplements	Production rate	Yield	U
Propionic acid:					
ACCOAL, SUCCOAS, AKGDH			0.50	0.05	0.95
MCITD, MTHFC, PFL			0.90	0.09	0.91
Itaconic acid:					
GLUDy, ICL, SUCCOAS		L-glu	7.64	0.764	1.10
GLNS, ICL, SUCCOAS		L-gln	0.24	0.024	1.11
ACKr, AKGDH, ICL, PGL, POX		L-ile	5.68	0.568	0.29
AKGDH, G6PDH2r, ICL, MDH, MGSA, PYK		L-asp	6.32	0.632	0.60
Product methylation:					
SERAT	CYSTL, CYSTGL	L-met	0.10	0.01	1.02
ASPTA	AHSERL2, HSERTA	L-met	2.69	0.269	0.97

While the itaconic acid growth-coupling by Harder et al. (2016) results in a high production with yields of up to 0.68 mol/mol glucose, the methylation growth-coupling by Luo and Hansen (2016) has the disadvantage that only a relatively small flux is forced through the target pathway. Since methylation is required for the cell to synthesise cysteine, the growth-coupling will not drive methylation to exceed the cellular demand for cysteine which is quite low (Orth et al., 2011). We therefore used OptCouple to predict alternative growth-coupling strategies, which would be able to force a higher flux through the target methylation reaction. One such strategy was discovered, that uses product methylation to convert supplemented methionine into the amino acids aspartate, threonine and isoleucine, while disabling the native production of these. This will demand a higher flux through the methylation reaction at a given growth rate than the original design coupling methylation to cysteine biosynthesis. Figure 5 shows the two growth-coupling designs and their respective production envelopes. The production envelope for the alternative design (Figure 5C) shows a larger potential production rate by growth-coupling (indicated by the height of the right-

most point) than the original design (Figure 5B), consistent with the combined higher cellular demand for aspartate, threonine and isoleucine compared to cysteine (Orth et al., 2011).

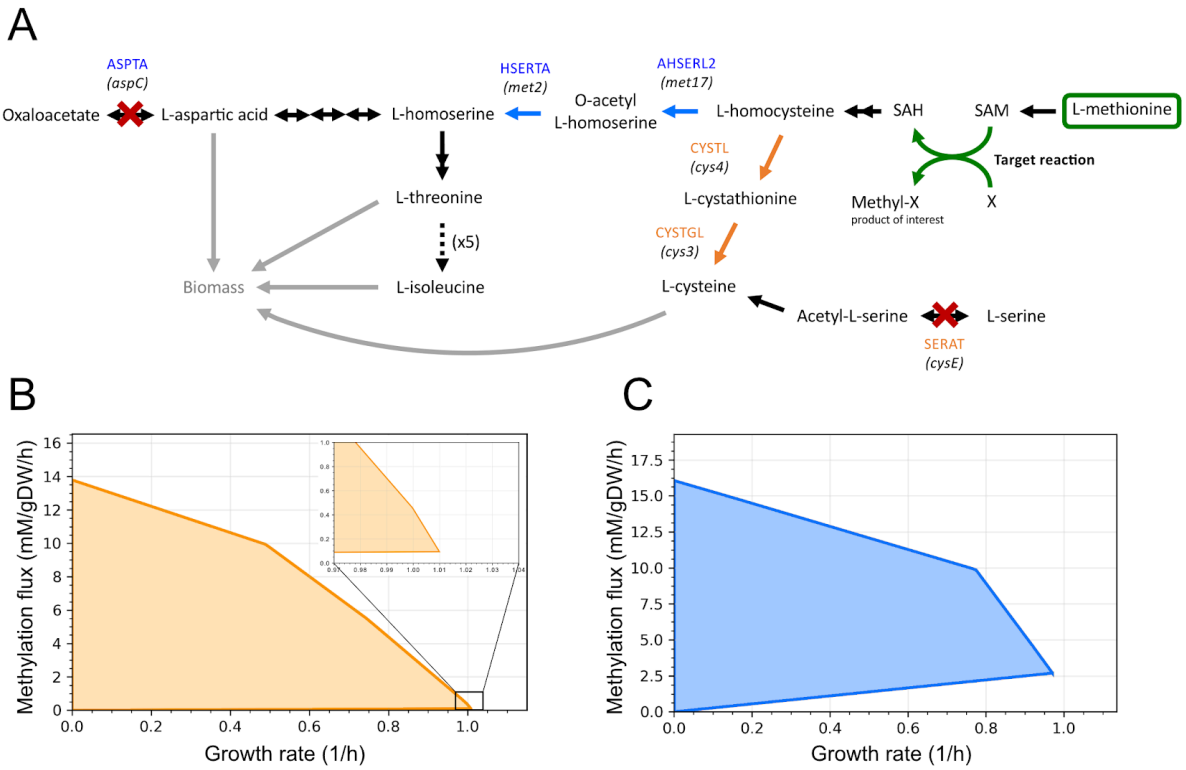

Figure 5: *Overview of a subset of the predicted growth-coupling designs for product methylation. A) Pathway map showing the mechanisms of two growth-coupling strategies. The design of Luo & Hansen (2018) (orange) converts L-homocysteine into L-cysteine. The alternative design found here (blue) converts L-homocysteine in to L-threonine, L-isoleucine and L-aspartic acid. Both designs require supplementing the medium with methionine. B) Production envelope of the growth-coupling design of Luo & Hansen (2018). C) Production envelope of the alternative growth-coupling design found in this study.*

The above results prove that OptCouple can be used to identify combinations of knockouts, gene insertions and medium supplements that make production of various compounds coupled to growth in *E. coli*. The algorithm could easily find designs allowing up to 7 modifications with running times less than 24 hours. The fact that OptCouple identifies designs that are identical or very similar to prominent, experimentally validated growth-coupling designs indicates that it will also be able to find novel valid growth-coupling designs.

The main novelty and advantage of OptCouple is the possibility of simultaneously identifying complex combinations of three different types of modifications. Currently, other strain design algorithms exist that attempt to find growth-coupled designs through the identification of one or

two types of modifications simultaneously. Recent examples are SimOptStrain (Kim et al., 2011) that simultaneously identifies gene knockouts and insertions, whereas SelFi (Hassanpour et al., 2017) can suggest all three types of modifications, but only medium supplements and gene knockouts are identified simultaneously. Several successful designs, however, such as the product methylation growth-coupling (Luo and Hansen, 2018), show that considering all three types of modifications at once can enable the identification of new growth-coupling strategies.

OptCouple guarantees that the resulting designs are truly growth-coupled. This is in contrast to e.g. SimOptStrain, which uses the same objective function as OptKnock, and thus does not specifically predict growth-coupling, as competing pathways are still allowed. A potential drawback of using the growth-coupling potential as objective function in OptCouple is that there is no explicit optimization of the target flux that can be achieved by growth-coupling. An example of this issue is seen in the identified growth-coupling strategies for propionic acid. The design identified by OptCouple ensures the production of propionic acid to supply the cell with either NAD or methionine, lysine and murein, all of which are only needed in relatively small amounts. The consequence is that the growth-coupled production rate of propionic acid will not be sufficient for a commercially viable process, given the modest market price of propionic acid (Rodriguez et al., 2014). Even though this limits the practical utility of some growth-coupling strategies identified by OptCouple, it does not significantly reduce the utility of the algorithm itself. Computationally predicted strain designs should always be assessed manually before being implemented in the laboratory, as their feasibility can also be affected by a range of factors not considered in the models, e.g. thermodynamics, regulation, toxicity, etc. Through the use of suboptimal solution pools, OptCouple can quickly identify many design alternatives, which means that many candidate designs are obtained, increasing the likelihood that at least one will be deemed feasible and have a high growth-coupled production rate.

As with all model-based predictions, the quality of the results strongly depends on the quality of the model that was used. As one of the most commonly used organisms for metabolic modeling, the *E. coli* genome-scale model is relatively comprehensive. While nothing prevents OptCouple from being used in other organisms, the predicted designs should be curated even more thoroughly if a less complete metabolic model is used. The *in vivo* presence of enzymes that are not accounted for in the model can effectively abolish the growth-coupling of a predicted design, as they can allow the

cell to circumvent the growth-coupling mechanism. Conversely, if a model contains reactions that are not active *in vivo*, e.g. due to transcriptional repression, some growth-coupling strategies will require more modifications *in silico* than they would in practice. This is seen in the experimentally validated itaconic acid growth-coupling design (Harder et al., 2016), which does not show growth-coupling when simulated with iJO1366, whereas the reduced model EColiCore2 did allow production at optimal growth. However, during optimization with ALE, repressed reactions could become active allowing the cell to circumvent growth-coupling mechanisms predicted with reduced models. Therefore, it would most likely be preferable to use the most complete model available for the chosen organism.

5.5 Conclusion

OptCouple is an MILP-based optimization algorithm that can find combinations of gene knockouts, heterologous gene insertions, and additions to the growth medium, that allow the stoichiometric coupling of a product of interest to growth. In our validation tests OptCouple was able to reproduce successful growth-coupling designs from the published literature and find alternative designs that allow for a higher production flux. Furthermore, we showed that OptCouple can be used to predict novel candidate growth-coupling designs for target compounds where no growth-coupling has previously been demonstrated.

5.6 Acknowledgements

This project has received funding from the European Union's Horizon 2020 research and innovation programme under grant agreement No 686070. Furthermore, we acknowledge financial support from the Novo Nordisk Foundation. The funding agencies were not involved in planning or carrying out the study. ASLH declares financial interest as co-inventor of patent WO2018037098.

5.7 References

Alter, T.B., Blank, L.M., Ebert, B.E., 2018. Determination of growth-coupling strategies and their underlying principles. bioRxiv. https://doi.org/https://doi.org/10.1101/258996

Becker, J., Wittmann, C., 2015. Advanced biotechnology: Metabolically engineered cells for the bio-based production of chemicals and fuels, materials, and health-care products. Angew. Chemie

- Int. Ed. 54, 3328–3350. https://doi.org/10.1002/anie.201409033

Burgard, A.P., Pharkya, P., Maranas, C.D., 2003. OptKnock: A Bilevel Programming Framework for Identifying Gene Knockout Strategies for Microbial Strain Optimization. Biotechnol. Bioeng. 84, 647–657. https://doi.org/10.1002/bit.10803

Cardoso, J.G.R., Jensen, K., Lieven, C., Hansen, A.S.L., Galkina, S., Beber, M., Özdemir, E., Herrgård, M.J., Redestig, H., Sonnenschein, N., 2018. Cameo: A Python Library for Computer Aided Metabolic Engineering and Optimization of Cell Factories. ACS Synth. Biol. 7, 1163–1166. https://doi.org/10.1021/acssynbio.7b00423

Eş, I., Khaneghah, A.M., Hashemi, S.M.B., Koubaa, M., 2017. Current advances in biological production of propionic acid. Biotechnol. Lett. 39, 635–645. https://doi.org/10.1007/s10529-017-2293-6

Feist, A.M., Zielinski, D.C., Orth, J.D., Schellenberger, J., Herrgard, M.J., Palsson, B.O., 2010. Model-driven evaluation of the production potential for growth-coupled products of Escherichia coli. Metab. Eng. 12, 173–186. https://doi.org/10.1016/j.ymben.2009.10.003

Hädicke, O., Klamt, S., 2017. EColiCore2: A reference network model of the central metabolism of Escherichia coli and relationships to its genome-scale parent model. Sci. Rep. 7, 1–15. https://doi.org/10.1038/srep39647

Hansen, A.S.L., Lennen, R.M., Sonnenschein, N., Herrgård, M.J., 2017. Systems biology solutions for biochemical production challenges. Curr. Opin. Biotechnol. 45, 85–91. https://doi.org/10.1016/j.copbio.2016.11.018

Harder, B.J., Bettenbrock, K., Klamt, S., 2016. Model-based metabolic engineering enables high yield itaconic acid production by Escherichia coli. Metab. Eng. 38, 29–37. https://doi.org/10.1016/j.ymben.2016.05.008

Hassanpour, N., Ullah, E., Yousofshahi, M., Nair, N.U., Hassoun, S., 2017. Selection Finder (SelFi): A computational metabolic engineering tool to enable directed evolution of enzymes. Metab. Eng. Commun. 4, 37–47. https://doi.org/10.1016/j.meteno.2017.02.003

Ignizio, J.P., Cavalier, T.M., 1994. Duality and Sensitivity Analysis, in: Ignizio, J.P., Cavalier, T.M. (Eds.),

Linear Programming. Prentice Hall, Englewood Cliffs, NJ.

Jensen, K., G.R. Cardoso, J., Sonnenschein, N., 2017. Optlang: An algebraic modeling language for mathematical optimization. J. Open Source Softw. 2, 139. https://doi.org/10.21105/joss.00139

Kim, J., Reed, J.L., Maravelias, C.T., 2011. Large-Scale Bi-Level strain design approaches and Mixed-Integer programming solution techniques. PLoS One 6. https://doi.org/10.1371/journal.pone.0024162

Klamt, S., Gilles, E.D., 2004. Minimal cut sets in biochemical reaction networks. Bioinformatics 20, 226–234. https://doi.org/10.1093/bioinformatics/btg395

Klamt, S., Mahadevan, R., 2015. On the feasibility of growth-coupled product synthesis in microbial strains. Metab. Eng. 30, 166–178. https://doi.org/10.1016/j.ymben.2015.05.006

LaCroix, R.A., Palsson, B.O., Feist, A.M., 2017. A model for designing adaptive laboratory evolution experiments. Appl. Environ. Microbiol. 83. https://doi.org/10.1128/AEM.03115-16

Lee, S.Y., Kim, H.U., 2015. Systems strategies for developing industrial microbial strains. Nat. Biotechnol. 33, 1061–1072. https://doi.org/10.1038/nbt.3365

Luo, H., Hansen, A.S.L., 2018. Method of improving methyltransferase activity. WO2018037098.

Moretti, S., Martin, O., Van Du Tran, T., Bridge, A., Morgat, A., Pagni, M., 2016. MetaNetX/MNXref - Reconciliation of metabolites and biochemical reactions to bring together genome-scale metabolic networks. Nucleic Acids Res. 44, D523–D526. https://doi.org/10.1093/nar/gkv1117

Orth, J.D., Conrad, T.M., Na, J., Lerman, J. a, Nam, H., Feist, A.M., Palsson, B.Ø., 2011. A comprehensive genome-scale reconstruction of Escherichia coli metabolism. Mol. Syst. Biol. 7, 1–9. https://doi.org/10.1038/msb.2011.65

Phaneuf, P. V, Gos, D., Palsson, B.O., Feist, A.M., 2018. ALEdb 1.0: A Database of Mutations from Adaptive Laboratory Evolution Experimentation.

Pharkya, P., Burgard, A.P., Maranas, C.D., 2004. OptStrain: A computational framework for redesign of microbial production systems. Genome Res. 2367–2376. https://doi.org/10.1101/gr.2872004

Portnoy, V.A., Bezdan, D., Zengler, K., 2011. Adaptive laboratory evolution-harnessing the power of biology for metabolic engineering. Curr. Opin. Biotechnol. 22, 590–594. https://doi.org/10.1016/j.copbio.2011.03.007

Rodriguez, B.A., Stowers, C.C., Pham, V., Cox, B.M., 2014. The production of propionic acid, propanol and propylene via sugar fermentation: An industrial perspective on the progress, technical challenges and future outlook. Green Chem. 16, 1066–1076. https://doi.org/10.1039/c3gc42000k

Shepelin, D., Hansen, A.S.L., Lennen, R., Luo, H., Herrgård, M.J., 2018. Selecting the best: Evolutionary engineering of chemical production in microbes. Genes (Basel). 9. https://doi.org/10.3390/genes9050249

Stanford, N.J., Millard, P., Swainston, N., 2015. RobOKoD: microbial strain design for (over)production of target compounds. Front. Cell Dev. Biol. 3, 1–12. https://doi.org/10.3389/fcell.2015.00017

Tepper, N., Shlomi, T., 2009. Predicting metabolic engineering knockout strategies for chemical production: Accounting for competing pathways. Bioinformatics 26, 536–543. https://doi.org/10.1093/bioinformatics/btp704

von Kamp, A., Klamt, S., 2017. Growth-coupled overproduction is feasible for almost all metabolites in five major production organisms. Nat. Commun. 8, 1–10. https://doi.org/10.1038/ncomms15956

von Kamp, A., Klamt, S., 2014. Enumeration of Smallest Intervention Strategies in Genome-Scale Metabolic Networks. PLoS Comput. Biol. 10. https://doi.org/10.1371/journal.pcbi.1003378

Wong, B.G., Mancuso, C.P., Kiriakov, S., Bashor, C.J., Khalil, A.S., 2018. Precise, automated control of conditions for high-throughput growth of yeast and bacteria with eVOLVER. Nat. Biotechnol. 36, 614–623. https://doi.org/10.1038/nbt.4151

5.8 Supplementary Materials

Mathematical formulation of OptCouple

The metabolic model used in OptCouple is given by a set of metabolites $m_i \forall\ i \in N$, and a set of metabolic reactions $r_j\ \forall\ \ j \in R$. A stoichiometric matrix *S* encodes which metabolites participate in each reaction (Orth et al., 2010). R is partitioned by the three subsets, R_{native}, $R_{heterologous}$ and $R_{additions}$, representing native reactions, heterologous reactions and boundary reactions for potential medium additions, respectively. Furthermore, some reactions $r_j\ \forall\ j \in R_{irreversible}$ can only proceed in the forward direction, while the remaining reactions can proceed in both directions. Each reaction is associated with a binary control variable, $y_j \in Y\ \ \forall\ \ j \in R$.

The primal problem (M) optimizes biomass production subject to stoichiometric constraints, limited glucose uptake and genetic modifications, Y:

$Maximise_{\boldsymbol{v}}\ v_{biomass}$

subject to:

$\sum_{j \in R} s_{ij} \cdot v_j = 0\ \ \forall\ \ i \in N$

$v_j^{min} \cdot y_j \leq v_j \leq v_j^{max} \cdot y_j\ \ \ \forall\ \ j \in\ R$

$v_{glc\_uptake} \leq 10$

$v_j \geq 0\ \ \forall\ j \in R_{irreversible}$

$y_j \in \{0, 1\},\ \ \forall\ j \in R$

$\sum_{j \in R_{native}} (1 - y_j) \leq K_{native}$

$\sum_{j \in R_{heterologous}} y_j \leq K_{heterologous}$

$\sum_{j \in R_{additions}} y_j \leq K_{additions}$

The problem can be modified to not allow flux in the target reaction r_{target}, resulting in M*:

$Maximise_{\boldsymbol{v}}\ v_{biomass}$

subject to:

$\sum_{j=1}^{|R|} s_{ij} \cdot v_j = 0, \quad \forall\ i \in N$

$v_j^{min} \cdot y_j \leq v_j \leq v_j^{max} \cdot y_j, \quad \forall\ j \in R$

$v_{target} = 0$

$v_{glc\_uptake} \leq 10$

$v_j \geq 0, \quad \forall\, j \in R_{irreversible}$

$y_j \in \{0, 1\},\ \forall\, j \in R$

$\sum_{j \in R_{native}} (1 - y_j) \leq K_{native}$

$\sum_{j \in R_{heterologous}} y_j \leq K_{heterologous}$

$\sum_{j \in R_{additions}} y_j \leq K_{additions}$

M* can then be converted to its dual form, M_D^* (as described by Burgard et al. (2003)):

$Minimise_{\boldsymbol{\mu},\boldsymbol{\lambda}}\ 10 \cdot \mu_{glucose\_uptake}$

subject to:

$\sum_{i=1}^{|N|} \lambda_i^{stoich} \cdot s_{ij} + \mu_j = 0, \quad \forall\, j \in R,\ j \neq biomass$

$\sum_{i=1}^{|N|} \lambda_i^{stoich} \cdot s_{i,biomass} + \mu_{biomass} = 1$

$\mu_j^{min} \cdot (1 - y_j) \leq\ \mu_j \leq\ \mu_j^{max} \cdot (1 - y_i), \quad \forall\, j \in R,\ j \neq target$

$y_j \in \{0, 1\},\ \forall\, j \in R$

$\sum_{j \in R_{native}} (1 - y_j) \leq K_{native}$

$\sum_{j \in R_{heterologous}} y_j \leq K_{heterologous}$

$\sum_{j \in R_{additions}} y_j \leq K_{additions}$

Here λ_i^{stoich} represent dual variables of the stoichiometric constraints in the primal, while μ_i represent other flux bounds. The minimum and maximum values, μ_j^{min} and μ_j^{max} as well as

v_j^{min} and v_j^{max} can be found by sequentially minimizing and maximizing the variables or by using a sufficiently large constant (the big-M method).

The two problems M and M_d^* are combined and optimized simultaneously, together with the binary variables Y:

$Maximise_{\boldsymbol{v},\boldsymbol{\lambda},\boldsymbol{\mu},\boldsymbol{Y}}\ v_{biomass} - 10 \cdot \mu_{glucose\_uptake}$ **OptCouple**

subject to:

$\sum_{j=1}^{|R|} s_{ij} \cdot v_j = 0\ \forall\ i \in N$

$v_j^{min} \cdot y_j \leq v_j \leq v_j^{max} \cdot y_j\ \ \forall\ j \in\ R$

$v_{glc\_uptake} \leq 10$

$v_j \geq 0\ \forall\, j \in R_{irreversible}$

$\sum_{i=1}^{|N|} \lambda_i^{stoich} \cdot s_{ij} + \mu_j = 0,\ \ \forall\, j \in R,\ j \neq biomass$

$\sum_{i=1}^{|N|} \lambda_i^{stoich} \cdot s_{i,biomass} + \mu_{biomass} = 1$

$\mu_j^{min} \cdot (1 - y_j) \leq\ \mu_j \leq\ \mu_j^{max} \cdot (1 - y_i),\ \ \forall\, j \in R,\ j \neq target$

$y_j \in \{0, 1\},\ \forall\, j \in R$

$\sum_{j \in R_{native}} (1 - y_j) \leq K_{native}$

$\sum_{j \in R_{heterologous}} y_j \leq K_{heterologous}$

$\sum_{j \in R_{additions}} y_j \leq K_{additions}$

References

Burgard, A.P., Pharkya, P., Maranas, C.D., 2003. OptKnock: A Bilevel Programming Framework for Identifying Gene Knockout Strategies for Microbial Strain Optimization. Biotechnol. Bioeng. 84, 647–657. https://doi.org/10.1002/bit.10803

Orth, J.D., Thiele, I., Palsson, B.Ø., 2010. What is flux balance analysis? Nat. Biotechnol. 28, 245–248. https://doi.org/10.1038/nbt.1614

Concluding remarks

Adaptive laboratory evolution (ALE) can be a valuable addition to rational engineering during development of microbial cell factories. Sequencing of evolved isolates can reveal new engineering targets for the evolved phenotype that could not have been predicted from preexisting knowledge. Additionally, studying the evolved strains can yield insight into the mechanisms with which the targeted phenotype improved.

In this thesis, it was shown that ALE could be used to improve chemical tolerance of *Escherichia coli* – a phenotype that is difficult to engineer rationally due to a lack of knowledge about toxicity mechanisms. The concentrations of chemicals that the evolved strains could tolerate were high enough to be relevant in the context of bioproduction. Although only little information could be gained about the mechanisms of tolerance, cross-compound screenings revealed that tolerance to one compound tends to be generalizable to a wide range of chemically similar compounds. This demonstrates that it is possible to use broadly tolerant platform strains for production of several products, without having to evolve tolerance to each individual product. For two compounds it was also shown that some evolved tolerant strains were able to produce the respective compounds at higher rates than the background strain, further demonstrating the utility of ALE in cell factory development.

Metabolomic characterization of the evolved strains showed a high degree of convergent evolution on the metabolic level despite only limited convergence on the genetic level. This suggests that metabolism plays a significant role in tolerance against the tested chemicals. The metabolic profiles of the evolved strains were also used to develop a method for predicting the impact of a mutation on the gene that it affects. This method can be beneficial in interpreting the mutations that are observed after an ALE experiment and is not limited to strains evolved for tolerance. Another method for interpreting mutations observed in ALE was presented, which was based on deep neural networks. While artificial intelligence and machine learning have the potential to revolutionize the field of metabolic engineering like it has other fields, it is still limited by the comparatively small datasets available in biology.

The greatest challenge of using ALE in cell factory engineering is finding ways to select for the phenotype that is to be improved. In particular it is desirable to be able to select for mutants that produce a target compound at high rates. This is possible by making production coupled to growth such that the target compound becomes a necessary by-product. Although growth-coupling production usually requires complicated rewiring of metabolism, it can be done through the use of mathematical models of metabolism. This thesis presented a new model-based algorithm for identifying genetic modifications that cause growth-coupling in combination with one or more supplements to the growth medium. The algorithm allowed prediction of promising design strategies for growth-coupling, however these strategies need to be validated *in vivo* and are not guaranteed to work. Future work might focus on directly integrating experimental data into algorithms for predicting growth-coupling in order to improve predictions and make the predicted designs more likely to function *in vivo*, which would further increase the effectiveness of ALE for cell factory development.